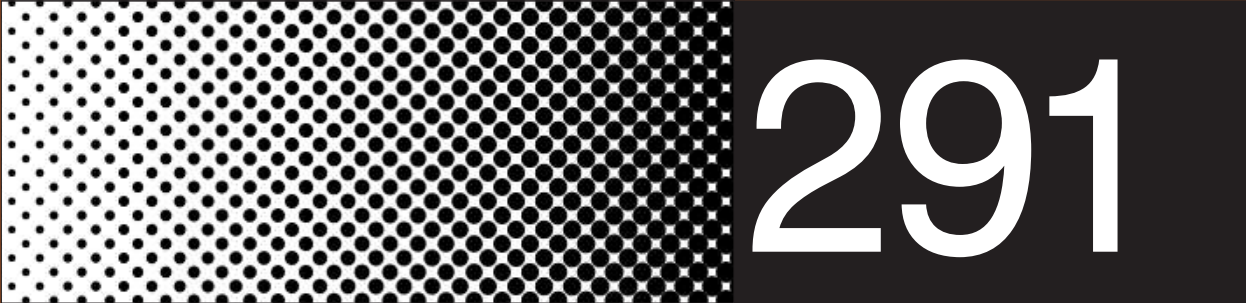


ROZPRAWY MONOGRAFIE



291

DANUTA SZELIGA

Identification problems in metal forming.
A comprehensive study



AGH UNIVERSITY OF SCIENCE AND TECHNOLOGY PRESS

KRAKOW 2013

Published by AGH University of Science and Technology Press

Editor-in-Chief:

Jan Sas

Editorial Committee:

Zbigniew Kąkol (Chairman)

Marek Cała

Borys Mikułowski

Tadeusz Sawik

Mariusz Ziółko

Reviewers:

prof. dr hab. inż. Maciej Pietrzyk, AGH University of Science and Technology, Poland

dr hab. inż. Waclaw Kuś, Silesian University of Technology, Poland

The author of the monograph is an employee of
AGH University of Science and Technology
Faculty of Metals Engineering and Industrial Computer Science
Department of Applied Computer Science and Modelling
al. A. Mickiewicza 30
30-059 Krakow, Poland

Desktop publishing: Danuta Szeliga

©Wydawnictwa AGH, Kraków 2013

ISSN 0867-6631

ISBN 978-83-7464-625-3

Wydawnictwa AGH

al. A. Mickiewicza 30, 30-059 Kraków

tel. 12 617 32 28, tel./fax 12 636 40 38

e-mail: redakcja@wydawnictwoagh.pl

www.wydawnictwa.agh.edu.pl

Contents

Summary	7
Streszczenie	9
The list of main symbols	11
1 State of the art in inverse analysis of metal forming	13
2 The thesis and the structure of the book	20
2.1 The thesis and the objectives of the work	20
2.2 The structure of the book	21
3 Inverse problems. The mathematical background	23
3.1 Modeling of metal forming processes	23
3.2 Inverse problems for the thermomechanical deformation problem	26
3.3 General formulation of the inverse problem	26
3.4 Regularization	29
3.5 Methods of regularizations	30
3.5.1 Tikhonov regularization	32
3.5.2 Iteration methods	33
3.5.3 Regularization by projection	36
3.6 Numerical computation	37
3.6.1 Regularization in the finite dimension setting	38
3.6.2 Practical aspects and problems	39
4 Sensitivity analysis	41
4.1 Local sensitivity analysis	42
4.1.1 A scheme for semi-analytical sensitivity calculations	44
4.1.2 An optimization algorithm enriched with sensitivity analysis	45
4.2 Global sensitivity analysis	49
4.2.1 An algorithm based on the Morris design	53
4.2.2 Variance based methods	56
4.3 The implementation of sensitivity analysis algorithms	61
5 A strategy for the identification of the model parameters	63
6 Case studies	66
6.1 Rheological and friction models	67
6.1.1 Objectives of the work	67
6.1.2 The experiments	68

6.1.3	The numerical model of the plastometric test	70
6.1.4	The identification task	77
6.1.5	The estimation of the functional minimum	78
6.1.6	The results of the parameter identification	83
6.1.7	Sensitivity analysis	88
6.1.8	Discussion of the results	95
6.2	A quantitative fracture criterion	96
6.2.1	Objectives of the work	97
6.2.2	The experiment	97
6.2.3	A numerical model of the SICO test	98
6.2.4	Sensitivity analysis	99
6.2.5	Discussion of the results	101
6.3	The strain localization model	102
6.3.1	Objectives of the work	102
6.3.2	The experiment	102
6.3.3	The numerical model of a shearing test	103
6.3.4	Sensitivity analysis	104
6.3.5	Discussion of the results	107
6.4	The phase transformation model	107
6.4.1	Objectives of the work	108
6.4.2	Phase transformation models	108
6.4.3	Sensitivity analysis	112
6.4.4	Identification of the model parameters	115
6.4.5	Discussion of the results	116
6.5	Design of the hot rolling technology of dual phase steel strips	117
6.5.1	Objectives of the work	118
6.5.2	The experiment	118
6.5.3	The numerical model of the process	119
6.5.4	Sensitivity analysis	120
6.5.5	Discussion of the results	122
6.6	Design of the continuous annealing process	123
7	Conclusions	128
7.1	Summary	128
7.2	Future prospects	130
A	Functional analysis - fundamentals	133
	Bibliography	136

DANUTA SZELIGA

Identification problems in metal forming.

A comprehensive study

Summary

The work presents an identification problem of the parameters of models applied in the numerical simulation of metal forming processes. The main thesis of the work is a supposition that it is possible to obtain *optimal* solutions to ill-posed inverse problems of identification with the application of sensitivity analysis methods combined with optimization procedures. The objectives defined and executed in the work, as well as the application of the developed methods to solve practical identification problems of metal forming, prove the work thesis. Identification problems are inverse problems transformed into optimization tasks for which a minimum is searched. These problems are ill-posed, thus, the main objective of the work was to develop a method based on the sensitivity analysis algorithms coupled with optimization procedures which would constitute a robust tool to solve inverse problems and which would allow to obtain solutions close to the exact ones.

The application of sensitivity algorithms to decrease computational costs of identification is presented. The application was the next objective of the work. The methods of reducing the space dimension of decision variables dedicated to the identification of parameters of the highest importance, based on sensitivity analysis algorithms, are provided in the work. This problem is particularly important for numerical models of metal forming, which are computationally expensive due to non-stationary nature of these problems and due to solvers of finite element method with *hp*-adaptation to improve the quality of the solution. Another advantage of this application of sensitivity analysis is the constraint of a possible number of solutions.

The application of sensitivity analysis as a preliminary step of optimization to bound or extend the parameters domain, to generate starting points for optimization or to investigate behavior of the functional defined in optimization is presented in the work. Another provided application of sensitivity analysis is a hybrid optimization procedure, such as a combination of nondeterministic optimization methods and local sensitivity analysis algorithms for exploring local minima.

The thesis was proved with the solution of practical problems presented in the work. The following problems were solved: identification of mechanical boundary condition (friction coefficient), identification of parameters of rheological models, identification of fracture criteria parameters, identification of parameters of multiscale models, parameters of the phase transformation model and identification of production cycle control parameters. All the listed problems were solved with the developed software and they are presented in the monograph.

The presentation starts with the state of the art of identification problems investigated in metal forming. The identification achievements are summarized and weaknesses of theoretical research are pointed out. The conclusions from this part were basis to formulate the thesis of the work. Next general equilibrium equations used in the modeling of metal forming processes and the formulation of inverse problems for these equations are provided. The mathematical background of inverse operators and an attempt to apply mathematical formalism to construct the inverse operator for metal forming equations is included. Then, a description of sensitivity analysis methods and the ability to apply sensitivity analysis algorithms to inverse calculations as a supporting tool is presented. The performed investigations allowed to develop an algorithm dedicated to the parameters identification of models with the application of sensitivity analysis methods described in the work. The algorithm was implemented and all the calculations of identification problems presented in the work were computed with the designed software. The monograph ends with conclusions which summarize the work achievements and which prove the formulated thesis that it is possible to effectively solve ill-posed identification problems of metal forming with the developed application of identification strategy algorithm, based on sensitivity analysis methods coupled with optimization procedures.

DANUTA SZELIGA

Zagadnienie identyfikacji parametrów modeli procesów przeróbki plastycznej w ujęciu kompletnym

Streszczenie

W pracy przedstawiono zagadnienie identyfikacji parametrów modeli wykorzystywanych w modelowaniu procesów przeróbki plastycznej metali. Główną tezę pracy jest stwierdzenie, że możliwe jest otrzymanie *optymalnych* rozwiązań dla źle uwarunkowanych problemów identyfikacji z wykorzystaniem metod analizy wrażliwości połączonych z procedurami optymalizacyjnymi. Tezę udowodniono realizując cele postawione w pracy oraz stosując opracowane metody do rozwiązania praktycznych zagadnień identyfikacji parametrów modeli procesów przeróbki plastycznej. Zagadnienia identyfikacji parametrów modeli są zadaniami odwrotnymi. Dla zadań tych poszukuje się rozwiązań przekształcając problem odwrotny w zadanie optymalizacji i poszukując jego minimum. Zadania te są źle uwarunkowane, dlatego podstawowym celem pracy było opracowanie metody opartej na algorytmach analizy wrażliwości, które w połączeniu z procedurami optymalizacji stanowią wydajne narzędzie do rozwiązywania zagadnień odwrotnych i pozwalają na otrzymywanie rozwiązań wystarczająco bliskich rozwiązaniu dokładnego.

Praca zawiera również zastosowanie algorytmów analizy wrażliwości do obniżenia kosztów obliczeniowych problemów identyfikacji, co było jej kolejnym celem. Przedstawiono metody redukcji wymiaru przestrzeni zmiennych decyzyjnych procesu optymalizacji wykorzystujące algorytmy analizy wrażliwości do identyfikacji parametrów modeli mających największy wpływ na wyjście modelu. Zagadnienie to jest szczególnie istotne dla problemów rozwiązywanych w przeróbce plastycznej jako zadań kosztownych obliczeniowo, formułowanych jako różniczkowe zadania niestacjonarne i rozwiązywanych z wykorzystaniem metody elementów skończonych, często z *hp*-adaptacją dla otrzymania rozwiązań wystarczająco dokładnych. Dodatkowo zastosowanie algorytmów analizy wrażliwości pozwoliło na zawężenie przedziałów zmienności poszczególnych parametrów.

Ponadto w ramach pracy zaprezentowano i zastosowano algorytmy analizy wrażliwości jako wstępny krok optymalizacji dla ograniczenia bądź poszerzenia przestrzeni

poszukiwań parametrów, do generowania punktu początkowego dla zadania optymalizacji oraz dla badania zachowania się funkcjonału w optymalizacji. W pracy przedstawiono również wykorzystanie analizy wrażliwości w hybrydowych metodach optymalizacji, takich jak kombinacja niedeterministycznych metod optymalizacji z algorytmami analizy wrażliwości dla przeszukiwania obszarów minimów lokalnych.

Teza pracy została udowodniona poprzez przedstawienie rozwiązań praktycznych zagadnień identyfikacji modelowania problemów przeróbki plastycznej metali. Rozwiązano następujące problemy: zadanie identyfikacji mechanicznych warunków brzegowych (współczynnik tarcia), zadanie identyfikacji parametrów równań reologicznych, zadanie identyfikacji parametrów kryterium pęknięcia, zadanie identyfikacji parametrów w modelu wieloskalowym, zadanie identyfikacji parametrów równań opisujących przemiany fazowe oraz zadanie identyfikacji parametrów kontrolujących cykl produkcyjny. Wszystkie wymienione zagadnienia zostały rozwiązane z wykorzystaniem opracowanego autorskiego oprogramowania.

W pierwszej części monografii przedstawiono aktualny stan zagadnień związanych z problemami identyfikacji przeróbki plastycznej metali. Zostały wymienione zarówno dotychczasowe osiągnięcia, jak i słabe strony rozwiązań z punktu widzenia rozważań teoretycznych. Wnioski z tej części pozwoliły na sformułowanie tezy pracy. Następnie zostały przedstawione różniczkowe równania równowagi, które stosowane są w rozwiązywaniu zagadnień przeróbki plastycznej wraz ze sformulowaniem zadań odwrotnych dla tych równań. Matematyczne podstawy operatorów odwrotnych oraz próba zastosowania formalizmu matematycznego do konstrukcji operatora odwrotnego dla zadań przeróbki plastycznej stanowiły tematykę dalszej części pracy. W pracy przedstawiono algorytm analizy wrażliwości jako narzędzia wspomagającego rozwiązywanie zadań identyfikacji (zadań odwrotnych). Przeprowadzone badania pozwoliły na realizację głównego celu pracy, jakim było opracowanie algorytmu strategii identyfikacji. Zaprojektowany algorytm został opisany oraz zaimplementowany, a wszystkie przedstawione w pracy obliczenia wykonano z jego użyciem. Monografię kończą wnioski podsumowujące osiągnięcia, które udowodniają sformułowaną w pracy tezę, że możliwe jest efektywne rozwiązywanie źle uwarunkowanych zadań identyfikacji przeróbki plastycznej metali z wykorzystaniem opracowanego w pracy algorytmu strategii identyfikacji łączącego metody analizy wrażliwości i procedury optymalizacji.

The list of main symbols

In the identification procedure

α	regularization parameter
$\mathcal{D}(K)$	domain of the mapping K
δ	perturbation, $\delta > 0$
$\dim X$	dimension of the X space
$\tilde{\eta}_i^2$	estimated correlation ratio of the x_i parameter (the variance based method)
K	mapping between the Hilbert spaces: $K : X \rightarrow Y$
$\tilde{\mu}$	normalized mean (the Morris design procedure)
N	number of the measurements/calculated points in the experiment
$\mathcal{N}(K)$	kernel of the mapping K
Φ	functional of the optimization problem
\mathbb{R}	the set of real numbers
$\mathcal{R}(K)$	image (range) of the mapping K
R_α	regularization strategy
\mathbf{S}	sensitivity matrix
$\hat{\mathbf{S}}$	normalized sensitivity matrix
S_i	Sobol' index for the x_i parameter
$\tilde{\sigma}$	normalized standard deviation (the Morris design procedure)
w	weighted coefficient
\mathbf{x}	vector of the identified quantities: inputs and/or parameters
X, Y	Hilbert spaces
x, y	elements of the Hilbert spaces, $x \in X, y \in Y$
$\mathbf{x}^{(i)}$	vector \mathbf{x} in the i^{th} iteration
\mathbf{x}^i	i^{th} vector

X^\perp	orthogonal complement of X
\mathbf{x}^*	solution of the optimization problem
x_i	i^{th} component of the vector \mathbf{x}
ξ_i	elementary effect of the x_i parameter (the Morris design procedure)
\mathbf{y}	vector of the model outputs
\mathbf{y}^δ	measured/perturbed vector \mathbf{y}
y_i	i^{th} component of the vector \mathbf{y}

In modeling of metal forming processes

d	inner/outer diameter of the ring; diameter of the cylindrical sample
ε	strain
$\dot{\varepsilon}$	strain rate
$\dot{\boldsymbol{\varepsilon}}$	tensor of the strain rate
$\underline{\dot{\varepsilon}}_i$	effective strain
F	load calculated with the model
\tilde{F}	load measured in the experiment
h	height of the sample
m_c	friction factor in the Tresca friction model
m_c	friction coefficient in the Chen-Kobayashi friction model
$\boldsymbol{\sigma}$	the Cauchy stress tensor
$\underline{\sigma}_i$	effective stress
σ_p	flow stress
\hat{T}	temperature, in °C
T	temperature, in K
t	time
τ	shear stress
\mathbf{u}	velocity vector
\mathbf{x}	material point coordinates

1 State of the art in inverse analysis of metal forming

Numerical modeling of metal forming processes is commonly used to aid the design of new technologies, to design materials of new properties and to study in details the phenomena occurring in the analyzed processes. The accuracy of modeling depends, except proper, mathematical description of physical phenomena and an analytical or numerical solver, on correctly, in terms of quantity, defined boundary and initial conditions and constitutive relations. In this work, the problem of determining both constitutive relations and boundary or initial conditions is considered and the identification problem is equivalent to the estimation of parameters of these equations.

The problem of parameter estimation has been investigated by many researchers and there are a lot of papers related to this subject area. In the chapter, an overview of selected identification problems and methods of their solutions is provided. The investigations are grouped into the following classes:

- estimation of material properties,
- determination of thermal or mechanical initial/boundary conditions,
- initial shape finding,
- mix-problems.

Problems of the first two classes, which are directly related to the work subject area, are discussed further in the chapter.

Estimation of material properties. Determination of plastic properties of the material is performed based on the results of plastometric tests: compression (axisymmetric or plane strain), tension or torsion. During the test, loads in the function of displacements are measured and this data set is an input for the parameter estimation. The experiments are carried out for various strain rates and temperatures, according to the assumed function which defines the flow stress σ_p . The flow stress σ_p is approximated with various functions of parameters gathered in vector \mathbf{x} , designed in an empirical way. The basic function of the flow stress σ_p is the relation of strain ε and strain rate $\dot{\varepsilon}$:

$$\sigma_p = f(\varepsilon, \dot{\varepsilon}, \mathbf{x}) \quad (1.1)$$

for processes performed in the room temperature. For hot forming processes, the relation (1.1) is extended for temperature T of the process:

$$\sigma_p = f(\varepsilon, \dot{\varepsilon}, \mathbf{x}, T) \quad (1.2)$$

While the deformation process depends on its history, e.g. the strain rate is changed during the process, the flow stress is also a function of internal variables of the material:

$$\sigma_p = f(\varepsilon, \dot{\varepsilon}, \mathbf{x}, T, \mathbf{x}^{in}) \quad (1.3)$$

where \mathbf{x}^{in} is a vector of internal variables, e.g. dislocation density.

The estimation of the flow stress function parameters has been investigated by many researchers. Selected papers are presented below. In all of them, the problem of parameter determination was transformed to the following, equivalent task: find vector \mathbf{x}^* of the estimated parameters such that

$$\mathbf{x}^* = \min_{\mathbf{x}} \Phi(\mathbf{x}) \quad (1.4)$$

where the functional Φ is defined as

$$\Phi(\mathbf{x}) = \sum_{i=1}^N w_i^\sigma [\tilde{\sigma}_i - \sigma_i(\mathbf{x})]^2 \quad (1.5)$$

or

$$\Phi(\mathbf{x}) = \sum_{i=1}^N w_i^F [\tilde{F}_i - F_i(\mathbf{x})]^2 \quad (1.6)$$

where $\tilde{\sigma}_i$ is the *experimental* stress, calculated as the ratio of the load \tilde{F}_i to the surface between the tool and the sample with regard to the constant volume condition, $\sigma_i(\mathbf{x})$ is the flow stress calculated based on one of Equations (1.1)-(1.3), \tilde{F}_i is the load measured in the plastometric test, which is dedicated to an experiment to determine the material flow stress, $F_i(\mathbf{x})$ is the load calculated with the numerical model of the plastometric test that includes one of the flow stress equations (1.1)-(1.3), w_i^σ , w_i^F are weighted coefficients, N is the number of measurements in all the performed tests. The task (1.4) is called *inverse* problem, while the *direct* problem is to estimate flow stress σ_p given by one of Equations (1.1)-(1.3) and known equation parameters.

The minimization problem (1.4) with the functional (1.5) requires to solve the optimization problem of the system of equations. If this system is linear with respect to parameters \mathbf{x} , minimization of (1.4) provides exactly one minimum - a unique solution of the identification problem. However, in most cases, the problem (1.5) is not linear with respect to \mathbf{x} and the functional (1.5) has many local minima. Therefore, as the minimization result, not one value \mathbf{x}^* is obtained but the vector of solutions $[\mathbf{x}_i^*]_{i \in I}$ is determined, such that for each component \mathbf{x}_i^* Equation (1.4) is fulfilled, i.e. $\Phi(\mathbf{x}_i^*) \leq \delta \forall i \in I$, where δ is a small value.

Another disadvantage of the functional (1.5) minimization is that it does not take into account disturbances occurring in plastometric tests: nonuniform stress and strain field, nonuniform temperature field, heat generated due to friction and due to deformation. Following that, the functional (1.6) with loads, calculated based on the numerical model of the plastometric test, is applied. Plastometric tests are thermomechanical deformation processes defined by partial differential equations

(a detailed description of the thermomechanical model is provided in Chapter 3, section 3.2). It means that the loads in the functional (1.6) are computed by solving these equations. The most commonly used numerical algorithm to solve thermomechanical equilibrium equations is the finite element method ([147]).

The first papers on the inverse approach in the identification of material parameters are the works [31, 26, 27, 28] where the identification was performed for the thermoviscoplastic model of the plastometric test. The direct problem was simulated with commercial code Forge, initially for the 2D problem and next extended to the 3D problem, to include material anisotropy. Due to time costs of direct calculations, the gradient optimization algorithm with semi-analytical computations of differential coefficients was applied to reduce those costs. In the paper [45], a similar approach was used, the optimization problem was solved with different gradient optimization procedures to compare their efficiency and robustness. It should be emphasized that the application of the gradient optimization methods excludes the existence of many minima: the methods determine the closest local minimum.

The problem of the identification of rheological parameters based on the axisymmetrical plastometric test results was the subject of the author's PhD thesis [133] and next continued for other experiments [120, 118], tested for various materials [79, 114] and developed for a wide class of rheological models [116, 96]. The experiments were modeled as a rigid-plastic thermomechanical problem. As distinct from the works quoted above, the optimization was performed, first of all, with deterministic, non gradient procedures. The selection of a starting point for calculations is crucial for these algorithms, which was investigated in [122]. The results of that part of the work were summarized and a computer program dedicated to the identification of rheological parameters was developed and described in [48]. Another approach, the application of a two-criterion optimization to increase the robustness of inverse calculations, was studied in [30]. The investigations were continued and genetic algorithms were applied. Stochastic methods do not restrict the number of solutions but the computational costs increase due to the population size. To avoid the problem of a time-consuming direct problem solver, alternative methods in which a finite element solver of the direct problem was replaced with a metamodel of the process, were developed. Hence, stochastic optimization procedures were applied with no constraints to the population size and the number of the solver evaluations. Metamodels based on the approximation based technique are presented in [54, 127]. Neural networks applied to the optimization problem of material processing are provided in [148], the same approach used to the identification of metal flow stress is described in [129, 131]. The application of neural networks to the identification of material properties based on the industrial process results is presented in [130]. The summary of the current work on inverse computation is provided in [56]. One should remember that such an approach is computationally effective but the problem of selecting one, *the best* solution, still remains open.

Other identification tasks, dedicated to the estimation of material parameters in the extrusion process, are presented in [150, 151, 152].

Mechanical boundary conditions. For numerical modeling of metal forming processes, the estimation of friction between a deformed material and a tool is as essential as the determination of the material properties. Following that experimental investigations and the numerical interpretation of the results of mechanical boundary conditions are performed. One of the most commonly used method to estimate friction coefficient is the ring compression test [3]. In the test, according to the original procedure, the inner diameters of a deformed ring are measured along its height. The next averaged length of the inner diameter is compared to calibration curves and the friction coefficient value is read from the chart. More precise predictions of friction coefficients are obtained while the ring compression is modeled with the finite element method applied to thermomechanical equations which define this process, and numerical predictions of the ring shape after compression are compared to the shape obtained in the experiment [133]. In this approach, not only the information on the inner shape of the ring, but the information on the outer shape is considered, as well. Thus, the friction identification problem is defined by Equation (1.4) and the functional Φ is expressed as:

$$\Phi(\mathbf{x}) = \sum_{i=1}^N w_i^d [\tilde{d}_i - d_i(\mathbf{x})]^2 \quad (1.7)$$

where \mathbf{x} is an one dimensional vector, i.e. a scalar which represents the friction coefficient, \tilde{d} , d are the inner/outer diameters of the ring after the compression measured and calculated along the height of the ring, respectively, w_i^d are weighted coefficients, N is the number of measurements along the ring height. The investigations of the identification of the friction coefficient based on this test are presented in [115, 136, 29]. A similar procedure, but for the extrusion process, is provided in [149].

Thermal boundary/initial conditions. A wide group of the metal forming processes are hot forming processes. Hence, determination of thermal boundary and initial conditions is crucial to perform a proper and accurate process analysis. Temperature measurements are carried out with thermocouples located in the selected area of the deformed material, tool or ambient. These measurements are compared to temperature predictions calculated with the process model. Thermal problems are described with heat transport differential equation. Precise evaluation of the temperature distribution during the process is possible, while the finite/boundary element method or the finite difference algorithm is applied to solve this equation. Following that, for the identification task (1.4) the functional Φ is defined as:

$$\Phi(\mathbf{x}) = \sum_{i=1}^N w_i^T [\tilde{T}_i - T_i(\mathbf{x})]^2 \quad (1.8)$$

where \mathbf{x} is the vector of boundary or initial condition parameters, \tilde{T} is the temperature measured in the process, T is the temperature calculated with the numerical model of the process, w_i^T are weighted coefficients, N is the number of measurements.

There are a lot of papers on the identification of thermal parameters for various processes, selected examples are referred to here. In the works [137, 138], the problem of the estimation of thermal conductivity of steels was described, the papers [13, 33] present the problem of the determination of the heat transfer coefficient and in the work [11] both of these problems are discussed. In turn, the identification of thermal parameters for solidification problems are presented in [70, 72].

The existence, uniqueness and stability of a solution is not widely discussed in the cited references although their authors were aware of these problems. Presented identification problems were transformed to the optimization problem (1.4) with a functional including information on the measured and calculated quantities and the optimization objective was to find a minimum of the functional (1.4) with respect to the identified parameters. In most cases, the problem was described with partial differential equations and equilibrium equations were solved with numerical methods. The question is why those problems were transformed to the optimization task, whether the selected minimum is the solution to the original identification problem, whether this is the only procedure to solve these problems and whether it is possible to construct the inverse operator to identify the parameters directly from the equations describing the problem. The answers to these questions are provided in Chapter 3 but now let us consider the general identification problem for differential operators and the problem solution stability, which are presented below.

The identification problems are expressed, in terms of the functional analysis, with the following form:

$$\Phi(x) = \|Kx - y^\delta\|_Y^2 \quad (1.9)$$

where $K : X \rightarrow Y$ is the mapping (e.g. model), such that $Kx = y$, X, Y are Hilbert spaces, y^δ is the measured data. Posedness of the problem depends on the properties of mapping K and the norm in space Y . If the mapping K is a differential operator, the inverse problem is always ill-posed (the formal definition is provided in Chapter 3, section 3.3). To explain the ill-posedness, the following problem [21] is presented: let f be any function such that $f \in C^1[0, 1]$, $\delta \in (0, 1)$, $n \in \mathcal{N}$, $n \geq 2$ are selected arbitrarily. Let us define:

$$f_n^\delta(x) := f(x) + \delta \sin \frac{nx}{\delta}, \quad x \in [0, 1] \quad (1.10)$$

Let us differentiate the function f with respect to x :

$$(f_n^\delta)'(x) := f'(x) + n \cos \frac{nx}{\delta}, \quad x \in [0, 1] \quad (1.11)$$

and estimate the error in the uniform norm:

$$\|f - f_n^\delta\|_\infty = \delta \quad (1.12)$$

but:

$$\left\| f' - (f_n^\delta)' \right\|_\infty = n \quad (1.13)$$

The functions f and f_n^δ can be considered as the exact and perturbed data, respectively. Then, for arbitrarily small error δ , the error in the result - the derivative, can

be arbitrarily large, equal n . Hence, the derivative does not depend continuously on the data for the uniform norm. Continuing, f' solves the simple integral equation of the first kind:

$$(Kx)(s) := \int_0^s x(t) dt = f(s) - f(0) \quad (1.14)$$

which is solvable in $C[0, 1]$ only if $f \in C^1[0, 1]$. The corresponding *direct* problem is to compute f from x , namely to integrate. Note that integration is a stable process on $C[0, 1]$ and a smoothing process, i.e. high errors in x expressed by (1.13) are damped out to $\delta \sin(nx/\delta)$ (see (1.12)) and have a very small effect on the data for the *inverse* problem. Thus, whenever a direct problem has smoothing properties it has to be expected that oscillations appear which come from the small data perturbation in the solution of the inverse problem. The question is whether it is possible to differentiate a function in spite of these problems. The answer is positive if data errors are able to be excluded. It can be done for the known bound of f'' . In this example, such a bound can be expressed as a bound for n in terms of δ . In terms of the functional analysis, the problem is described as follows: if the operator K , given by (1.14), is considered on $C[0, 1]$, then it is a continuous linear injective operator whose inverse operator, defined on $C^1[0, 1]$, considered as a subspace of $C[0, 1]$, is unbounded. However, if K is restricted to the set $\{x \in C^1[0, 1] : \|x\|_\infty + \|x''\|_\infty \leq \gamma\}$, then the inverse of this operator is continuous on its domain, i.e. it is possible to "restore stability" by assuming an a-priori bound for f' and f'' . The methods which allow to keep the problem are called regularization methods. They are discussed in Chapter 3.

The uniqueness of the identification problem solution is the next crucial problem. If the problem has more than one solution, the standard procedure is to bound the parameters domain. For complex problems which include many empirical parameters, the bounding operation is not a trivial task and this problem has to be solved with other methods. One of the approaches is to keep the original domain and to use stochastic optimization algorithms to obtain a set of solutions instead of a global one. The *best* solution is selected arbitrarily by an expert. Such a procedure was applied in some references on the material parameters identification, but it was also successfully applied to other problems, see, e.g. the paper [9] on the shape optimization of bodies by heat exchanging, the works [7, 98] on the optimization of material structures, the investigations on the identification of voids in a microstructure in [53] or the identification of the parameters of microscale heat transfer in [12] and the paper [69] on the inverse problem of solidification.

Another solution is to use sensitivity analysis algorithms as a supporting tool for the identification problem. *Local* sensitivity analysis procedures, calculating Jacobian, have been just applied to solve various tasks, e.g. for non-linear mechanical problems [44, 109, 108] or for thermal problems [68, 67, 71]. However, there are other sensitivity algorithms, called *global* procedures, which allow to estimate the global impact of the parameters to model outputs. Both groups of methods, the local and the global ones, are helpful to reduce the number of solutions, to estimate the quality

of the solutions, to select the most important model parameters and to eliminate parameters which do not affect the model. The sensitivity analysis methods, the local and the global ones, are the subject of this work, and they are applied to support identification problems in metal forming.

Two problems: stability and uniqueness, are essential for the proper solution of the identification inverse problems. They are discussed in the work in terms of the functional analysis. To date, identification tasks in metal forming have been transformed to the optimization problems defined by (1.4) and, only in a few investigations, the results were validated. In this work, the problem of solution regularity is considered. The sensitivity analysis methods have been developed and applied to validate new models introduced to the solver, to determine the accuracy of the parameter estimation, and to verify the robustness of inverse calculations.

2 The thesis and the structure of the book

2.1 The thesis and the objectives of the work

The main thesis of this work is expressed as follows:

It is possible to obtain an optimal solution for ill-posed inverse problems of identification with the application of sensitivity analysis methods combined with the optimization procedures. Sensitivity analysis decreases the computational costs of the identification and increases reliability of the solution.

The primary objective of the work is to develop a method which will allow for the identification of model parameters used in numerical simulations of the metal forming processes. Numerical models of metal forming processes are complex, they include several equations, at least the mechanical model of continuum and the heat transfer equation. Thus, the problem of identification is an ill-posed inverse problem. Available regularization algorithms do not support such a complex model and the problem of identification becomes a hard one. It is expected that the development of the sensitivity analysis procedures derived from the original sensitivity methods and the design of the identification strategy algorithm will enable to solve identification problems in metal forming and to obtain results close enough to the optimal ones.

The next objective of the work is to decrease computational costs of the identification. Due to a non-stationary nature of the problem and due to solvers, based on the finite element method with *hp*-adaptation for high quality of the solution, numerical models of the metal forming processes are computationally expensive. The identification task requires to run the solver many times, particularly if the number of parameters to be identified is large. Therefore, a supporting tool for the reduction of the number of solver evaluations is of the interest. This tool is based on sensitivity analysis which indicates the parameters of high importance and these parameters are decision variables in the optimization task. The computational cost is lower because of reducing the space dimension of decision variables. Another advantage of the application of sensitivity analysis is that the number of possible solutions is constraint.

The results of sensitivity analysis can be applied as a preliminary step of optimization to bound or extend the parameters domain, generate starting points for optimization or to investigate the behavior of the functional defined in optimization.

Another application of sensitivity analysis is to develop hybrid optimization procedures, such as a combination of nondeterministic optimization methods and the local sensitivity analysis algorithms for exploring local minima.

Practical results of the work is the application of sensitivity analysis combined with the inverse solver. The following problems were solved in the work: identification of mechanical boundary condition (friction coefficient), identification of parameters of rheological models, parameters of the phase transformation model, identification of control parameters of the production cycle. All the listed problems were solved with the developed software.

2.2 The structure of the book

The monograph consists of seven chapters and, in addition, one appendix. The presentation starts in Chapter 1 with state of the art of identification problems investigated in metal forming. Most of these problems are transformed to optimization tasks with a wide range of the optimization methods applied; however, there is weak justification of the properties of the obtained results, particularly in terms of the mathematical background. Another group of problems discussed in this chapter are applications of sensitivity analysis. To date, sensitivity analysis in metal forming has been understood as calculations of partial derivatives and sensitivity matrix in numerical methods of solving partial differential equations. The application of the global sensitivity methods has not been investigated. At the end of this chapter, up to date achievements are summarized and the weaknesses of theoretical research are focused on. The conclusions from Chapter 1 were basis to formulate the thesis and the contents of the work, presented in Chapter 2.

Chapter 2, section 2.1 includes the main thesis of the work as well as the objectives of the work and the list of problems solved with the identification strategy algorithm developed in the work. This section 2.2 provides a brief overview of the book.

Chapter 3 provides general equilibrium equations used in the modeling of metal forming processes and formulates inverse problems for these equations. The mathematical background of inverse operators and an attempt to apply mathematical formalism to construct the inverse operator for these equations is included.

Chapter 4 provides a description of sensitivity analysis methods and the ability to apply sensitivity analysis algorithms to inverse calculations as a supporting tool. The application of sensitivity methods to direct problems are included in the chapter, as well. A description of local sensitivity procedures with the algorithm of semi-analytical derivative computation and the application of accelerated nondeterministic optimization method is presented. In the second part of the chapter, global sensitivity procedures for the estimation of the parameters importance are provided.

Chapter 5 presents a developed algorithm dedicated to the parameters identification of models with the application of the sensitivity analysis methods described in Chapter 4. In the identification strategy algorithm the inverse problem is solved with the mathematical background provided in Chapter 3 to construct an inverse operator and sensitivity methods presented in Chapter 4 applied to the direct problem and

to functional defined in the optimization task. The developed algorithm was implemented and all the calculations of identification problems included in Chapter 6 were performed with the designed software.

In Chapter 6 solutions of various inverse problems of metal forming, including identification of material models, boundary conditions and a design of the production cycle, are discussed. The problems were solved with the identification strategy algorithm developed in the work (see: Chapter 5).

The book ends with Chapter 7 which is a synthesis of the work achievements. This chapter outlines the directions for future research, as well. The conclusions are followed by Appendix which includes some definitions of the functional analysis helpful in understanding Chapter 3.

3 Inverse problems.

The mathematical background

The problems of identification presented in Chapter 1 clearly show that the inverse problems solved in metal forming did not have good mathematical background and any statement of uniqueness, quality of the solution or convergence and stability of the applied algorithm could not be made. Therefore, the theoretical and mathematical background of inverse problems were investigated to verify whether there are well-established mathematical methods which allow to solve inverse problems in metal forming. This chapter is dedicated to the mathematical formalism of inverse operators.

Physical phenomena in metal forming processes are described by differential, phenomenological/empirical equations or are a combination of those two equation types. To analyze the process, a series of physical experiments and mathematical calculations are performed. Nowadays, mathematical modeling supported with physical experiments are a powerful tool to understand the processes run. The processes modeling is being performed in the following steps:

- identification of physical phenomena and the selection of physical laws,
- mathematical description of the physical model,
- calculation model; a selection of the solution: analytical or numerical; if the numerical method is applied: a selection of the method including the estimation of the approximation error,
- identification of the material properties, initial and boundary conditions; the estimation of the error/sensitivity of the model output with respect to the material and initial/boundary parameters,
- model runs/performing calculations; an analysis of the results.

In these investigations, the problem of the material characteristics and the accuracy of initial/boundary properties is considered. The assumption is made that the physical phenomena, the mathematical description and the solution method are well assigned.

3.1 Modeling of metal forming processes

Two phenomena are considered in modeling of metal forming processes in the basic form: mechanical equilibrium of state and heat transport. Both phenomena are described by differential equations with boundary and/or initial conditions.

Mechanical equilibrium. Let the body concerned be defined in subset $\Omega \subset \mathbb{R}^n$ with boundary $\Gamma = \partial\Omega$. Equilibrium equation (total momentum equal zero) is expressed as [24, 80]:

$$\operatorname{div}(\boldsymbol{\sigma}) = \nabla \cdot \boldsymbol{\sigma} = 0 \quad (3.1)$$

where $\boldsymbol{\sigma}$ is the Cauchy stress tensor, dependent on the velocity field $\mathbf{u} \in \mathbf{V}$ and \mathbf{V} is a function space where the solution is determined. On boundary Γ , the following conditions are defined:

$$\mathbf{u} = \mathbf{u}_0 \quad \text{on } \Gamma_D \quad (3.2)$$

$$\mathbf{n} \cdot \boldsymbol{\sigma} = \boldsymbol{\tau} \quad \text{on } \Gamma_N \quad (3.3)$$

where \mathbf{u}_0 is the assumed velocity field on the boundary Γ_D , $\boldsymbol{\tau}$ is the load acting on the body applied to the boundary Γ_N (the unit is load on boundary Γ_N unit), \mathbf{n} is the unit vector normal to the boundary Γ oriented outside, and $\Gamma_D \cup \Gamma_N = \Gamma$, $\Gamma_D \cap \Gamma_N = \emptyset$. The assumption is made that during deformation the volume of the body is constant, i.e. elastic strains are very small compared to plastic strains [36]. The tensor of strain rate is defined as a symmetric part of the velocity gradient tensor $\nabla \mathbf{u}$:

$$\dot{\boldsymbol{\varepsilon}} = \frac{1}{2} (\nabla \mathbf{u} + \nabla^T \mathbf{u}) \quad \text{or} \quad \varepsilon_{ij} = \frac{1}{2} \left(\frac{\partial u_i}{\partial x_j} + \frac{\partial u_j}{\partial x_i} \right) \quad (3.4)$$

Incompressibility of the body is equivalent to the volume strain rate being a zero:

$$\dot{\boldsymbol{\varepsilon}}_V(\mathbf{u}) = \dot{\boldsymbol{\varepsilon}}_{ii}(\mathbf{u}) = 0 \quad \text{or} \quad \operatorname{tr}(\dot{\boldsymbol{\varepsilon}}) = \operatorname{div}(\mathbf{u}) = \nabla \cdot \mathbf{u} = 0 \quad (3.5)$$

and it restricts the velocity space \mathbf{V} . Equations (3.1)-(3.5) define the problem of plastic deformation of a body with incompressibility.

In the flow theory of plasticity, the strain rates $\dot{\boldsymbol{\varepsilon}}$ are related to stresses $\boldsymbol{\sigma}$ by the Levy-Mises flow rule:

$$\boldsymbol{\sigma} = \frac{2}{3} \frac{\underline{\sigma}_i}{\underline{\dot{\varepsilon}}_i} \dot{\boldsymbol{\varepsilon}} \quad (3.6)$$

where $\underline{\sigma}_i$ is the effective stress and $\underline{\dot{\varepsilon}}_i$ is the effective strain rate. According to the Huber-Mises yield criterion, the effective stress $\underline{\sigma}_i$ is equal to the flow stress σ_p which characterizes plastic material properties and is a phenomenological function of strain ε , the strain rate $\dot{\varepsilon}$ and/or temperature T : $\sigma_p = f(\varepsilon, \dot{\varepsilon}, T)$.

In the considered deformation problem, there is friction between the deformed body and the tool. Two basic models, and the modifications derived from them, are applied:

- The classic Coulomb model for static friction. In tensor form the friction is expressed as:

$$\boldsymbol{\tau} = \mu \sigma_N \frac{\mathbf{u}_s}{|\mathbf{u}_s|} \quad (3.7)$$

where $\boldsymbol{\tau}$ is the shear stress, μ is the friction coefficient, σ_N is the normal stress (caused by tool stress) and \mathbf{u}_s is the slip velocity of the body in relation to tool.

- The Tresca model which assumes that friction stress τ is the function of shear strength of the material:

$$\boldsymbol{\tau} = m\tau_{max} \frac{\mathbf{u}_s}{|\mathbf{u}_s|} \quad (3.8)$$

where m is called the friction factor, and τ_{max} yields stress in shear equals $\tau_{max} = \sigma_p/\sqrt{3}$ according to Huber-Mises yield criterion.

- The Chen-Kobayashi friction model [14] of the form:

$$\boldsymbol{\tau} = -m_c\sigma_p \left[\frac{2}{\pi} \arctan \left(\frac{\mathbf{u}_s}{a} \right) \right] \quad (3.9)$$

where a is a constant, few order smaller than an average slip velocity. If the slip velocity \mathbf{u}_s is large, the formula (3.9) is equivalent to the Tresca's friction law (3.8) and $m = \sqrt{3}m_c$.

Heat transport equation. Primary heat transport equation is defined as [62, 145]:

$$\nabla \cdot (k\nabla T) + \dot{Q} = \rho c_p \frac{\partial T}{\partial t} \quad (3.10)$$

where t is time, $T = T(\mathbf{x}, t)$ is the temperature distribution, k is the conductivity, ρ is the material density, c_p is the specific heat, \dot{Q} is the density of inner heat source energy (the rate of heat generation due to deformation work). The following convection boundary condition is applied:

$$k(\mathbf{n} \cdot \nabla) T = \dot{q} + \alpha(T_o - T) \quad (3.11)$$

where α is the heat transfer coefficient, T_o is ambient or tool temperature, \dot{q} is the heat flux due to friction on the boundary Γ .

The initial condition is expressed as:

$$T(\mathbf{x}, 0) = T_0(\mathbf{x}) \quad (3.12)$$

where T_0 is the initial temperature distribution at time $t = 0$.

Quantities \dot{Q} and \dot{q} describe heat generated due to plastic deformation and heat generated due to friction between the material and the tool, respectively. Following [36, 46, 95, 145], they are defined as:

$$\begin{aligned} \dot{Q} &= \nu \int_{\Omega} \sigma_p \dot{\underline{\epsilon}}_i d\Omega & \nu \in [0.9, 1] \\ \dot{q} &= \int_{\Gamma} m_c \sigma_p |\mathbf{u}_s| d\Gamma \end{aligned} \quad (3.13)$$

Equations (3.1)-(3.13) define a thermomechanical problem of deformation for rigid-plastic material. The problem is quasi-stationary, i.e. in every time step the problem is solved as a stationary problem which satisfies the equilibrium condition. The results of the solution in time t are input data for the next time step $t + 1$. The solution is obtained with the finite element method. A detailed description of the rigid-plastic approach coupled with the solution of the heat transport equation is presented in [46, 61].

3.2 Inverse problems for the thermomechanical deformation problem

A *direct problem* for the thermomechanical problem described by Equations (3.1)-(3.13) is defined as

- for boundary conditions given by Equations (3.2) and (3.3) with the known parameters of friction model (3.7), (3.8) or (3.9), known constitutive relation (3.6), particularly the function of flow stress σ_p , and all the parameters included in the heat transport equations (3.10)-(3.11) to determine velocity field \mathbf{u} , temperature field $T(\mathbf{x})$, and the next displacement field, strain-stress distribution.

Inverse problems for the thermomechanical problem (3.1)-(3.13) are as follows:

- for known velocity field \mathbf{u} to determine mechanical boundary conditions, i.e. friction coefficient in Equation (3.7), (3.8) or (3.9),
- for known velocity field \mathbf{u} to determine parameters of the flow stress function σ_p in constitutive relation (3.6),
- for known temperature field $T(\mathbf{x})$ to determine the initial temperature field $T_0(\mathbf{x})$,
- for known temperature field $T(\mathbf{x})$ to determine parameters of thermal boundary conditions (3.11).

To solve the inverse problems listed above, the inverse operator should be designed for the determination of input data or process parameters. The question is whether it is possible to construct an inverse operator. Therefore, in section 3.3, mathematical background of inverse operators is presented.

3.3 General formulation of the inverse problem

Mathematical formulation of the material properties or initial/boundary conditions estimation is called an inverse problem. To analyze and solve that problem it is convenient to apply functional analysis.

Let $K : X \rightarrow Y$ be a mapping between two normed spaces X and Y :

$$Kx = y \quad x \in X, y \in Y \quad (3.14)$$

The mapping K describes a process under study. For the operator K two problems can be defined:

- *a direct problem*: for known x , evaluate Kx ,
- *an inverse problem*: for known y , solve the equation $Kx = y$ for x .

In particular the mapping K can be a linear differential equation of the generalized form:

$$Kx = y \quad \text{where} \quad Kx = \sum_{|\alpha| \leq n} A_\alpha(x) D^\alpha x \quad (3.15)$$

where A_α and y are the functions defined on $\Omega \subset \mathbb{R}^n$, function x defined as $x : \Omega \rightarrow \mathbb{R}$, multi-index α is n -tuple such that $\alpha = (\alpha_1, \dots, \alpha_n) \in \mathbb{N}_0^n$ and $|\alpha| = \alpha_1 + \alpha_2 + \dots + \alpha_n$, $D^\alpha = \partial_1^{\alpha_1} \partial_2^{\alpha_2} \dots \partial_n^{\alpha_n}$ where $\partial_i^{\alpha_i} = \frac{\partial^{\alpha_i}}{\partial x_i^{\alpha_i}}$.

If the analyzed phenomena are described with Equation (3.15), two classes of inverse problems are distinguished:

- a reconstruction problem: determination of initial condition x_0 ,
- an identification problem: estimation of quantities characterizing material properties - determination of functions $A_\alpha(x)$.

To solve a physical problem, its mathematical model must be well-posed, which means that a solution to the problem exists, it is unique and it continuously depends on the data (the stability property). If the solution does not exist, the solution space must be extended. If there is more than one solution, additional, more restriction conditions must be included in the model. The property of the continuous dependence on the data is the most important one. If it is not held, any calculations cannot be performed due to uncontrolled disturbances. It is not possible to determine the right problem estimation if the answer to the question whether the obtained results are the solution or a noise is not known. To eliminate the lack of stability, more information about the solution is needed. The formal definition of a well-posed problem was proposed by Hadamard [34]:

Definition 3.3.1 (Well-posed problems). *Let $K : X \rightarrow Y$ be a mapping between normed spaces X and Y . The equation $Kx = y$ is well-posed (properly-posed) if the following properties are held:*

1. *Existence. For every $y \in Y$ there is, at least one, $x \in X$ such that $Kx = y$:
 $\forall y \in Y \exists x \in X : Kx = y$*
2. *Uniqueness. For every $y \in Y$ there is at most one $x \in X$ such that $Kx = y$:
 $\forall y_1, y_2 \in Y : y_1 = Kx_1, y_2 = Kx_2 \wedge y_1 = y_2 \Rightarrow x_1 = x_2$*
3. *Stability. The solution x depends continuously on y :
 \forall sequence $(x^{(n)}) \subset X, Kx^{(n)} \rightarrow Kx(n \rightarrow \infty) \Rightarrow x^{(n)} \rightarrow x(n \rightarrow \infty)$*

If at least one of these conditions is not held, the equation is called ill-posed (improperly posed).

Regarding the definition 3.3.1, to solve any inverse problem a specification of the triple $\{X, Y, K\}$ with their norms is required. The first two properties, existence and uniqueness, depend only on the algebraic characteristic of the spaces and the operator (considering if the operator is onto or one-to-one). The stability depends also on the spaces topologies, i.e. whether the inverse operator $K^{-1} : Y \rightarrow X$ is continuous. Solving the problems presented in Chapter 1 leads, except some trivial cases, to the variational (integral) formulation [60, 147]. Integral operators are compact operators in many natural topologies. It can be proved that for the compact operator K , the inverse problem of the linear equation $Kx = y$ is always ill-posed [43]:

Theorem 3.3.1. *Let $K : X \rightarrow Y$ be a linear compact operator over normed spaces X and Y with kernel $\mathcal{N}(K) := \{x \in X : Kx = 0\}$. Let the dimension of the factor space $X/\mathcal{N}(K)$ be infinite. Then there exists a sequence $(x^{(n)}) \subset X$ such that $K(x^{(n)}) \rightarrow 0$ but $(x^{(n)})$ does not converge. Moreover, there exists the sequence $(x^{(n)})$ such that $\|x^{(n)}\| \rightarrow \infty$. In particular, if K is one-to-one, the inverse operator $K^{-1} : Y \supset K(X) \rightarrow X$ is unbounded.*

To solve the problem of ill-posedness, it is convenient to introduce the definition of the best-approximation solution of $Kx = y$.

Definition 3.3.2. $K : X \rightarrow Y$ is a bounded linear operator, X, Y - Hilbert spaces.

1. $x \in X$ is the least-square solution of $Kx = y$ if $\|Kx - y\| = \inf \{\|Kz - y\| : z \in X\}$
2. $x \in X$ is the best-approximation solution of $Kx = y$ if x is the least-square solution of $Kx = y$ and x is of the minimal norm:

$$\|x\| = \inf \{z : z \text{ is the least - square solution of } Kx = y\}$$

The term of the best-approximation solution in the definition 3.3.2 is closely related to the Moore-Penrose inverse operator K^\wedge defined as follows:

Definition 3.3.3. *The Moore-Penrose (generalized) inverse operator K^\wedge of the linear operator $K : X \rightarrow Y$, where X, Y are Hilbert spaces, is defined as the unique linear extension of K^{-1} to:*

$$\mathcal{D}(K^\wedge) := \mathcal{R}(K) + \mathcal{R}(K)^\perp$$

and

$$\mathcal{N}(K^\wedge) = \mathcal{N}(K)^\perp$$

where

$$K^\wedge := K|_{\mathcal{N}(K)^\perp} : \mathcal{N}(K)^\perp \rightarrow \mathcal{R}(K)$$

Taking into account the theorem 3.3.1, the proper identification of material properties or boundary conditions in the computations of metal forming processes have to be supported by a method which will satisfy the definition 3.3.1 of well-posedness. Such a class of mappings is called regularization strategies which allow transformation of ill-posed problems to well-posed problems. The definition of the regularization and selected methods of this approach are presented in the next section.

3.4 Regularization

The main idea of regularization is to transform an ill-posed problem into a well-posed one. The formal definition of regularization is formulated as:

Definition 3.4.1 (Regularization). *A regularization strategy is a family of linear and bounded operators $R_\alpha : Y \rightarrow X$, $\alpha > 0$ such that $\lim_{\alpha \rightarrow 0} R_\alpha Kx = x \quad \forall x \in X$. It means that the operators $R_\alpha K$ convergence pointwise to identity.*

In many practical problems, the exact value of y is not known because this quantity is measured or derived from measurements. It means that the disturbed value y^δ for $\delta > 0$ is known:

$$\|y - y^\delta\| \leq \delta \quad (3.16)$$

The following equation (3.16) solving inverse problem for (3.14) is equivalent to find a value x^δ such that:

$$Kx^\delta = y^\delta \quad (3.17)$$

If no additional information of mapping K is known, one can not assume that the solution y^δ belongs to the K image $K(X)$. Therefore, one is estimating only a sufficiently good approximation x^δ of x .

The error between the exact value x and the approximated one $x_\alpha^\delta := R_\alpha y^\delta$ with the regularization strategy can be estimated with the use of the triangle inequality:

$$\begin{aligned} \|x_\alpha^\delta - x\| &\leq \|R_\alpha y^\delta - R_\alpha y\| + \|R_\alpha y - x\| \leq \|R_\alpha y^\delta - R_\alpha y\| + \|R_\alpha y - x\| \\ &\leq \|R_\alpha\| \|y^\delta - y\| + \|R_\alpha Kx - x\| \leq \|R_\alpha\| \delta + \|R_\alpha Kx - x\| \end{aligned} \quad (3.18)$$

The error (3.18) of approximation is the sum of two components. To estimate this error the behavior of the components has to be known. The component $\|R_\alpha Kx - x\|$ is increasing with an increase in α and it is going to zero while α is going to zero according to the definition 3.4.1 of regularization. To estimate the $\|R_\alpha\|$ component, let us consider the following theorem (the proof can be found in [43]):

Theorem 3.4.1. *R_α is the regularization strategy for a compact operator $K : X \rightarrow Y$ and $\dim X = \infty$. Then, the sequence $(R_\alpha Kx)$ does not converge uniformly on the bounded subset of X , i.e. there is no convergence of $R_\alpha K$ to identity I in the operator norm.*

Based on the theorem 3.4.1, it is observed that the component $\|R_\alpha\|$ is going to infinity while α is going to zero. It means that the formula (3.18) should be minimized with respect to α while the value of δ is fixed (Figure 3.1). These considerations lead to the definition of the *admissibility* of the regularization strategy.

Definition 3.4.2. *The regularization strategy $\alpha = \alpha(\delta)$ is admissible if the following property is held:*

$$\alpha(\delta) \rightarrow 0 \wedge \sup \{ \|R_{\alpha(\delta)} y^\delta - x\| : \|Kx - y^\delta\| \leq \delta \} \rightarrow 0, \quad \delta \rightarrow 0 \quad \forall x \in X.$$

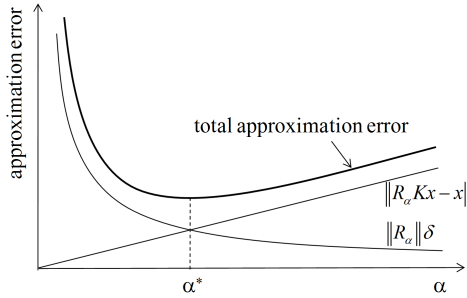


Figure 3.1: Total error of approximation.

The definitions 3.4.1 and 3.4.2 imply that to solve the inverse problem of the equation $Kx = y$ for $y \in Y$, one has to select not only a regularization operator R_α but a parameter α as well, in such a way that the regularized solution converges, in the norm, if the disturbance of y tends to zero. It means that one looks for a pair (R_α, α) that is called *the regularization method*. Then, the regularization procedure consists of the following steps:

- selection and construction of the regularization operator R_α ,
- determination of the parameter α of the regularization procedure with the property of the convergence to the solution.

The question is how this process should be designed to be efficient in terms of calculations. Some of the regularization methods, which are applied to the inverse metal forming problems, especially the identification problems, are presented in the next section.

In this section, the main definitions and theorems of inverse problems are presented, which are the background to investigate sufficient methods and tools to solve these problems. More details on the theory of inverse problems can be found in [21, 43].

3.5 Methods of regularizations

One of the methods to construct the admissible regularization strategy is using the singular system of the operator K (for the definition, see: A.0.9). If $K : X \rightarrow Y$ is

a linear compact operator with the singular system (μ_j, x_j, y_j) the solution x of the equation $Kx = y$ is concluded from the Picard theorem (A.0.5) and it is given by:

$$x = \sum_{j=1}^{\infty} \frac{1}{\mu_j} (y, y_j) x_j \quad (3.19)$$

for $y \in K(X)$.

Below there are presented theorems illustrating the functions that are admissible regularization strategies.

Theorem 3.5.1. *$K : X \rightarrow Y$ is a compact operator with the singular system (μ_j, x_j, y_j) and there is a function of the following form $q : (0, \infty) \times (0, \|K\|) \rightarrow \mathbb{R}$ such that:*

1. $|q(\alpha, \mu)| \leq 1$ for all $\alpha > 0$ and $0 < \mu \leq \|K\|$.
2. for every $\alpha > 0$ there exists $c(\alpha)$ such that $|q(\alpha, \mu)| \leq c(\alpha)\mu$ for all $0 < \mu \leq \|K\|$,
3. $\lim_{\alpha \rightarrow 0} q(\alpha, \mu) = 1$ for every $0 < \mu \leq \|K\|$.

Then the operator $R_\alpha : Y \rightarrow X$, $\alpha > 0$, defined as $R_\alpha := \sum_{j=1}^{\infty} \frac{q(\alpha, \mu_j)}{\mu_j} (y, y_j) x_j$ is a regularization strategy with $\|R_\alpha\| \leq c(\alpha)$. A choice $\alpha = \alpha(\delta)$ is admissible if $\alpha(\delta) \rightarrow 0$ and $\delta c(\alpha(\delta)) \rightarrow 0$ as $\delta \rightarrow 0$. The function q is a regularizing filter for operator K .

4. the item 3 can be replaced with another, stronger assumption:
There exists $c_1 > 0$ such that $|q(\alpha, \mu) - 1| \leq c_1 \frac{\sqrt{\alpha}}{\mu}$ for all $\alpha > 0$ and $0 < \mu \leq \|K\|$ and if $x \in K^*(Y)$, then $\|R_\alpha Kx - x\| \leq c_1 \sqrt{\alpha} \|z\|$, where $x = K^*z$,
5. the item 3 can be replaced with another, stronger assumption:
There exists $c_2 > 0$ such that $|q(\alpha, \mu) - 1| \leq c_2 \frac{\alpha}{\mu^2}$ for all $\alpha > 0$ and $0 < \mu \leq \|K\|$ and if $x \in K^*K(X)$, then $\|R_\alpha Kx - x\| \leq c_2 \alpha \|z\|$, where $x = K^*Kz$.

Every pair: a function $q : (0, \infty) \times (0, \|K\|) \rightarrow \mathbb{R}$ and the quantity α that satisfy the properties of the theorem 3.5.1 is a regularization strategy of the inverse equation $Kx = y$. Selected filters that are used to regularize inverse problems are presented next.

Let us define the function q of the form:

$$q(\alpha, \mu) = \mu^2 / (\alpha + \mu^2) \quad (3.20)$$

This function satisfies the assumption (2) of the theorem 3.5.1 for $c(\alpha) = 1/2\sqrt{\alpha}$, the assumption (4) for $c_1 = 1/2$ and the assumption (5) for $c_2 = 1$.

Let us define the function q of the form:

$$q(\alpha, \mu) = 1 - (1 - a\mu^2)^{1/\alpha} \quad (3.21)$$

for some parameter a such that $0 < a \leq \|K\|^2$. This function holds the assumption (2) of the theorem 3.5.1 for $c(\alpha) = \sqrt{a/\alpha}$, the assumption (4) for $c_1 = 1/\sqrt{2a}$ and the assumption (5) for $c_2 = 1/a$.

Let us define the function q of the form:

$$q(\alpha, \mu) = \begin{cases} 1 & \mu^2 \geq \alpha \\ 0 & \mu^2 < \alpha \end{cases} \quad (3.22)$$

This function holds the assumption (2) of the theorem 3.5.1 for $c(\alpha) = 1/\sqrt{\alpha}$ and the assumptions (4) and (5) for $c_1 = c_2 = 1/a$.

All of the functions (3.20)-(3.22) possess the assumptions (1), (2) and (3)-(5) of the theorem 3.5.1, respectively. It means, that these functions are regularizing filters and lead to admissible regularization strategies.

3.5.1 Tikhonov regularization

To construct the Tikhonov regularization strategy, let us consider the definition 3.3.2 of the best-approximation solution of $Kx = y$. It is noticed (and proved in [43, 21]) that there exists a set of the least-square solutions given by $x^\wedge + \mathcal{N}(K)$ and x^\wedge is the unique best-approximation solution, where $\mathcal{N}(K)$ is the kernel of K . Moreover, the least-square solution $x \in X$ of $Kx = y$ can be described by the *Gaussian normal equation* of the form:

$$K^*Kx = K^*y \quad (3.23)$$

where K^* is the adjoint operator of K (A.0.2). The Gaussian normal equation (3.23) is consistent with the definition 3.3.3 of the Moore-Penrose inverse operator K^\wedge .

Let us estimate the approximation error:

$$\begin{aligned} \|Kx - y\|^2 - \|K^\wedge x - y\|^2 &= \|K(x - x^\wedge)\|^2 + 2\operatorname{Re}(K^\wedge x - y, K(x - x^\wedge)) \\ &= \|K(x - x^\wedge)\|^2 + 2\operatorname{Re}(K^*(K^\wedge x - y), x - x^\wedge) \end{aligned} \quad (3.24)$$

If x^\wedge is the best-approximation solution of the problem $Kx = y$ and it solves the normal equation (3.23) then the error $\|Kx - y\|^2 - \|K^\wedge x - y\|^2 \geq 0$ and x^\wedge minimizes $\|Kx - y\|$.

Now, let us express $x \in X$ as $x = x^\wedge + c\bar{x}$ for any $c > 0$ and $\bar{x} \in X$. Thus, if x^\wedge minimizes $\|Kx - y\|$ and (3.24) is held, one arrives at:

$$\begin{aligned} 0 \leq \|Kx - y\|^2 - \|K^\wedge x - y\|^2 &= c^2 \|K\bar{x}\|^2 + 2c\operatorname{Re}(K^*(K^\wedge x - y), \bar{x}) \\ &= c \|K\bar{x}\|^2 + 2\operatorname{Re}(K^*(K^\wedge x - y), \bar{x}) \end{aligned} \quad (3.25)$$

Keeping in mind the estimation error (3.25), to determine the solution of the linear, bounded operator $Kx = y$ for given $y \in Y$, the minimization problem of the following form has to be solved:

$$\Phi_\alpha := \|Kx - y\|^2 + \alpha \|x\|^2 \quad \text{for } x \in X \quad (3.26)$$

The functional (3.26) is called Tikhonov functional. This functional has a unique minimum $x_\alpha \in X$ that can be expressed with normal equation:

$$\alpha x_\alpha + K^* K x_\alpha = K^* y \quad (3.27)$$

The functional (3.26) is well-defined and it is an admissible regularization strategy according to the definition (3.4.2). The minimum x_α - the solution of Equation (3.27), can be put as $x_\alpha = R_\alpha y$, where:

$$R_\alpha := (\alpha I + K^* K)^{-1} K^* : Y \rightarrow X \quad (3.28)$$

Selecting the singular system (μ_j, x_j, y_j) for the operator K , it is observed that R_α is of the form:

$$R_\alpha = \sum_{j=1}^{\infty} \frac{\mu_j}{\alpha + \mu_j^2} (y, y_j) x_j \quad y \in Y \quad (3.29)$$

Assuming the function $q(\alpha, \mu) = \frac{\mu^2}{\alpha + \mu^2}$, the regularization operator is represented by:

$$R_\alpha = \sum_{j=1}^{\infty} \frac{q(\alpha, \mu)}{\mu_j} (y, y_j) x_j \quad y \in Y \quad (3.30)$$

In Equation (3.30) q is the same function as the one defined by (3.20). Thus, q is the regularization filter for the operator R_α given by (3.29) according to the theorem (3.5.1) and the Tikhonov functional (3.26) is the admissible regularization strategy of the equation $Kx = y$ for the given $y \in Y$. Moreover, it can be proved that for the disturbed data y^δ the Tikhonov regularization strategy $R_\alpha y^\delta$ is admissible for every choice $\alpha(\delta) \rightarrow 0$, $\delta \rightarrow 0$ if $\delta^2/\alpha(\delta) \rightarrow 0$, $\delta \rightarrow 0$ (the parameter α should converge to 0 as δ is going to 0 but not so fast as δ^2).

3.5.2 Iteration methods

In this group of the regularization methods, the regularization parameter α is an equivalent to the iteration index and the method itself defines the stopping rule. Below, the iterative methods applied to inverse problems are listed. All of them are proved to be a regularization strategy:

- Landweber iteration,
- the conjugate gradient method,
- v -methods (semiiterative).

The first two algorithms have found practical applications and they are presented below. The descriptions of the last one is included in e.g. [21, 43].

Landweber iteration. Transforming the basic equation (3.14) with the normal form (3.23), the equation of the form is obtained $x = x + K^*(y - Kx)$ and next the iteration scheme is derived:

$$x^{(0)} := 0 \quad x^{(k)} = (I - \alpha K^* K) x^{(k-1)} + \alpha K^* y \quad \alpha > 0 \quad (3.31)$$

for $k = 1, 2, \dots$. This scheme is equivalent to the steepest descent algorithm applied to the quadratic functional $\Phi(x) = \|Kx - y\|^2$. The scheme (3.31) is the linear recursive formula of $x^{(k)}$. Applying induction with respect to k , it is observed that $x^{(k)}$ is of the form $x^{(k)} = R_k y$ where the operator $R_k : Y \leftarrow X$ is expressed as:

$$R_k := \alpha \sum_{i=0}^{k-1} (I - \alpha K^* K)^i K^* \quad k = 1, 2, \dots \quad (3.32)$$

If the singular system (μ_j, x_j, y_j) for the compact operator K is selected then $R_k y$ is given by:

$$\begin{aligned} R_k y &= \sum_{j=1}^{\infty} \mu_j \sum_{i=0}^{k-1} (1 - \alpha \mu_j^2)^i (y, y_j) x_j \\ &= \sum_{j=1}^{\infty} \frac{1}{\mu_j} \left[1 - (1 - \alpha \mu_j^2)^k \right] (y, y_j) x_j \\ &= \sum_{j=1}^{\infty} \frac{q(k, \mu_j)}{\mu_j} (y, y_j) x_j, \quad y \in Y \end{aligned} \quad (3.33)$$

where $q(k, \mu_j) = \left[1 - (1 - \alpha \mu_j^2)^k \right]$. The function $q(k, \mu_j)$ is a regularization filter q defined as in Equation (3.21) for $\alpha = 1/k$. Thus, according to the theorem 3.5.1, the operator R_k is an admissible regularization strategy with discrete parameter α .

In the most practical application solved with the iterative procedures, the following stopping rule is used: the algorithm is stopped at the first occurrence of $k \in \mathbb{N}$ such that $\|Kx^{(k),\delta} - y^\delta\| \leq r\delta$, where $r > 1$ is a constant. It is shown (e.g. in [43]) that the selection of k for the stopping rule is possible for the Landweber scheme and leads to the optimal regularization strategy.

Conjugate gradient method (CGM). Originally, the algorithm was developed for the least squares problems for the system of linear equations of the form $\mathbf{K}\mathbf{x} = \mathbf{y}$, where $\mathbf{K} \in \mathbb{R}^{m \times n}$, $m \geq n$. In the method, the error defined as $\Phi(\mathbf{x}) := \|\mathbf{K}\mathbf{x} - \mathbf{y}\|^2$ is minimized, where $\mathbf{x} \in \mathbb{R}^n$, $\|\cdot\|$ denotes the Euclidean norm in \mathbb{R}^m ([55, 84]). For the purpose of the inverse problem consideration, the operator equation $Kx = y$ is given with $K : X \rightarrow Y$ linear, bounded, injective operator, X, Y are Hilbert spaces and $K^* : Y \rightarrow X$ is an adjoint operator of K . Now, the functional Φ is defined as:

$$\Phi(x) := \|Kx - y\|^2 = (Kx - y, Kx - y), \quad x \in X \quad (3.34)$$

The derivative $\nabla\Phi$ is the Frechet derivative of Φ at x , and it is equal $\nabla\Phi(x) = 2K^*(Kx - y) \in X$ (from the Riesz theorem).

The procedure of the conjugate gradient method is listed in the algorithm 3.1.

Algorithm 3.1 The conjugate gradient method (CGM)

```

1:  $x^{(0)} \leftarrow 0, k \leftarrow 0$ 
2: if  $K^*y = 0$  then
3:   return  $x^{(0)}$ 
4: else
5:    $p^{(0)} \leftarrow -K^*y = \frac{1}{2}\nabla\Phi(x^{(0)})$ 
6: end if
7: while true do
8:    $t^{(k)} \leftarrow \frac{(Kx^{(k)}-y, Kp^{(k)})}{\|Kp^{(k)}\|^2}$ 
9:    $x^{(k+1)} \leftarrow x^{(k)} - t^{(k)}p^{(k)}$ 
10:  if  $K^*(Kx^{(k+1)} - y) = 0$  then
11:    return  $x^{(k+1)}$ 
12:  else
13:     $\gamma^{(k)} \leftarrow \frac{\|K^*(Kx^{(k+1)}-y)\|^2}{\|K^*(Kx^{(k)}-y)\|^2}$ 
14:     $p^{(k+1)} \leftarrow K^*(Kx^{(k+1)} - y) + \gamma^{(k)}p^{(k)}$ 
15:     $k \leftarrow k + 1$ 
16:  end if
17: end while

```

From the Fletcher-Reeves theorem ([43]), the CGM method is well-defined and either stops or produces sequences $(x^{(k)}), (p^{(k)}) \subset X$ such that:

$$\left(\nabla\Phi(x^{(k)}), \nabla\Phi(x^{(j)})\right) = 0 \quad \text{and} \quad \left(Kp^{(k)}, Kp^{(j)}\right) = 0 \quad \forall j \neq k \quad (3.35)$$

i.e. the gradients are orthogonal and the directions $p^{(k)}$ are K -conjugate. Moreover, it yields:

$$\left(\nabla\Phi(x^{(j)}), K^*Kp^{(k)}\right) = 0 \quad \forall j < k \quad (3.36)$$

The sequence $(p^{(k)})$ defines the space $V_k := \text{span}\{p^{(0)}, \dots, p^{(k)}\}$, which is called a *Krylov* space. The following forms are equivalent for V_k :

$$\begin{aligned} V_k &= \text{span}\left\{\nabla\Phi(x^{(0)}), \dots, \nabla\Phi(x^{(k)})\right\} \\ &= \text{span}\left\{p^{(0)}, K^*Kp^{(0)}, \dots, (K^*K)^k p^{(0)}\right\}, \quad k = 0, 1, \dots \end{aligned} \quad (3.37)$$

Furthermore, $x^{(k)}$ is the minimum of Φ on V_k for every $k \geq 1$, and $x^{(k)}$ can be expressed as:

$$x^{(k)} = -\mathcal{P}_{k-1}(K^*K)p^{(0)} = -\mathcal{P}_{k-1}(K^*K)K^*y \quad (3.38)$$

where \mathcal{P}_{k-1} is a well-defined polynomial of degree $k-1$.

To show that the CGM is a regularization strategy, let us assume that (μ_j, x_j, y_j) is a singular system for the operator K . The operator $\mathcal{P}_{k-1}(K^*K)K^* : Y \rightarrow X$ corresponds to the regularization operator R_α of the general regularization theory, although it depends on the right-hand side y . Thus, the mapping $y \rightarrow \mathcal{P}_{k-1}(K^*K)K^*y$ is nonlinear.

Let us consider a special case, such that $y = \sum_{j=1}^n \alpha_j y_j \in Y_n := \text{span}\{y_1, \dots, y_n\}$, $n \in \mathbb{N}$, then $x^{(k)} = \mathcal{P}_{k-1}(K^*K)K^*y = \sum_{j=1}^n \alpha_j \mathcal{P}_{k-1}(\mu_j^2) \mu_j x_j$ and $x^{(k)} \in X_n := \text{span}\{x_1, \dots, x_n\}$. In this special case, the algorithm stops after at the most n iterations since the dimension of space X_n is at most n and the gradients $\nabla\Phi(x^{(i)})$ are orthogonal to each other. This is the explanation why CGM applied to matrix equations terminates after the finite number of iterations. Generally, for operator equations defined in infinite-dimensional Hilbert spaces, CGM produces infinitely many elements.

3.5.3 Regularization by projection

For numerical calculations the regularization algorithms implementable in finite-dimensional spaces are looked for. Let us consider the operator equation of the form $Kx = y$. One of the approaches to approximate x^\wedge is *the least-squares projection*, i.e. to find the minimum of $Kx = y$ in terms of the norm in Y space, in a finite-dimensional subspace of X . It is obtained by defining a sequence $X_1 \subset X_2 \subset \dots$ of finite-dimensional subspaces of X whose union is dense in X . Let $x^{(k)}$ be the least-squares solution of the minimal norm in the space X_k and:

$$x^{(k)} = K_k^\wedge y \quad (3.39)$$

where $K_k = K\mathcal{P}_k$, \mathcal{P}_k is an orthogonal projector onto X_k , K^\wedge is defined as 3.3.3. Since K_k is of a close range, the operator K_k^\wedge is bounded and thus $x^{(k)}$ is a stable approximation of x^\wedge . To ensure the convergence of $x^{(k)}$ to x^\wedge , additional assumptions are required:

Theorem 3.5.2. *Let $y \in \mathcal{D}(K^\wedge)$ and $x^{(k)}$ is defined as 3.39. Thus:*

- $x^{(k)} \rightarrow x^\wedge$ if and only if $\{\|x^{(k)}\|\}$ is bounded,
- $x^{(k)} \rightarrow x^\wedge$ if and only if $\limsup_{k \rightarrow \infty} \|x^{(k)}\| \leq \|x^\wedge\|$

The strong convergence introduced in the theorem 3.39 in the second item is hard to control since the true solution norm is not known in most cases. Instead of this condition, another one is assumed of the following form:

$$\limsup_{k \rightarrow \infty} \left\| (K_k^\wedge)^* x^{(k)} \right\| = \limsup_{k \rightarrow \infty} \left\| (K_k^*)^\wedge x^{(k)} \right\| \quad (3.40)$$

The condition (3.40) is sufficient for the convergence of $(x^{(k)})$ to x^\wedge (for the proof, see: [21]).

Finite-dimensional approximation algorithms like discretization methods: collocation, Galerkin or Ritz approximation belong to *the regularization by projection* group of regularization methods. The details of these algorithms are presented in [21] for example.

3.6 Numerical computation

Most of the direct problems that are discussed in metal forming are solved with numerical methods. Thus, to solve an inverse problem, the regularization method should be established by the finite-dimension approximation procedure in the finite-dimension space. This regularization procedure most often consists of three main steps: discretization, transformation to the standard form and the regularization of it. Even though the discretization methods are regularization algorithms by themselves, as it was mentioned in section 3.5.3, some further regularization is recommended to increase the algorithm stabilization and to extend the discretization subspaces.

Let subspaces of discretization be denoted by $X^n \subset X$ and $Y^m \subset Y$ with the bases expressed as:

$$X_n = \text{span} \{e_1^X, \dots, e_n^X\}, \quad Y_m = \text{span} \{e_1^Y, \dots, e_m^Y\} \quad (3.41)$$

Let $x^* \in X_n$ be the approximation of the exact solution x . Now x^* is defined with the projection equation:

$$\mathcal{P}_m K x_n = \mathcal{P}_m y \quad (3.42)$$

where $\mathcal{P}_m : Y \rightarrow Y_m$. $x^* \in X_n$ is represented using the coordinate vector $\mathbf{x} \in \mathbb{R}^n$ corresponding to the combination:

$$x^* = \phi_1 e_1^X + \phi_n e_n^X, \quad \mathbf{x} = (\phi_1, \dots, \phi_n)^T \quad (3.43)$$

In this form, the projection equation (3.42) yields a system of equation for the n unknown coordinates $\{\phi_i\}$. In many practical applications, this system is still ill-conditioned to be numerically solved and further regularization is needed, like iterative methods or the Tikhonov regularization described in this chapter.

Reduction to standard form. There are two regularization forms: a *general form* and a *standard form*. The regularization is in the standard form if the coordinate space \mathbb{R}^n , where the unknown vector \mathbf{x} belongs to, is equipped with the Euclidean norm. If this norm is not defined in space \mathbb{R}^n , the regularization is in a general form. In the general regularization, *the weighted generalized inverse solution* is used. The definition 3.3.2 of the best least-square solution can be extended to the following form:

$$\|Lx_L^\wedge\| = \inf \{\|Lz\| : z \text{ is the least square solution of } Kx = y\} \quad (3.44)$$

Equation (3.44) minimizes the primary problem 3.3.2 with a different norm, called a *semi-norm*. The problem of the minimization (3.44) will be well defined (the solution will exist and will be unique) if the operator L is of appropriate properties [21]. In the space $\mathcal{D}(L)$ with $*$ -inner product, there are unique *Moore-Penrose generalized inverses*: of $L : \mathcal{D}(L) \rightarrow Z$, denoted as L_K^\wedge , and of $K : \mathcal{D}(L) \rightarrow Y$, denoted as K_L^\wedge . The operators L and K are bounded with respect to $\|\cdot\|_*$ norm. The operators L_K^\wedge and K_L^\wedge are noticed to be different from the Moore-Penrose inverses of L^\wedge and K^\wedge described in the definition 3.3.3 and derived from the original product in X . The inverses L_K^\wedge and K_L^\wedge are called *weighted Moore-Penrose generalized inverses* because they are obtained with the weighted inner product $\|\cdot\|_*$.

Important selections of L are those of nontrivial nullspaces, i.e. if L is a differential operator, L is taken to be the second derivative operator. For the computation implementation, on account of the calculation efficiency, instead of the operator K_L^\wedge , the continues operator B is introduced, defined as $B := KL_K^\wedge : Z \rightarrow Y$.

Based on Equation (3.44), the theorem 3.3.1, the definition 3.3.3, substituting in the projection equation (3.42) $\mathcal{P}_m K$ for A , and foregoing investigations, the weighted generalized inverse B_A^\wedge of B is applied:

$$\mathbf{x} = \mathbf{x}_0^\wedge + B_A^\wedge \mathbf{z} \quad (3.45)$$

where \mathbf{x}_0^\wedge is a component of the nullspace of B and \mathbf{z} is approximated by:

$$\mathbf{z}_\alpha = g_\alpha (\bar{A}^K \bar{A}) \bar{A}^K \bar{\mathbf{b}}, \quad \bar{A} = AB_A^\wedge, \quad \bar{\mathbf{b}} = \mathbf{b} - A\mathbf{x}_0^\wedge$$

\mathbf{z}_α is called a *regularized solution* of the standard form problem:

$$\bar{A}\mathbf{z} = \bar{\mathbf{b}}. \quad (3.46)$$

3.6.1 Regularization in the finite dimension setting

Tikhonov regularization in the finite dimension setting. In this case, the problem is transformed to the search for the minimum of the quadratic functional (see Equation (3.26)):

$$\|\mathbf{b} - A\mathbf{x}\|_2^2 + \alpha \|\mathbf{B}\mathbf{x}\|_2^2 = (\mathbf{b} - A\mathbf{x})^T (\mathbf{b} - A\mathbf{x}) + \alpha \mathbf{x}^T \mathbf{B}^T \mathbf{B} \mathbf{x} \quad (3.47)$$

where $\|\cdot\|_2$ is the Euclidean norm and the matrix \mathbf{B} estimates the way of the smoothness of \mathbf{x} to be consistent with $\|x\|_X$ (the norm of x in space X). According to the projection scheme (3.42), matrix \mathbf{A} and vector \mathbf{b} should be selected in the following way:

$$\|\mathbf{b} - A\mathbf{x}\| \approx \|\mathcal{P}_m (y - Kx)\|_Y \quad (3.48)$$

The vector \mathbf{x} that minimized the functional (3.47), satisfies the $n \times n$ system of equations:

$$(\mathbf{A}^T \mathbf{A} + \alpha \mathbf{B}^T \mathbf{B}) \mathbf{x} = \mathbf{A}^T \mathbf{b} \quad (3.49)$$

where the matrix \mathbf{B} is such that:

$$\|\mathbf{B}\mathbf{x}\|_2 \approx \|x^*\|_X = \|\phi_1 e_1^X + \dots + \phi_n e_n^X\|_X \quad (3.50)$$

From Equation (3.50) it is seen that the selection of the matrix \mathbf{B} equal identity matrix ($\mathbf{B} = \mathbf{I}$) is possible only if the functions ϕ_i are the functions for the subset of piecewise constants and then it is regularization in the standard form. Otherwise, the regularization is of the general form and the correct norm is expressed with the Gramian matrix:

$$\mathbf{G} = \left[(e_i^X, e_j^X)_X \right], \quad \|\phi_1 e_1^X + \dots + \phi_n e_n^X\|_X^2 = \sum_{i,j=1}^n \phi_i \phi_j (e_i^X, e_j^X)_X = \mathbf{x}^T \mathbf{G} \mathbf{x} \quad (3.51)$$

More details on the Gramian matrix can be found in [21].

Iterative methods in finite dimension space. If regularization is performed to a different norm in the coefficient space, i.e. $\mathbf{B} \neq \mathbf{I}$, taking Equation (3.45) and using a standard form problem (3.46), the following iteration scheme is obtained:

$$\mathbf{x}^{(k)} = \mathbf{x}^{(k)\wedge} + B_A^\wedge \mathbf{z}^{(k)}, \quad \mathbf{z}^{(k)} = g^{(k)} \left((B_A^\wedge)^T A^T A B_A^\wedge \right) (B_A^\wedge)^T A^T \bar{\mathbf{b}}$$

For the Landweber algorithm the iteration of $\mathbf{z}^{(k)}$ is given by:

$$\mathbf{z}^{(k)} = \mathbf{z}^{(k-1)} + (B_A^\wedge)^T A^T \left(\bar{\mathbf{b}} - A B_A^\wedge \mathbf{z}^{(k-1)} \right)$$

where $k \in \mathbb{N}$, $\mathbf{z}^{(0)} = 0$. After backsubstitution the relation is formed:

$$\mathbf{x}^{(k)} = \mathbf{x}^{(k-1)} + B_A^\wedge (B_A^\wedge)^T A^T \left(\mathbf{b} - A \mathbf{x}^{(k-1)} \right), \quad k \in \mathbb{N}$$

and $\mathbf{x}^{(0)} = \mathbf{x}_0^\wedge$. It means that regularization is performed with multiplication of the normal equation system by generalized inverses of B and B^T .

3.6.2 Practical aspects and problems

Based on the investigations provided in sections 3.3-3.6, the method (operator) developed to solve an inverse problem should be proved to be a regularizator in terms of the theorem 3.5.1 and the definition 3.3.1 of well-posedness. Metal forming modeling is a complex task since the problems are not stationary and they include mechanical and thermal phenomena, as presented in section 3.1. In addition, the models involve phenomenological laws and relations. The problems are solved with numerical methods, the computations are performed separately for mechanical and thermal models and the results are interchanged and integrated between the solvers at particular time steps. These aspects and investigations provided in this chapter are the reason for which the construction of an inverse operator of thermomechanical metal forming task is a hard problem.

It was mentioned in section 3.1 that equations of metal forming thermomechanical problems are solved with finite element methods. Hence, the regularization procedures for finite dimensional spaces, presented in section 3.6.1, are going to be applied.

It should be once again highlighted that it is possible to use these algorithms since the considered problem has a unique solution. In practical applications, the assumption of a unique solution is not true or the information on the number of possible solutions is not known. Thereby, the classical regularization algorithms listed above do not assure proper solution. According to the definition 3.3.1 of well-posedness and the conclusions from this definition, in case when there are more than one solution, the parameters domain should be narrowed. Such an operation is hard to perform for real problems. Although the regularization methods are used to hold the stability of the identification process, e.g. the Tikhonov functional (3.47), the Landweber iteration scheme (3.31) or the CGM algorithm (3.34), but there is no confirmation that the obtained results indeed solved the considered problems. Thus, one of the approaches is that the minima of the functionals defined in classic regularization methods are searched with nondeterministic, stochastic optimization algorithms or the Pareto front is applied to determine the set of solutions [55, 19, 42, 86]. The question is of the convergence of such an application. Propositions of the stochastic methods convergence are not trivial, some theorems of these problems are presented in [5, 40, 102].

Taking into account all the problems listed above and high computational cost of metal forming solvers, other, alternative methods were looked for to reduce the number of possible inverse solutions, enhance reliability of the obtained results and decrease computational costs of the calculations. The methods of sensitivity analysis were selected to solve these problems. The algorithms of sensitivity analysis are presented in Chapter 4 and the developed identification strategy and the software in Chapter 5.

4 Sensitivity analysis

The problem of parameters identification defined as an inverse problem is a kind of a hard problem due to the lack of a unique solution and high computational costs (see Chapter 3). In many practical applications the most important issue is to obtain a solution in a relatively short time. Following that, the supporting algorithms were looked for to make the inverse calculations more reliable and to decrease the calculations cost of calculating the inverse problem solving. A wide range of methods, like data mining, experts systems and the algorithms derived from artificial intelligence, were browsed and finally the sensitivity analysis techniques were selected as most suitable.

Sensitivity Analysis (SA) is the field of knowledge investigating the model (mathematical and physical description of the phenomenon under study) behavior for various input data and model parameters [101]. It determines how the variations of input data and parameters are distributed on the variations of model outputs and influence them. A good practice of the numerical modeling is to validate the model and SA provides techniques enabling this evaluation. The main goals of SA application are:

- verification whether a model simulates the phenomenon under study in a proper way (e.g. according to physical laws),
- determination of the model parameters which the most contribute to the model outputs variations,
- identification the parameters which are not significant for the analyzed model outputs,
- determination the parameters domain of the highest influence of the model variations,
- estimation of parameters uncertainty,
- verification whether parameters interact with each other,
- for inverse problems:
 - verification whether the norm defined in the output space is proper to solve the defined inverse problem,
 - verification whether the goal function in optimization task includes information allowing to perform the optimization,
 - determination of the parameters identification accuracy,
 - reduction of calculation cost of optimization procedure (decrease the number of direct problem solver evaluations),

- as the preliminary step - to select the starting point/the first region of interest or the first population for optimization algorithm,
- in optimization process - to construct hybrid algorithms (e.g. the combination of an evolutionary algorithm to select local minima and a gradient method to explore those minima) or modified algorithms (e.g. evolutionary procedure enriched with the information about the local sensitivities [128]) to increase the efficiency of the procedure.

The SA methods are classified using various criteria. One of the possibility is to group the algorithms with respect to the manner of parameter analysis:

- global methods - they calculate one (global) value expressing the sensitivity of a parameter for the whole parameter domain; these methods are derived from statistics and the probability theory,
- local methods [44] - they calculate the sensitivity of a parameter for a small interval of parameter variation; local sensitivities are defined as the partial derivatives of a model with respect to the input model parameters.

In the next sections, there are presented algorithms derived from the classical SA methods which were adopted and next applied to the problems of parameter identification in the numerical modeling of metal forming processes. The results of the calculations are presented in Chapter 6.

4.1 Local sensitivity analysis

As was mentioned at the beginning of this chapter, local SA methods estimate parameter sensitivity for a narrow interval of the parameter variation. Local sensitivities are determined by means of the differential analysis. The sensitivity measure in these methods is derived right from the partial derivative definition calculated for a model output with respect to a model input parameter. Let us consider the problem described by the time-dependent equation:

$$\mathbf{y} = \mathbf{y}(t, \mathbf{x}) \quad (4.1)$$

where \mathbf{x} is the vector of model inputs and parameters, t - time.

The effect of parameter change on the solution at time t can be expressed through a Taylor series expansion:

$$\mathbf{y}(t, \mathbf{x} + \Delta\mathbf{x}) = \mathbf{y}(t, \mathbf{x}) + \sum_i \frac{\partial \mathbf{y}}{\partial x_i} \Delta x_i + \frac{1}{2} \sum_i \sum_j \frac{\partial^2 \mathbf{y}}{\partial x_i \partial x_j} \Delta x_i \Delta x_j + \dots \quad (4.2)$$

The partial derivatives $\partial \mathbf{y} / \partial x_i$ are called the first-order local sensitivities, $\partial^2 \mathbf{y} / \partial x_i \partial x_j$ are called the second-order local sensitivities. The first-order local sensitivities define the sensitivity matrix

$$\mathbf{S} = [s_{ji}] = \left[\frac{\partial y_j}{\partial x_i} \right] \quad (4.3)$$

The sensitivity matrix \mathbf{S} in Equation (4.3) is defined for the case when the parameters are perturbed at the simulation time equal 0, and therefore the initial time of the sensitivity computation is equal to the initial time of the simulation. In general case, the initial times of the calculations of the model and the sensitivities differ. Let us assume that the simulation starts at time 0, the parameters are perturbed in time t_1 and the sensitivities are estimated in t_2 . Thus, the perturbed solution \mathbf{y}' is approximated by the double time dependent sensitivity matrix $\mathbf{S}(t_1, t_2)$:

$$\mathbf{y}'(t_2) \approx \mathbf{y}(t_1) + \mathbf{S}(t_1, t_2) \Delta \mathbf{x}_{t_1} \quad (4.4)$$

The best way to determine the sensitivity matrix \mathbf{S} is to perform analytical calculation. However, the problem description is complex in many cases and such analytical calculations are not possible. Instead of that, e.g. *the finite-difference approximation* scheme is applied:

$$\frac{\partial \mathbf{y}}{\partial x_i} \cong \frac{\mathbf{y}(x_i + \Delta x_i) - \mathbf{y}(x_i)}{\Delta x_i} \quad (4.5)$$

The formula (4.5) is also called *the indirect* or *the brute-force method*. The advantage of this procedure is that no modifications of the original solution are needed, it can be run for any model. The disadvantage is that there are no guidelines how to determine the disturbance Δx_i . In many cases, the value of 1% of x_i for Δx_i is a good choice, but it should be estimated precisely, especially for highly non-linear models, to keep the reliability of the calculations and accuracy. Local sensitivities calculated with the scheme (4.5) require $n + 1$ model runs, where n is the dimension of the vector \mathbf{x} . If the central differences scheme is applied, the number of the model evaluation increases to $2n$. The procedure is also time consuming.

Another solution is to use *the semi-analytical approximation* which is the combination of the finite-difference method and analytical calculations: the model outputs \mathbf{y} are first analytically differentiated while differentiation for the inner functions is feasible, next, the finite-difference algorithm is applied. The error of approximation can be reduced in that way.

The elements of a sensitivity matrix (4.3) estimated for various parameters x_i are expressed by the (physical or empirical) units assigned to the parameters x_i and the model outputs \mathbf{y} , therefore, the comparison between the coefficients for the sensitivities of various x_i is not permitted. To avoid this problem and to make the sensitivity coefficients independent of the parameters and the model outputs units, they are normalized:

$$\hat{\mathbf{S}} = [\hat{s}_{ji}] = \left[\frac{x_i}{y_j} \frac{\partial y_j}{\partial x_i} \right] \quad (4.6)$$

Sensitivity coefficients \hat{s}_{ji} represent a relative variation of the model output y_j while the relative change of the parameter x_i is introduced to the model.

The practical application of the local sensitivities of the first and the second order: they are used first of all in gradient optimization algorithms and inverse problems, as well as in numerical solutions of physical problems [44]. The local methods are not suitable to compare the effects of more than one parameter at a time. If the model is

of strong nonlinearity, it is not possible to extend the calculated local parameter sensitivity to other values of the parameter. Moreover, if the sensitivities are estimated numerically, they can be of high errors. If a large number of the model parameters is under study, it is difficult to manage the information of the local sensitivities and to summarize it.

4.1.1 A scheme for semi-analytical sensitivity calculations

The main steps of the sample semi-analytical calculations of the sensitivity matrix \mathbf{S} is presented in this section. Let us consider the thermomechanical problem described in Chapter 3.1 defined by Equations (3.1)-(3.13). The equations are solved with the finite element method as a quasi-stationary problem. Thus, the discrete form of virtual work in every time step t is described as:

$$W^{(t)}(\mathbf{x}, \mathbf{u}^{(t)}, T^{(t-\Delta t)}) = 0 \quad (4.7)$$

where \mathbf{x} is the vector of the identified model parameters, e.g., parameters of the rheological equation or the friction model, $\mathbf{u}^{(t)}$ is velocity vector, $T^{(t-\Delta t)}$ is temperature.

The inverse problem solved with iteration methods (see Chapter 3.1, section 3.5.2), is defined as:

$$\min_{\mathbf{x} \in X} \Phi(\mathbf{x}) \quad \Phi(\mathbf{x}) = \|\mathbf{y}(\mathbf{x}, \mathbf{u}, T) - \mathbf{y}^\delta\|^2 \quad (4.8)$$

where X is the space of admissible values of the identified vector \mathbf{x} , \mathbf{y} and \mathbf{y}^δ are the vectors of calculated and measured model outputs, respectively. The functional (4.8) can be rewritten as:

$$\Phi(\mathbf{x}) = \sum_{i=1}^m w_i [y_i(\mathbf{x}) - y_i^\delta]^2 \quad (4.9)$$

where m is the dimension of the model outputs space, $w_i = 1/(y_i^\delta)^2$ are weighted coefficients.

If, to select the minimum of the functional (4.9), the gradient Gauss-Newton iteration method is applied, the iteration scheme is following:

$$\mathbf{x}^{(k)} = \mathbf{x}^{(k-1)} - \mathbf{J}(\mathbf{x}^{(k-1)}) \frac{d\Phi}{d\mathbf{x}}(\mathbf{x}^{(k-1)}) \quad (4.10)$$

where

$$\frac{d\Phi}{d\mathbf{x}} = 2 \sum_{i=1}^m w_i (y_i(\mathbf{x}) - y_i^\delta) \frac{dy_i}{d\mathbf{x}} \quad (4.11)$$

$$\mathbf{J} \approx 2 \sum_{i=1}^m w_i \frac{dy_i}{d\mathbf{x}} \left[\frac{dy_i}{d\mathbf{x}} \right]^T$$

where \mathbf{J} is the Jacobian matrix of $\frac{d\Phi}{d\mathbf{x}}$ with respect to \mathbf{x} ignoring the second order derivatives.

The algorithm convergence depends on sensitivity of the model outputs \mathbf{y} with respect to the vector \mathbf{x} . The sensitivity matrix $\mathbf{S} = \frac{d\mathbf{y}}{d\mathbf{x}}$ from Equation (4.11) can be computed with the finite-difference approximation (4.5) or with the semi-analytical algorithm presented below.

Sensitivity matrix \mathbf{S} , from the derivative definition, is expressed by:

$$\mathbf{S} = \frac{d\mathbf{y}}{d\mathbf{x}} = \lim_{\Delta\mathbf{x} \rightarrow 0} \frac{\mathbf{y}(\mathbf{x} + \Delta\mathbf{x}, \mathbf{u}^{(\Delta)}, T^{(\Delta)}) - \mathbf{y}(\mathbf{x}, \mathbf{u}^{(t)}, T^{(t-\Delta t)})}{\Delta\mathbf{x}} \quad (4.12)$$

where

$$\mathbf{u}^{(\Delta)} = \mathbf{u}^{(t)} + \frac{d\mathbf{u}^{(t)}}{d\mathbf{x}} \Delta\mathbf{x}, \quad T^{(\Delta)} = T^{(t-\Delta t)} + \frac{dT^{(t-\Delta t)}}{d\mathbf{x}} \Delta\mathbf{x}$$

and the velocity derivative $d\mathbf{u}$ with respect to the vector \mathbf{x} , $\frac{d\mathbf{u}^{(t)}}{d\mathbf{x}}$, is calculated based on the differentiation of the direct problem (4.7):

$$\frac{dW^{(t)}}{d\mathbf{x}} = \left. \frac{dW}{d\mathbf{x}} \right|_{\mathbf{u}} + \frac{\partial W}{\partial \mathbf{x}} \frac{d\mathbf{u}^{(t)}}{d\mathbf{x}} = 0 \quad (4.13)$$

And from Equation (4.13) one obtains:

$$\frac{d\mathbf{u}^{(t)}}{d\mathbf{x}} = - \left(\frac{\partial W}{\partial \mathbf{x}} \right)^{-1} \left. \frac{dW}{d\mathbf{x}} \right|_{\mathbf{u}} = -\mathbf{H}^{-1}(\mathbf{u}) \left. \frac{dW}{d\mathbf{x}} \right|_{\mathbf{u}} \quad (4.14)$$

where $\mathbf{H}^{-1}(\mathbf{u})$ is inverse of Hessian matrix which is computed while the problem (4.7) is solved. The partial derivative of W with respect to the vector \mathbf{x} , while the velocity vector \mathbf{u} is constant (see Equation (4.14)), are calculated with the finite-difference scheme (4.5) due to nonlinear equations included vector \mathbf{x} . If these equations are temperature dependent as well, the differential quotient is of the form:

$$\left. \frac{dW}{d\mathbf{x}} \right|_{\mathbf{u}} = \lim_{\Delta\mathbf{x} \rightarrow 0} \frac{W(\mathbf{x} + \Delta\mathbf{x}, \mathbf{u}^{(\Delta)}, T^{(\Delta)}) - W(\mathbf{x} + \Delta\mathbf{x}, \mathbf{u}^{(t)}, T^{(t-\Delta t)})}{\Delta\mathbf{x}} \quad (4.15)$$

where $\frac{dT^{(t-\Delta t)}}{d\mathbf{x}}$ is calculated based on the last time step of the heat transfer equation (3.10) for which the same procedure is applied as for mechanical part of the solution. The details of the provided semi-analytical approach are presented in [112].

4.1.2 An optimization algorithm enriched with sensitivity analysis

One of the applications of local sensitivity analysis is to include local sensitivities information into optimization algorithm to accelerate optimization process. The approach is presented for particle swarm optimization (PSO) procedure.

The original (oPSO) method [41] is based on the mechanisms observed in the nature, namely on the behavior of the individuals' population. Particles (identified with the solutions of the problem considered) traverse the decision space (the area inhabited by the population) following the particle representing the best hitherto behavior, at the same time remembering the best position, in which they have been so far. Each

particle is described by two vectors: the position vector \mathbf{x} and the velocity vector \mathbf{v} . In each algorithm iteration, a new velocity vector is determined and the change of the particle position occurs based on it. Let us assume that the optimization functional is denoted by Φ . The procedure pseudo code is shown in the algorithm 4.1.

Algorithm 4.1 Particle swarm optimization algorithm (oPSO).

Require:

```

     $k \leftarrow 0$ 
     $R^k$  swarm initialization
1: repeat
2:   for  $i \in R^k$  do
3:     compute function  $\Phi^i$ 
4:   end for
5:   update the best position  $\mathbf{x}^b$  of  $R^k$ 
6:   for  $i \in R^k$  do
7:     update the best position  $\mathbf{x}^{i(b)}$  of  $i^{th}$  particle
8:     determine velocity vector  $\mathbf{v}^{i(k)}$ 
9:     determine position vector  $\mathbf{x}^{i(k)}$ 
10:  end for
11:   $k \leftarrow k + 1$ 
12: until not stop-condition for  $R^k$ 
13: return  $\mathbf{x}^b$ 

```

The initialization of the swarm R^k , $k = 0$, consists in giving the particles a random position and velocity. The position should be sampled from the permissible area. The size of this area should be considered when sampling the velocity. If the velocity is too low, the swarm will not be able to search the entire permissible area; while excessively high velocity makes, the particles 'bump' against the limits. The velocity vector changes according to the relationship:

$$\mathbf{v}^{i(k+1)} = w\mathbf{v}^{i(k)} + c_1r_1 \left(\mathbf{x}^b - \mathbf{x}^{i(k)} \right) + c_2r_2 \left(\mathbf{x}^{i(b)} - \mathbf{x}^{i(k)} \right), \quad (4.16)$$

where $\mathbf{x}^{i(k)}$ and $\mathbf{v}^{i(k)}$ are the position and the velocity of the i^{th} particle in the k^{th} iteration, respectively, \mathbf{x}^b defines the best position found so far by the whole swarm, $\mathbf{x}^{i(b)}$ is the best position found so far by the i^{th} particle, w is defined as the inertia coefficient; c_1 and c_2 are acceleration coefficients (called also learning coefficients), r_1 and r_2 are random numbers from the $[0, 1]$ interval of the uniform distribution. The new particle position is defined as follows:

$$\mathbf{x}^{i(k+1)} = \mathbf{x}^{i(k)} + \mathbf{v}^{i(k+1)} \quad (4.17)$$

After displacement of all the particles to their new position, they are subjected to assessment and the swarm leader is selected. The determination of the coefficients values affects the swarm behavior. The value of the inertia coefficient is usually selected from the $[0, 1]$ interval. A higher value is favorable for the global searching for the solution space, and a lower value for the local searching. Usually, this value is

constant throughout the entire optimization process. However, it also may change. Then, at the beginning, it assumes a high value, enabling global searching, and while approaching the maximum that is sought, it gradually decreases. Acceleration coefficients are usually equal and selected from the $[0, 2]$ interval. When selecting their values, the maximum velocities, which the particles should not exceed, should be considered. Exceeding of the maximum number of iterations or obtaining a satisfactory solution is taken as the criteria of the computation completion (stop criteria).

The oPSO was enriched by local sensitivity analysis. SA allows to apply some extra information on functional defined in the optimization task which can accelerate the algorithm convergence. In the modified PSO (mPSO), a correction vector \mathbf{v}_c^i is added to the velocity vector \mathbf{v}^i of i^{th} particle such that the particle moves toward potentially better areas. A correction vector requires to determine the neighborhood of i^{th} particle which is defined as:

$$N^i = \{i \in I : \|\mathbf{x}^i - \mathbf{x}^j\| < d\} \quad (4.18)$$

where I is a set of all population R indices, $d \geq 0$ is the constant describing the neighborhood. The correction vector \mathbf{v}_c^i of i^{th} particle is defined as:

$$\mathbf{v}_c^i = - \sum_{j \in N^i} \frac{\|\Phi(\mathbf{x}^j) - \Phi(\mathbf{x}^i)\|}{\|\mathbf{x}^j - \mathbf{x}^i\|^2} \cdot (\mathbf{x}^j - \mathbf{x}^i) \quad (4.19)$$

In addition, the uncertainty coefficient which describes accuracy of information included in the correction vector is determined:

$$\alpha^i = \frac{\sum_{j \in N^i} \|\mathbf{x}^j - \mathbf{x}^i\|}{|N^i| \cdot l} \quad (4.20)$$

where l is length of the decision space diagonal.

Therefore, the velocity vector (4.16) is modified and computed as:

$$\mathbf{v}^{i(k+1)} = w' \mathbf{v}^{i(k)} + c'_1 r_1 (\mathbf{x}^b - \mathbf{x}^{i(k)}) + c'_2 r_2 (\mathbf{x}^{i(b)} - \mathbf{x}^{i(k)}) + c'_3 r_3 \mathbf{v}_c^i \quad (4.21)$$

where \mathbf{v}_c^i is the correction velocity vector of i^{th} particle, w' is the inertia coefficient and c'_1, c'_2, c'_3 are acceleration coefficients modified according to information on the initial values and sensitivity analysis calculations. The values of these coefficients depend on the uncertainty coefficient (4.20):

$$\begin{aligned} \text{if } \alpha^i > \delta : & \quad w' = w, \quad c'_1 = c_1, \quad c'_2 = c_2, \quad c'_3 = 0 \\ \text{else} & \quad w' = w \sqrt{\frac{\alpha^i}{\delta}}, \quad c'_1 = c_1 \sqrt{\frac{\alpha^i}{\delta}}, \quad c'_2 = c_2 \sqrt{\frac{\alpha^i}{\delta}}, \quad c'_3 = c_3 \left(1 - \sqrt{\frac{\alpha^i}{\delta}}\right) \end{aligned}$$

where δ is the threshold of the sensitivity analysis activation.

Based on the new velocity vectors of the particles (4.21), the new positions are determined according to Equation (4.17). The mPSO procedure is presented in the algorithm (4.2).

Algorithm 4.2 The particle swarm optimization algorithm + sensitivity analysis (mPSO).

Require: $k \leftarrow 0$

R^k swarm initialization

d constant describing particles neighborhood

δ threshold for sensitivity analysis activation

```

1: repeat
2:   for  $i \in R^k$  do
3:     compute function  $\Phi^i$ 
4:   end for
5:   update the best position  $\mathbf{x}^b$  of  $R^k$ 
6:   for  $i \in R^k$  do
7:     update the best position  $\mathbf{x}^{i(b)}$  of  $i^{th}$  particle
8:     determine neighborhood  $N^i$ 
9:     determine correction vector  $\mathbf{v}_c^i$ 
10:    determine uncertainty coefficient  $\alpha^i$ 
11:    determine coefficients  $w', c'_1, c'_2, c'_3$ ,
12:    determine velocity vector  $\mathbf{v}^{i(k)}$  according to Equation (4.21)
13:    determine position vector  $\mathbf{x}^{i(k)}$ 
14:  end for
15:   $k \leftarrow k + 1$ 
16: until not stop-condition for  $R^k$ 
17: return  $\mathbf{x}^b$ 

```

The mPSO algorithm was tested for benchmark functions. Selected results are presented below. The effectiveness of oPSO and mPSO was compared for two benchmark functions: Rastrigin [139] and Rosenbrock [100], the two-dimensional searching space was limited to the intervals $[-1, 1] \times [-1, 1]$ and $[0, 2] \times [0, 2]$, respectively. The stop criterion was solution less than 10^{-5} , the maximum number of function evaluations was 2000. The results are shown in Table 4.1 and in Figure 4.1.

Table 4.1: Comparison of oPSO and mPSO results.

Function		mPSO		oPSO	
		No. of runs	Estimation	No. of runs	Estimation
Rastrigin	MIN	440	2.8060×10^{-7}	920	3.0274×10^{-7}
	AVE	734	0.0123	1356	0.0243
	MAX	2000	0.1225	2000	0.1216
Rosenbrock	MIN	340	9.9679×10^{-8}	860	3.0282×10^{-7}
	AVE	482	4.1418×10^{-6}	1086	4.2531×10^{-6}
	MAX	580	9.1182×10^{-6}	1440	9.4049×10^{-6}

In Figure 4.1 and Table 4.1 it is observed that the function values obtained by mPSO and oPSO are close to each other for both test functions. However, the number of function evaluations was much lower for mPSO. On average, that number dropped by 46% for the Rastrigin function and 56% for the Rosenbrock function. Determination

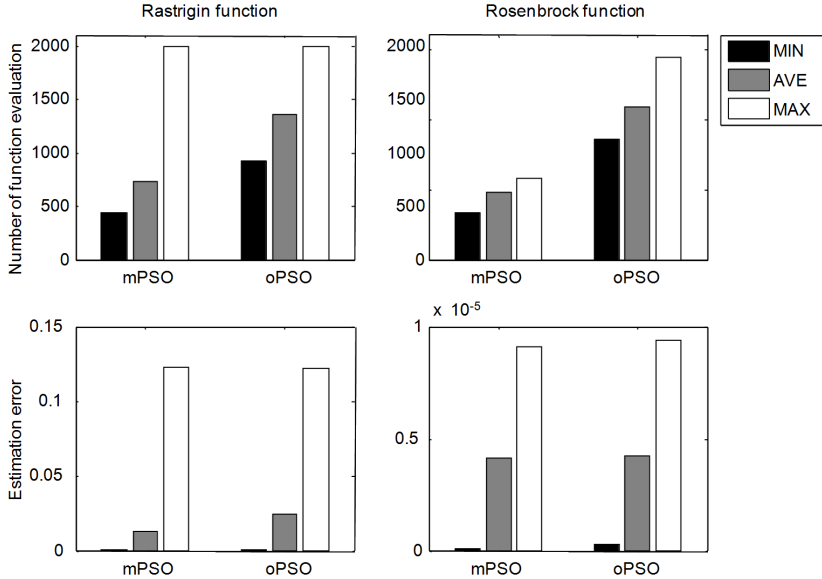


Figure 4.1: Comparison of oPSO and mPSO results.

of the global minimum or maximum for multimodal functions is never guaranteed, there is possibility that the optimization result is a local minimum/maximum instead of the global one. That behavior of the nondeterministic optimization procedure for multimodal function was tested, as well. The procedures were run 1000 times for the Rastrigin function. The oPSO algorithm stopped in the local minimum 113 times, whereas the mPSO stopped 181 times. Following the obtained calculation results, the mPSO method allows to reduce the number of function evaluation of the optimization procedure and reduce computation costs of the optimization but for multimodal functions the probability of the local minimum or maximum determination is slightly higher. The details of the investigation are presented in [128].

4.2 Global sensitivity analysis

As distinct from local sensitivities, the global ones estimate the effect of a parameter described with one quantity for the whole parameter domain. Global SA requires a definition of the following terms:

- expression which characterizes the measure of model output/outputs (it should be a scalar value),
- definition of the variation interval for each input parameter,
- selection of the points in the parameters domain (design of experiment techniques are applied),

- sensitivity measure - the sensitivities are estimated based on the model outputs measure variations caused by changes in the model parameters.

The first three items are the problems that are independent of the applied global SA algorithm. The last one, a sensitivity measure, is strictly related to the method.

If the model output is a time-dependent vector $\mathbf{y}(t)$, where t is time, the scalar expression describing the output has to be introduced. The measure can be defined as:

$$\tilde{y} = \int_{t_1}^{t_2} \|\mathbf{y}(t)\| dt \quad (4.22)$$

where $\|\cdot\|$ is the norm in the output space, or:

$$\tilde{y} = \int_{t_1}^{t_2} \|\mathbf{y}(t) - \mathbf{y}^*(t)\| dt \quad (4.23)$$

where \mathbf{y}^* is the *reference point* of the model calculated for the selected model conditions and assumptions. The reference point should be close to *the best* problem solution or, if such a solution is not known, close to the experimental conditions (physical, technological ones).

The difference between the measures (4.22) and (4.23) is presented in Figure 4.2.

The next problem is to define the variations intervals for each model parameter. If the model is not complex and the parameters are directly derived from physical laws, determination of the extreme points is relatively simple. This problem is non trivial if the parameters are coefficients of the phenomenological equations and their meaning is far from the physical background. Expert knowledge is helpful in this case. If the variation intervals are too narrow or too wide, sensitivity indices estimated with them can be weighed down with an error and, in consequence, the conclusion drawn with them will be improper.

Another problem is the selection of the points the model is run for and next, based on the outputs, sensitivity indices are calculated. There are three main sampling procedures commonly used:

- random sampling,
- importance sampling,
- Latin hypercube sampling.

To generate the points of the input vector $\mathbf{x} = [x_1, x_2, \dots, x_n]^T$, where $\mathbf{x} \in \mathbb{R}^n$, the corresponding probability distribution F_i of each component x_i of \mathbf{x} should be known.

If *random sampling* is applied, the set of k points is generated as follows:

$$\mathbf{x}^j = [x_1^j, x_2^j, \dots, x_n^j], \quad j = 1 \dots k \quad (4.24)$$

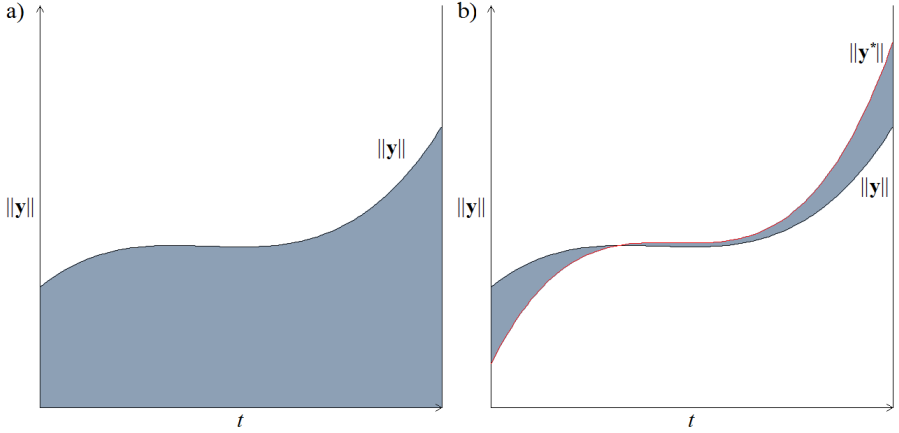


Figure 4.2: Comparison between two model output measures: a) for time-dependent output vector \mathbf{y} , b) for difference between output vector \mathbf{y} and the reference point \mathbf{y}^* .

where x_i^j component of \mathbf{x}^j is selected according to the probability distribution F_i and each point \mathbf{x}^j is selected independently of all the remaining points.

If more information is known about the input vector \mathbf{x} , especially if any subdomain of \mathbf{x} is more interesting, the *importance sampling* can be useful. In the importance sampling, the variation domain of \mathbf{x} is divided into p separable subintervals. Then, for the l subinterval k_l points are generated in consistency with the probability distribution F_i for each i^{th} component:

$$\mathbf{x}^j = \left[x_1^j, x_2^j, \dots, x_n^j \right], \quad j = 1, 2, \dots, \sum_{l=1}^p k_l \quad (4.25)$$

If one value is sampled for each subdomain, the set (4.25) is of the form:

$$\mathbf{x}^j = \left[x_1^j, x_2^j, \dots, x_n^j \right], \quad j = 1, 2, \dots, p \quad (4.26)$$

An example of the importance sampling is presented in Figure 4.3.

The idea of the coverage the whole input domain in a specific way was extended in the *Latin hypercube sampling* [78]. In this procedure the variational interval of each component x_i of \mathbf{x} input vector is divided into k subintervals of equal probability and the next random value is generated from each interval. The k values obtained for x_1 are randomly coupled with k values generated for x_2 . These k pairs of x_1 and x_2 are next combined with randomly selected k values of x_3 forming k triples. The procedure is continued till a set of k n -tuples is generated. The n -tuples are expressed as:

$$\mathbf{x}^j = \left[x_1^j, x_2^j, \dots, x_n^j \right], \quad j = 1, 2, \dots, k \quad (4.27)$$

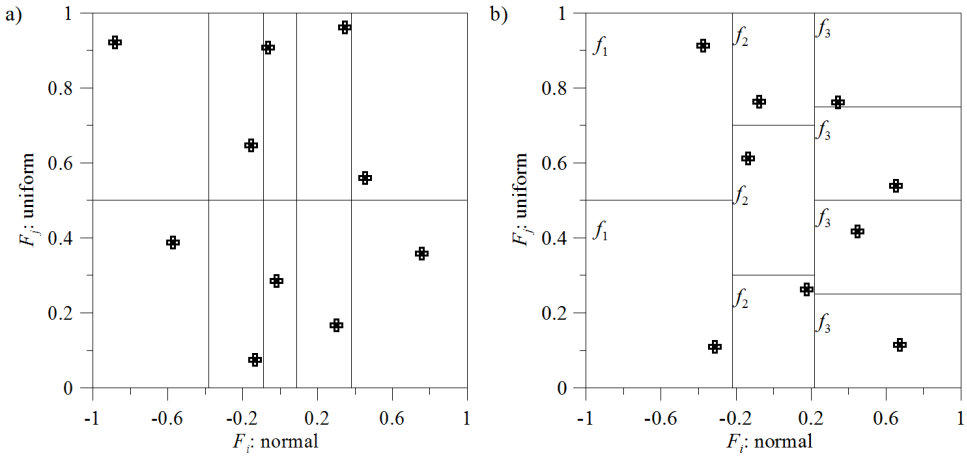


Figure 4.3: Examples of the importance sampling $p = 10$ for the input data x_i of the normal probability distribution function F_i and x_j of the uniform probability distribution function F_j , a) equal subintervals probability of 0.1, b) unequal subintervals probability of $f_1 = 0.2$, $f_2 = 0.1$, $f_3 = 0.06$.

and they constitute the Latin hypercube sampling (LHS). The pairing process is not unique and many LHSs can be obtained. Examples of LHSs are presented in Figure 4.4.

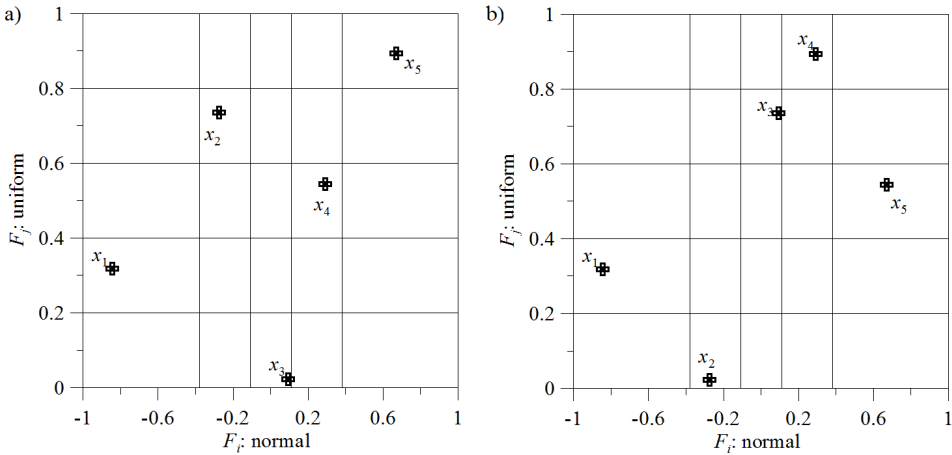


Figure 4.4: Examples of the Latin hypercube sampling $k = 5$ for the input data x_i of the normal probability distribution function F_i and x_j of the uniform probability distribution function F_j . Various pairing: plots a) and b).

To control the proper sampling of points in the variation domain, for each component of the input vector conformity of mean, standard deviation or quantiles plot with its

probability distribution should be investigated. Random sampling is a method which is convenient to implement, but it can be applied if the calculation of large number of model outputs is not of high computational costs. To avoid large sets of points, a better way is to use importance sampling. However, it is not trivial to determine the number of subintervals, the start and the end of each subinterval, as well as to estimate the probability for them. Another solution to reduce the cardinality of the sampling set is the application of the Latin hypercube sampling technique. This algorithm is often used to estimate the effect of input parameters defined by mean, conditional expected value and variation and for unbiased estimations. LHS gives reliable results if the number of generated points is low. It is also applied for calculations when information on probability distribution functions of input parameters is not available and importance sampling cannot be used.

4.2.1 An algorithm based on the Morris design

The term *screening design* characterizes the method of the input parameters domain processing. The methods of this group calculate the parameter sensitivities as the global indices and they search systematically the whole parameters domain - thus, they are called *screening methods*. The main idea of these algorithms is to investigate the model parameters, which have the biggest influence on variability of the model output, and to keep computational costs as low as possible. The methods deal with the question which model parameters are really important. The assumption of not high calculation costs makes these procedures estimate the importance of the input parameters qualitatively, not quantitatively. i.e. they state that one parameter is more important than another one. The methods were designed for processes of a large number of parameters. Identification problems in metal forming include up to 50 parameters, but the computational cost of the problems solvers is often very high. Following this, screening methods have found practical application in metal forming problems. Among various procedures, the One-At-a-Time (OAT) approach, originally developed by Morris [81], was selected. This technique investigates the impact of the variation of each parameter in turn. The OAT design is called a global sensitivity analysis, because the algorithm explores the entire space over which the parameters vary. In the algorithm, the term of parameter *main effect* is introduced and it is determined by computing a number of *local measures* at different points in the input space and next estimated by *mean value* and *standard deviation*. The key definitions and steps of Morris design are presented below.

Assumptions and definitions. Let \mathbf{x} be an n -dimensional vector of model parameters x_i . The primary assumption of the algorithm is that all x_i components are defined on $[0, 1]$ interval. In most practical problems x_i components are of various physical units and the parameters have to be rescaled to $[0, 1]$. Linear or logarithmic transformation can be applied. The conversion is necessary to compare the results obtained for various parameters. It is feasible only if estimated elementary effects are expressed with the same units for all parameters.

Let the components x_i , $i = 1 \dots n$, accept k values in the set $\{0, 1/(k-1), 2/(k-1), \dots, 1\}$. Then the parameters domain $\Omega \subseteq \mathbb{R}^n$ forms an n -dimensional k -level grid. Let Δ depend on k and describe the side length of the grid element:

$$\Delta = \frac{1}{k-1} \quad (4.28)$$

The *elementary effect* ξ_i of the i^{th} parameter at a given point \mathbf{x} calculated for \tilde{y} model output is defined as:

$$\xi_i(\mathbf{x}) := \frac{\tilde{y}(x_1, \dots, x_{i-1}, x_i + \tilde{\Delta}_i, x_{i+1}, \dots, x_n) - \tilde{y}(\mathbf{x})}{\Delta} \quad (4.29)$$

where \mathbf{x} is any value in the Ω domain such that the perturbed point $\mathbf{x} + \Delta$ is also in Ω , $\tilde{\Delta}_i = \Delta(x_{i,s} - x_{i,e})$ and $x_{i,s}$, $x_{i,e}$ are start and end points of parameter x_i variation interval, respectively. A finite distribution F_i for each parameter x_i is obtained by sampling \mathbf{x} in Ω . The number of elements of F_i is equal to $(k-1)k^{n-1}$.

Distribution F_i of elementary effects is described by *mean* μ and *standard deviation* σ . A mean characterizes the sensitivity of the model output with respect to i^{th} parameter. A high mean indicates that the parameter is important and it substantially influences the output. A high standard deviation implies that the parameter interacts with other parameters or its effect to the model is nonlinear.

The naive algorithm calculates in sequence r values from distribution F_i of each parameter x_i and in summary there are $2rn$ solver runs to determine elementary effects. Another, more effective procedure with the orientation matrix \mathbf{B}^* introduced to the algorithm was proposed by Morris [81]. The rows of the matrix \mathbf{B}^* represent input vectors \mathbf{x} and n corresponding model runs providing n elementary effects ξ_i , one for each parameter x_i , are computed for them. Thus, the dimension of the matrix \mathbf{B}^* is $(n+1) \times n$. The orientation matrix \mathbf{B}^* is randomly and independently selected r times. As a result, $r(n+1)$ model outputs are obtained forming a rn -elements set of F_i distribution for elementary effects ξ_i .

Construction of the matrix \mathbf{B}^* is listed in the algorithm 4.3. The algorithm 4.3 returns one orientation matrix \mathbf{B}^* such that every consecutive pair of the generated vectors - two consecutive rows of \mathbf{B}^* , differ for only one component. Any component i of the starting vector \mathbf{x}^* is increased or decreased by Δ exactly only once, enabling calculation of one elementary effect ξ_i for each parameter x_i .

In practical applications, it is convenient to use another algorithm of randomly selected orientation matrix \mathbf{B}^* , presented as the algorithm 4.4.

The algorithm for the estimation of mean μ_i and standard deviation σ_i of elementary effects ξ_i is printed in the algorithm 4.5.

The mean of elementary effects will be incorrect (underestimated) for the effects obtained simultaneously with positive and negative signs, therefore, instead of the

Algorithm 4.3 Construction of orientation matrix \mathbf{B}^*

Require: Randomly start vector \mathbf{x}^*

Ensure: Each component $x_i \in \{0, 1/(k-1), \dots, 1-\Delta\}$

- 1: Increase one or more of n components of \mathbf{x}^* with Δ such that the new vector $\mathbf{x}^{(1)}$ is still in Ω .
- 2: Calculate elementary effect $\xi_i(x^{(1)})$ following Equation (4.29):

$$\xi_i(\mathbf{x}^{(1)}) := \frac{\tilde{y}(x_1^{(1)}, \dots, x_{i-1}^{(1)}, x_i^{(1)} + \tilde{\Delta}_i, x_{i+1}^{(1)}, \dots, x_n^{(1)}) - \tilde{y}(\mathbf{x}^{(1)})}{\Delta} \quad (4.30)$$

if $\mathbf{x}^{(1)}$ is increased by $\tilde{\Delta}_i$, or

$$\xi_i(\mathbf{x}^{(1)}) := \frac{\tilde{y}(x_1^{(1)}, \dots, x_{i-1}^{(1)}, x_i^{(1)} - \tilde{\Delta}_i, x_{i+1}^{(1)}, \dots, x_n^{(1)}) - \tilde{y}(\mathbf{x}^{(1)})}{\Delta} \quad (4.31)$$

if $\mathbf{x}^{(1)}$ is decreased by $\tilde{\Delta}_i$.

- 3: $\mathbf{x}^{(2)} \leftarrow (x_1^{(1)}, \dots, x_{i-1}^{(1)}, x_i^{(1)} \pm \tilde{\Delta}_i, x_{i+1}^{(1)}, \dots, x_n^{(1)})$. Select the next vector $\mathbf{x}^{(3)}$ such that it differs from $\mathbf{x}^{(2)}$ for only one component j : either $x_j^{(3)} = x_j^{(2)} + \tilde{\Delta}_j$ or $x_j^{(3)} = x_j^{(2)} - \tilde{\Delta}_j$ and $j \neq i$. The elementary effect ξ_j of x_j parameter is then

$$\xi_i(\mathbf{x}^{(2)}) = \begin{cases} \frac{\tilde{y}(\mathbf{x}^{(3)}) - \tilde{y}(\mathbf{x}^{(2)})}{\Delta} & \text{if } \Delta > 0 \\ \frac{\tilde{y}(\mathbf{x}^{(2)}) - \tilde{y}(\mathbf{x}^{(3)})}{\Delta} & \text{if } \Delta < 0 \end{cases} \quad (4.32)$$

- 4: Repeat step 3 until $n+1$ vectors $\mathbf{x}^{(1)}, \mathbf{x}^{(2)}, \dots, \mathbf{x}^{(n+1)}$ are produced, forming a *trajectory* - one orientation matrix \mathbf{B}^*
 - 5: **return trajectory** $\mathbf{x}^{(1)}, \mathbf{x}^{(2)}, \dots, \mathbf{x}^{(n+1)}$ - matrix \mathbf{B}^*
-

elementary effect defined as (4.29), the absolute value of ξ_i is taken:

$$\xi_i(\mathbf{x}) := \left| \frac{\tilde{y}(x_1, \dots, x_{i-1}, x_i + \tilde{\Delta}_i, x_{i+1}, \dots, x_n) - \tilde{y}(\mathbf{x})}{\Delta} \right| \quad (4.34)$$

The results of the sensitivity of the model output with respect to the input model parameters expressed as the estimated mean of elementary effects are dependent on Δ value which is selected arbitrarily. This dependence rises with the non linearity of the model and the sensitivity calculations may be not reliable. Thus, the calculations with the Morris design algorithm are performed for various Δ and next the results are compared. The comparison is feasible for normalized quantities:

$$\tilde{\mu}_i = \frac{\mu_i}{\|\boldsymbol{\mu}\|} \quad \tilde{\sigma}_i = \frac{\sigma_i}{\|\boldsymbol{\sigma}\|} \quad (4.35)$$

where $\boldsymbol{\mu} = (\mu_1, \dots, \mu_n)$, $\boldsymbol{\sigma} = (\sigma_1, \dots, \sigma_n)$ are vectors of means and standard deviations calculated for all the input parameters x_i , $i = 1 \dots, n$.

If means and standard deviations computed for various Δ are close to each other, the sensitivities are properly estimated. If not, the value of Δ should be narrowed

Algorithm 4.4 A randomly selected orientation matrix \mathbf{B}^*

Require: Matrix $\mathbf{B} = (b_{ij})$ of $(n + 1) \times n$ dimension such that $b_{ij} = 0 \vee 1, i = 1, \dots, n, j = 1, \dots, n + 1$

Ensure: Every two columns of \mathbf{B} differ in only one element, e.g. \mathbf{B} can be defined as a strictly lower triangular matrix with values of 1.

1: Build diagonal n dimensional matrix \mathbf{D}^* such that

$$d_{ij}^* = \begin{cases} \pm 1 & i = j \text{ with equal probability} \\ 0 & i \neq j \end{cases}$$

2: Build random permutation matrix \mathbf{P}^* of $n \times n$ dimension such that every column contains one element equal 1 and others equal 0 and there are no two columns which have values of 1 at the same position. In particular $\mathbf{P}^* = \mathbf{I}$

3: Build the matrix \mathbf{B}^* following the formula:

$$\mathbf{B}^* = (\mathbf{J}_{n+1,1} \mathbf{x}^* + (\Delta/2) [(2\mathbf{B} - \mathbf{J}_{n+1,n}) \mathbf{D}^* + \mathbf{J}_{n+1,n}]) \mathbf{P}^* \quad (4.33)$$

where $\mathbf{J}_{n+1,1}$ and $\mathbf{J}_{n+1,n}$ are matrices with values 1 of dimensions appropriate $(n + 1) \times 1$ and $(n + 1) \times n$

4: **return** the orientation matrix \mathbf{B}^* providing a *trajectory* to calculate a single elementary effect ξ_i for parameter x_i

Algorithm 4.5 Estimation of mean μ and standard deviation σ

Require: r matrices \mathbf{B}^* generated with algorithm 4.3 or algorithm 4.4

Ensure: Matrices \mathbf{B}^* generated for a different starting point \mathbf{x}^* and provided r independent different trajectories for all n parameters x_i . It is equivalent to r values of distribution F_i for each parameter x_i

1: Estimate mean μ_i and standard deviation σ_i for each of x_i through the classic estimators for independent random samples

2: **return** mean μ_i and standard deviation σ_i estimated for each input model parameter x_i

down and the procedure is repeated. Another solution is to define Δ for each input parameter separately keeping in mind that the whole interval for each parameter should be screened (the value of r should be carefully examined).

4.2.2 Variance based methods

This section focuses on the methods of global sensitivity analysis derived from variance analysis [10, 99]. In particular, two algorithms were selected and presented: correlation ratio/importance measures [77, 38] and Sobol' technique [107]. The first itemized quantities are based on probability distributions and conditional variance of the model output which indicates the importance of an input parameter. The other one introduces the first order sensitivity indices that are equivalent to conditional variance.

Correlation ratios and importance measures

The measure of the input parameter importance can be expressed as *variance of the conditional expectation* (VCE) of model prediction. Let us assume that, with no loss of generality, there is one input model parameter x and the model output y is scalar. The importance of the parameter x can be evaluated with conditional probability distribution of the output y conditioned on x . The marginal distribution of Y is expressed with the conditional distribution of Y given x :

$$p_Y(y) = \int p_{Y|x}(y|x) p_X(x) dx \quad (4.36)$$

Analyzing Equation (4.36), one can conclude that the parameter x is important if for the fixed value of x the conditional variance of prediction is significantly reduced on the marginal prediction variance.

The notation used in Equation (4.36) is convenient because there are no assumptions of the functional relation between y and x , it can be applied to any model. Thus, let us consider the general analysis model of the n input parameters gathered in the vector \mathbf{x} defined as:

$$y = E(Y|\mathbf{x}) \quad (4.37)$$

where $E(Y|\mathbf{x})$ is the conditional expectation.

The prediction variance of Y is of the form:

$$\text{Var}(Y) = \text{Var}_{\mathbf{X}}(E(Y|\mathbf{x})) + E_{\mathbf{X}}(\text{Var}(Y|\mathbf{x})) \quad (4.38)$$

and

$$\begin{aligned} \text{Var}_{\mathbf{X}}(E(Y|\mathbf{x})) &= \int (E(Y|\mathbf{x}) - E(Y))^2 p_{\mathbf{X}}(\mathbf{x}) d\mathbf{x} \\ E_{\mathbf{X}}(\text{Var}(Y|\mathbf{x})) &= \int \int (y - E(Y|\mathbf{x}))^2 p_{Y|\mathbf{x}}(y) dp_{\mathbf{X}}(\mathbf{x}) d\mathbf{x} \\ E(Y|\mathbf{x}) &= \int y p_{Y|\mathbf{x}}(y) dy \end{aligned} \quad (4.39)$$

In Equation (4.38) the first component $\text{Var}_{\mathbf{X}}(E(Y|\mathbf{x}))$ is the *variance of the conditional expectation* VCE and the second one $E_{\mathbf{X}}(\text{Var}(Y|\mathbf{x}))$ is the residual part. The VCE is the variance of the conditional expectation of Y , conditioned on \mathbf{x} and it is a measure of the importance of \mathbf{x} . In particular, if the total variation in y is controlled by the variability in $E(Y|\mathbf{X} = \mathbf{x})$ while \mathbf{x} varies, it implies that the vector of the input parameters \mathbf{x} is very important. The residual part in Equation (4.38) measures extant variability in y of other unobserved inputs while \mathbf{x} is fixed.

The *correlation ratio* introduced by McKay [76] measures the magnitude of VCE in relation to prediction variance:

$$\eta^2 = \frac{\text{Var}_{\mathbf{X}}(E(Y|\mathbf{x}))}{\text{Var}(Y)} \quad (4.40)$$

Another measure, called the *importance measure*, was defined in [39] as:

$$\frac{\text{Var}_{\mathbf{X}}(E(\log Y|\mathbf{x}))}{\text{Var}(\log Y)} \quad (4.41)$$

where $E(\log Y|\mathbf{x})$ is estimated using linear regression for numerical robustness. Detailed information on the idea of correlation ratio and its extensions are presented e.g. in [76].

For numerical calculations, the correlation ratio defined in (4.40) for the input parameter x_i considered a random variable X_i , is estimated by a ratio of two estimators:

$$\tilde{\eta}^2 = \frac{\widetilde{\text{VCE}}(X_i)}{\widetilde{\text{Var}}(Y)} \quad (4.42)$$

where $\widetilde{\text{VCE}}(X_i)$ is the estimator of $\text{Var}_{X_i}(E(Y|X_i))$ and $\widetilde{\text{Var}}(Y)$ is the estimator of $\text{Var}(Y)$. Therefore, the procedures for computation of these estimators are required.

Determination of quantities from Equation (4.42) for the random variables X_i , $i = 1, \dots, n$, and the corresponding model inputs x_i , is performed using r -LHS of size m with r replicates. An LHS of size m for n model inputs is described with the matrix \mathbf{D}_0 :

$$\mathbf{D}^0 = [\mathbf{x}^1, \mathbf{x}^2, \dots, \mathbf{x}^n] \quad (4.43)$$

where \mathbf{x}^i , $i = 1, \dots, n$ represents an m -dimensional vector of x_{ji} values, $j = 1, \dots, m$, sampled from intervals of the same probability, and randomized within the positions in the vector. A \mathbf{D} for all r replicates is a r -LHS $_m$ matrix of the form:

$$\mathbf{D} = \begin{bmatrix} \mathbf{D}^1 \\ \mathbf{D}^2 \\ \vdots \\ \mathbf{D}^r \end{bmatrix} \quad (4.44)$$

where $\mathbf{D}^k = [\tilde{\mathbf{x}}^{1,k}, \tilde{\mathbf{x}}^{2,k}, \dots, \tilde{\mathbf{x}}^{n,k}]$, $k = 1, \dots, r$, and $\tilde{\mathbf{x}}^{i,k}$ is an independent permutation of the rows of the vector \mathbf{x}^i defined in Equation (4.43). The model outputs form the matrix $[y_{jk}]$, $j = 1, \dots, m$, $k = 1, \dots, r$ (each \mathbf{D}^k provides a vector of m outputs values \mathbf{y}^k). Now, the estimator of the output variance can be calculated as:

$$\widetilde{\text{Var}}(Y) = \frac{1}{mr} \sum_{j=1}^m \sum_{k=1}^r (y_j^k - \bar{y})^2 \quad (4.45)$$

where \bar{y} is the grand mean equal $\bar{y} = \frac{1}{mr} \sum_{j=1}^m \sum_{k=1}^r y_j^k$.

The variance of conditional expectation can be, as McKay suggested in [76], expressed by:

$$\widetilde{\text{VCE}}(X_i) = \frac{1}{m} \sum_{j=1}^m (\bar{y}_{j\cdot} - \bar{y}) - \frac{1}{mr^2} \sum_{j=1}^m \sum_{k=1}^r (y_j^{k,i} - \bar{y}_{j\cdot})^2 \quad (4.46)$$

where $[y_j^{k,i}]$ is obtained by fixing m quantities of the i^{th} column, corresponding to the parameter x_i in all r replicates, to the values from the i^{th} column of the matrix \mathbf{D}^0 , $\bar{y}_{j\cdot} = \frac{1}{r} \sum_{k=1}^r y_j^k$ are the means calculated for this matrix.

Finally, the correlation ratio η^2 for x_i is estimated with Equation (4.42) by inserting Equations (4.45) and (4.46) into it. After some transformations, the value of $\tilde{\eta}^2$ is given by:

$$\tilde{\eta}_i^2 = \frac{r \sum_{j=1}^m (\bar{y}_j - \bar{y})^2 - \frac{1}{r} \sum_{j=1}^m \sum_{k=1}^r (y_j^{k,i} - \bar{y}_j)^2}{\sum_{j=1}^m \sum_{k=1}^r (y_j^k - \bar{y})^2} \quad (4.47)$$

The estimator defined as (4.47) is resistant to bias induced by the sample design, but its disadvantage is that it produces negative values in some cases. McKay in [77] proposed another formula for the estimation η^2 :

$$\tilde{\eta}_{i,bias}^2 = \frac{r \sum_{j=1}^m (\bar{y}_j - \bar{y})^2}{\sum_{j=1}^m \sum_{k=1}^r (y_j^k - \bar{y})^2} \quad (4.48)$$

Although the correlation ratio determined with Equation (4.48) includes bias, but by increasing the number of replicates this problem is mostly solved.

The procedure of computing the estimated values of correlation ratio η^2 is listed in the algorithm 4.6.

Algorithm 4.6 The estimation of correlation ratios η_i^2 for parameter x_i

Require: Matrix \mathbf{D}^0 of r -LHS of size m defined by (4.43)

- 1: Generate the design matrix \mathbf{D} as described in Equation (4.44)
 - 2: Calculate grand mean \bar{y}
 - 3: Estimate variance $\text{VAR}(Y)$ with Equation (4.45)
 - 4: **for** each parameter $x_i, i = 1 \dots n$ **do**
 - 5: Calculate model outputs $\left[y_j^{k,i} \right]$
 - 6: Calculate means \bar{y}_j .
 - 7: Estimate $\tilde{\eta}^2$ with Equation (4.47) or (4.48)
 - 8: **end for**
 - 9: **return** the estimated correlation ratios η_i^2 for all the parameters x_i
-

The algorithm 4.6 for calculation of correlation ratios for all input parameters x_i requires $rm(n+1)$ model runs and it is quite computationally expensive. The algorithm of Sobol' provided in the next section presents lower computational cost.

Sobol' method

Sobol' in [107] developed the method of the global SA based on the variance analysis and the Monte Carlo algorithm. Let us assume that the domain of the input model parameters $x_i, i = 1, \dots, n$, is defined as an n -dimensional cube Ω :

$$\Omega = \{ \mathbf{x} : 0 \leq x_i \leq 1 \quad \forall i = 1, \dots, n \} \quad (4.49)$$

Let the function $y = y(\mathbf{x})$ represents a model. Sobol' defined the decomposition of $y(\mathbf{x})$ as the sum of the increasing dimensionality addends:

$$y(x_1, \dots, x_n) = y_0 + \sum_{i=1}^n y_i(x_i) + \sum_{1 \leq i < j \leq n} y_{ij}(x_i, x_j) + \dots + y_{1,2,\dots,n}(x_1, \dots, x_n) \quad (4.50)$$

The decomposition (4.50) is held if y_0 is constant and the integrals of every addend over its own variables is zero:

$$\int_0^1 y_{i_1, \dots, i_s}(x_{i_1}, \dots, x_{i_s}) dx_{i_k} = 0 \quad \forall k : 1 \leq k \leq s \quad (4.51)$$

From (4.50) and (4.51) it is concluded that all the addends in (4.50) are orthogonal:

$$\int_{\Omega} y_{i_1, \dots, i_s}(x_{i_1}, \dots, x_{i_s}) y_{j_1, \dots, j_k}(x_{j_1}, \dots, x_{j_k}) d\mathbf{x} = 0 \quad \forall (i_1, \dots, i_s) \neq (j_1, \dots, j_k) \quad (4.52)$$

and

$$y_0 = \int_{\Omega} y(\mathbf{x}) d\mathbf{x} \quad (4.53)$$

Sobol' in [107] proved that the decomposition (4.50) is unique and all the decomposition addends can be evaluated as multidimensional integrals:

$$\begin{aligned} y_i(x_i) &= -y_0 + \int_0^1 \dots \int_0^1 y(\mathbf{x}) d\mathbf{x}_{\sim i} \\ y_{ij}(x_i, x_j) &= -y_0 - y_i(x_i) - y_j(x_j) + \int_0^1 \dots \int_0^1 y(\mathbf{x}) d\mathbf{x}_{\sim (ij)} \end{aligned} \quad (4.54)$$

where $d\mathbf{x}_{\sim i}$ and $d\mathbf{x}_{\sim (ij)}$ denote integration over all the variables except x_i and x_i, x_j , respectively.

Bearing in mind the consideration presented above, the total variance is of the form:

$$\widetilde{\text{Var}} = \int_{\Omega} y^2(\mathbf{x}) d\mathbf{x} - y_0^2 \quad (4.55)$$

and partial variances are estimated based on the terms in Equation (4.50):

$$\widetilde{\text{Var}}_{i_1 \dots i_s} = \int_0^1 \dots \int_0^1 y_{i_1 \dots i_s}^2(x_{i_1} \dots x_{i_s}) dx_{i_1} \dots dx_{i_s} \quad (4.56)$$

where $1 \leq i_1 < \dots < i_s \leq n$, $s = 1, \dots, n$. Squared and integrated over Ω Equation (4.50) gives:

$$\widetilde{\text{Var}} = \sum_{i=1}^n \widetilde{\text{Var}}_i + \sum_{1 \leq i < j \leq n} \widetilde{\text{Var}}_{ij} + \dots + \widetilde{\text{Var}}_{1,2,\dots,n} \quad (4.57)$$

Thus, the sensitivity measures $S_{i_1 \dots i_s}$ are defined by:

$$S_{i_1 \dots i_s} = \frac{\widetilde{\text{Var}}_{i_1 \dots i_s}}{\widetilde{\text{Var}}} \quad (4.58)$$

S_i is called the *first order sensitivity index* for the parameter x_i and it measures the main effect of x_i on the model output. S_{ij} , $i \neq j$, is the *second order sensitivity index* and it measures the interacted effect of the two parameters x_i and x_j on the model output. The higher order sensitivity indices can be defined in the same way.

The Sobol's algorithm is listed in the algorithm 4.7. The multidimensional integration is performed with the Monte Carlo method [22], hence the efficiency of Sobol's algorithm depends mostly of efficiency of the Monte Carlo procedure.

Algorithm 4.7 Computation of Sobol' sensitivity indices S_i of the first order

Require: Rescaled model input parameters space to n -dimensional unit cube Ω

- 1: Calculate addend y_0 of (4.50) with Equation (4.53)
 - 2: Calculate total variance $\widetilde{\text{VAR}}$ with Equation (4.55)
 - 3: **for** each input parameter $x_i, i = 1 \dots n$ **do**
 - 4: Calculate partial variance $\widetilde{\text{VAR}}_i$ with Equation (4.56)
 - 5: Determine the sensitivity index S_i according to Equation (4.58)
 - 6: **end for**
 - 7: **return** computed sensitivity indices S_i for all input parameters x_i
-

4.3 The implementation of sensitivity analysis algorithms

Within the work, sensitivity analysis software was developed and implemented. All methods presented in this chapter were included in this application.

There are many applications with the implemented methods of sensitivity analysis, e.g. the commercial one: MATLAB numerical computing environment [75] or STATISTICA software [110], through plug-ins for Excel worksheet up to many open-source and shareware applications. The commercial software is dedicated to a broad multitude of customers and the implemented algorithms include a lot of options. The second group of programs is dedicated to solve some specific problems. In both cases it is almost impossible to employ the existing applications to identification problems in metal forming and to keep the convenience of computations. Thus, within the work, software for sensitivity analysis was developed.

The application provides the following functionalities:

- local sensitivity algorithm based on the brute-force method: left-handed, right-handed and central finite-differences schemes are available,

- algorithms of the global sensitivity methods: Morris design, McKay algorithm, Sobol' method,
- sampling algorithms: random, importance, Latin hypercube sampling,
- simple selection of the parameters for analysis,
- interface for communication with inverse problem software,
- definition of new goal functions of inverse problem,
- interface to run external solvers provided as *dll* libraries or *ready-to-run* programs.

The software was implemented in mixed C++ and Fortran languages and it can be run in both Unix/Linux and Windows systems. The procedures are able to be easily modified if there are any requirements of the considered problem. Moreover, the home-made application favors better understanding of the performed computations and an accurate, more detailed analysis of the obtained results. All the sensitivity calculations presented in Chapter 6 were performed with the developed software.

5 A strategy for the identification of the model parameters

The main steps of the numerical modeling of physical phenomena were listed at the beginning of the Chapter 3. In this chapter the solution of identification problem of material properties or/and initial and boundary conditions is presented. It is assumed that the mathematical model describing physical phenomena under consideration is properly defined and the method of solving the equations of the mathematical model is well established. The mathematical background and the formal definition of the identification problem was presented in section 3.3 and numerical solutions for some specific cases are described in section 3.6. There are still methods dedicated to solving a large group of problems that are not fully mathematically proved or with some open questions of the solution properties, as it was mentioned in the last paragraph *Selected practical aspects and problems* of section 3.6. Here, in Chapter 5, there is an attempt to solve such a kind of problems, based on investigated, well established algorithms aided with the methods of sensitivity analysis presented in Chapter 4. The combination of the developed procedures allowed to propose the method called *The parameters identification strategy* presented in the algorithm 5.1.

The initial step of the algorithm 5.1, called *the Require*, consists of three items: (a), (b) and (c). The first one, (a), is the problem description. It includes all the physical phenomena characterizing the considered problem, $\tilde{x} \in X$ represents input data including the model parameters, $K : X \rightarrow Y$ is a mapping and $y \in Y$ is the model output. The item (b) is the problem solver. To solve the equations defined in (a), first an analytical solution is looked for. If it does not exist, numerical methods are applied. For K - differential operator, the problem is discretized and solved in the finite dimensional space. Therefore, the solver is denoted as $\tilde{K}(\tilde{\mathbf{x}}) = \mathbf{y}$, where vectors $\tilde{\mathbf{x}}$ and \mathbf{y} belong to the finite dimensional spaces. The last item, (c), involves physical experiments, which are sources of the data gathered in \mathbf{y}^δ . The experimental data are the quantities derived right from physical measurements, not processed. The problem description from item (a) should be close to the conditions of the performed experiments to the obtained model output \mathbf{y} consistent with the experimental data \mathbf{y}^δ .

Statement no. 1 of the algorithm 5.1. The sensitivity analysis (SA) is applied to the solver in case of a modification of the original model, i.e. introducing new equations describing material properties and boundary/initial conditions, or extending the model with equations defining additional phenomena. Then SA is useful in model calibration and verification if the model outputs are consistent with physical predictions and if changes of the parameters of the newly introduced equations influence the model outputs (more information on the SA application was presented at the beginning of the Chapter 4).

Algorithm 5.1 The parameter identification strategy

Require:

- (a) Problem description: $K\tilde{x} = y$
 - (b) Solver of the problem: $\tilde{K}\tilde{\mathbf{x}} = \mathbf{y}$
 - (c) Set of the measured quantities \mathbf{y}^δ
- 1: Perform sensitivity analysis of the problem solver $\tilde{K}\tilde{\mathbf{x}} = \mathbf{y}$
 - 2: Determine the set of parameters \mathbf{x} to be identified: $\tilde{\mathbf{x}} = (\mathbf{x}, \mathbf{p})$,
 $\tilde{K}(\mathbf{x}, \mathbf{p}) = \mathbf{y}$
 - 3: Specify the inverse problem $\tilde{K}^\wedge(\mathbf{y}, \mathbf{p}) = \mathbf{x}$
 - 4: **if** \tilde{K}^\wedge is a *regularizator* in terms of the definition 3.4.1 **then**
 - 5: Determine vector \mathbf{x}^* by solving the equation $\tilde{K}^\wedge(\mathbf{y}^\delta, \mathbf{p})$
 - 6: **else**
 - 7: Define *least-square problem* of the following form:
 $\tilde{K}^\wedge := \Phi(\mathbf{x}, \mathbf{p}) = \left\| \tilde{K}(\mathbf{x}, \mathbf{p}) - \mathbf{y}^\delta \right\|^2$
 - 8: Perform sensitivity analysis of the functional Φ with respect to the components of vector \mathbf{x}
 - 9: Estimate the minimum \mathbf{x}^* of the functional Φ with respect to vector \mathbf{x} :
 $\Phi(\mathbf{x}^*, \mathbf{p}) = \min_{\mathbf{x}} \Phi(\mathbf{x}, \mathbf{p})$
 - 10: **end if**
 - 11: **return** Vector of identified parameters \mathbf{x}^*
-

Statement no. 2 of the algorithm 5.1. Vector $\tilde{\mathbf{x}}$ is composed of two vectors $\tilde{\mathbf{x}} = (\mathbf{x}, \mathbf{p})$, where \mathbf{x} is the vector of the model parameters/inputs to be identified and \mathbf{p} is the vector of the remaining model inputs. From the results of SA performed in step 1, there is certainty that the model is sensitive enough to the parameters which are going to be identified.

Statement no. 3 of the algorithm 5.1. In this step, the inverse task is defined, especially the inverse operator \tilde{K}^\wedge is constructed according to the guidelines presented in Chapter 3. It should be highlighted that the construction of the inverse operator \tilde{K}^\wedge is not a trivial task and for many complex solvers \tilde{K} it is not possible to define operator \tilde{K}^\wedge .

Statement no. 4 of the algorithm 5.1. The form of the inverse operator specified in step 3 is tested whether it is a *regularizator* in terms of the definition 3.4.1. If the condition is true, it is possible to use one of the just developed and well-established algorithms dedicated to inverse problems. Then, there is certainty that the obtained solution is unique and proper, and the identification task is solved. Otherwise, step no. 7 is executed.

Statement no. 7 of the algorithm 5.1. The following attempt is applied - the functional Φ is defined for the inverse operator \tilde{K}^\wedge :

$$\Phi(\mathbf{x}, \mathbf{p}) = \left\| \tilde{K}(\mathbf{x}, \mathbf{p}) - \mathbf{y}^\delta \right\|^2 \quad (5.1)$$

equipped with the Euclidean norm as a rule, but another norm can be used, as well. Such formulation invokes transformation to the optimization task. Since the solver of the original problem \tilde{K} is not linear with respect to the vector of the identified inputs \mathbf{x} , there is no guarantee that minimization of the functional Φ will result in one solution. The problem is not well-posed in the sense of the definition 3.3.1.

Thus, in *statement no. 8* of the algorithm 5.1 investigation of the functional Φ with respect to vector \mathbf{x} is performed with the sensitivity analysis methods (presented in Chapter 4). The SA provides substantial information on the dependence $\Phi - \mathbf{x}$ like information on the importance of the parameters (the components of vector \mathbf{x}) in relation to Φ and it allows to select an appropriate optimization approach and the optimization procedure. The SA results can be used as the input information for the optimization algorithm (e.g. the elimination of the parameters of the lowest importance), as the preliminary step of the optimization to generate the start points or the SA algorithm can be coupled with the optimization procedure to accelerate it. More applications of SA for optimization are listed at the beginning of Chapter 4. All these treatments lead to decreasing the complexity of the optimization task and to increasing the reliability of the solution.

Statement no. 9 of the algorithm 5.1 - optimization. The optimization task can be defined as a one- or multi- criteria optimization. Nondeterministic algorithms or deterministic algorithms with multi-start are used as optimization methods to obtain not one solution (due to the lack of the assumption of a unique solution) but the vector of the results. *Statement no. 11* of the algorithm 5.1. As a result, the algorithm returns the *optimal* parameters \mathbf{x}^* of the model.

The developed algorithm 5.1 of the identification strategy was applied to various problems of metal forming. The obtained results are presented in Chapter 6.

6 Case studies

The chapter provides solutions for the identification problems of metal forming with the methods presented in Chapters 3 and 4, particularly with the developed algorithm 5.1 of the identification strategy described in Chapter 5. The problems, being inverse tasks defined for differential partial equations, are ill-posed, as presented in section 3.3. Therefore, regularization methods are required to estimate their solutions. Regularization for the equation $\|Kx - y\|$, where K is an operator between Hilbert spaces X and Y (see section 3.4), transforms the equation to the Gaussian normal form (3.23): $K^*Kx = K^*y$. The approach leads to a minimization problem of the functional $\Phi := \|Kx - y\|^2$ (the details are included in section 3.5).

The case studies are presented in the order of the performed research and the development of the sensitivity analysis methods adopted to identification problems of the modeling of metal forming processes. In the first example, the identification problem of rheological and friction parameters is considered. That problem was investigated in the author's PhD dissertation [133] and next it was continued for a wide class of rheological equations and various materials. However, the results were equivocal, many sets of parameters were obtained with the same value of the optimization functional while the optimization procedures were started from various points or non-deterministic algorithms were applied. That was the reason for the search of the methods which would allow to clarify the equivocal observations. The investigations resulted in the selection of the sensitivity analysis to support the problem of the parameters identification. Due to the original problem of rheological or friction identification, the parameters were just estimated, local sensitivity algorithms, presented in Chapter 4, section 4.1, were applied to estimate the importance of the parameters and to estimate the solution. To search for the minimum of the functional defined in the identification task, a modified with sensitivity results non-gradient optimization procedure, gradient algorithms with semi-analytical sensitivity coefficients (see section 4.1.1) and an enriched non-deterministic method (see 4.1.2) were used.

A local sensitivity analysis approach is also sufficient for models of not very high computational costs or in case when sensitivity is considered for small intervals of the parameter variability. As an example, the identification problem of quantitative fracture criteria was provided in the case studies. Sensitivity analysis allowed to estimate the experimental and material parameters which strongly influence the test and it supported the design of the fracture criterion critical value as the function of the selected parameters.

In the following years, the application of sensitivity methods to identification problems of new models included in the simulations of the metal forming processes

was developed. Therefore, global sensitivity algorithms: screening design methods, algorithms based on the analysis of variance and Sobol' algorithm, were studied and adjusted for the metal forming problems. Their description is provided in Chapter 4, section 4.2. One of the example of the application is the identification problem of the strain localization model. Global sensitivity algorithms were used to validate the applicability of the experiment and the selected model responses in the identification procedure. Another case study is the identification problem of the material phase transformation model of laminar cooling or annealing, combined with the finite element method for modeling of the rolling process. These models were applied to simulate the strip production cycle. Due to a large number of model parameters and high computational costs, global sensitivity algorithms were applied to identify the parameters of the highest influence on the model outputs and the functional defined in the identification task. Sensitivity analysis allowed to reduce the dimension of the parameters domain and decrease calculation costs of the identification.

Selected identification case studies and the application of various sensitivity analysis methods as a supporting tool for the parameter identification procedure are presented in this chapter.

6.1 Rheological and friction models

The accuracy of the numerical modeling of metal forming processes depends, to a large extent, on the precise description of material properties and boundary conditions. The identification of quantities that define the material and boundary conditions during deformation is a crucial problem to obtain reliable numerical results. Therefore, this section deals with the problem of the identification of the material plastic properties and mechanical boundary conditions in the numerical modeling of the metal forming processes.

6.1.1 Objectives of the work

The main objective of the work was to determine the parameters of rheological and friction models for:

- cold and hot forming processes,
- various equations describing the flow stress of the material,
- a wide range of plastometric tests.

The computations were carried out with the identification strategy algorithm 5.1 provided in Chapter 5. In the algorithm, the identification task is transformed to the minimization problem. Thus, an increase in the robustness and efficiency of the calculations was the next work objective and that attempt was made by:

- a modification of classic non-gradient optimization algorithms with the results of the local sensitivity analysis performed with the methods presented in 4.1,

- the application of the gradient optimization method with semi-analytical sensitivity coefficients (see section 4.1.1),
- the development of a two-step identification procedure,
- a modification of the definition of the functional defined in the optimization task - the application of the multicriterion optimization.

Since the accuracy of the parameters estimation depends on the sensitivity of the model output to the identified parameters, sensitivity analysis was performed, which was the next objective of the work. The following calculations were performed:

- sensitivity of the models outputs with respect to the process parameters and the rheological model parameters,
- sensitivity of the inverse analysis results to the process parameters.

The sensitivity analysis results allowed to estimate suitability of the plastometric test type for inverse calculations and sensitivity of those calculations with respect to the process parameters or parameters determined in another experiment. The local sensitivity procedures described in Chapter 4, section 4.1 were used, considering the importance of the parameters, and they were investigated close to the point searched with the optimization algorithms.

This case study is the result of several years' work on the identification of rheological and friction model parameters originated from the author's PhD thesis [133]. The work was continued and presented in a number of papers, see [120, 29, 118, 117, 96, 124, 125, 126, 131].

6.1.2 The experiments

The first step of the identification algorithm 5.1 is to perform an experiment for the measured values to compare them to the calculated results obtained from the numerical model of the experiment ("Require", item c of the algorithm 5.1). The identification of the material rheological parameters is based on plastometric tests. Thus, the following plastometric tests are performed: the uniaxial compression of cylinders (UC), the compression of rings (RC), the plane strain compression (PSC), the plane strain compression in channel die (PSCc) and the compression of cubes (CC). A schematic illustration of various types of plastometric tests is presented in Figure 6.1.

In the presented investigations, two sets of experiments were carried out. The first set included hot tests for carbon-manganese steel containing 0.16%C, 0.43%Mn, 0.23%Si, 0.006%P, 0.015%S, 0.01%Cr, 0.03%Cu and 0.001%Nb. Three types of tests were investigated: UC, RC and PSC. Two different dimensions of samples were used in the PSC tests. All of the tests were performed in the same conditions of strain rate and temperature: $\dot{\epsilon} = 0.1 \text{ s}^{-1}$, 1 s^{-1} and 10 s^{-1} and $T = 900^\circ\text{C}$, 1000°C and 1100°C . The dimensions of the samples are given in Table 6.1. The width of the platen in the PSC tests was 10 mm for larger samples (PSC-L) and 5 mm for small samples

(PSC-S). Graphite foil with a nickel-based lubricant was used in all the hot compression tests. The tests were performed on the Gleeble 3800 simulator in the Institute for Ferrous Metallurgy in Gliwice. The second set of experiments included cold tests for copper. The UC tests were performed on the Gleeble 3800 simulator and on the INSTRON 4502 testing machine at Akademia Górniczo-Hutnicza in Kraków. The dimensions of the samples are given in Table 6.2. The strain of 0.8 was reached in all the tests except for the ring compression tests, where the strain of 0.5 was applied. The graphite-based paste was used as a lubricant in all the cold compression tests. Notation in both tables: d^{out} - outer diameter, d^{in} - inner diameter, h - height, l - length (perpendicular to the platen in the PSC and along the channel in the PSCc), b - width (along the platen in the PSC and perpendicular to the channel in the PSCc).

The load-displacement relationships were recorded during each test, and those data were used as an input for the identification procedure 5.1. The shape of the samples after the ring compression and the uniaxial compression were measured, as well, and that information was an additional input for the evaluation of both friction and rheological parameters. A detailed description of the experiments is given in [89, 29].

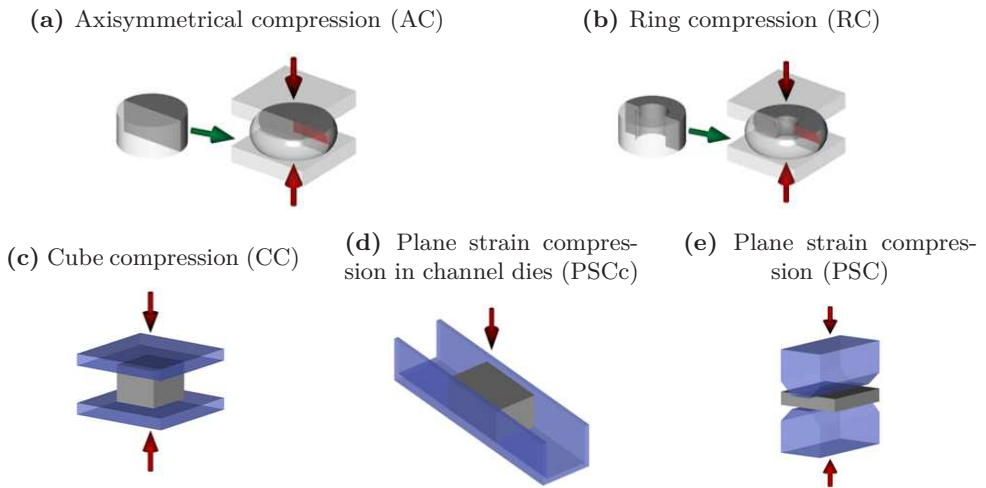


Figure 6.1: Schematic illustrations of various types of plastometric tests.

Table 6.1: Dimensions of the hot compression tests samples, mm.

Test	d^{out}	d^{in}	h	Test	h	l	b
RC	14.0	7.2	4.7	PSC-L	15	20	35
UC	10	-	12	PSC-S	10	15	20

Table 6.2: Dimensions of the cold compression tests samples, mm.

Machine	Test	h	b	l	Test	d^{out}	d^m	h
Gleeble	PSCc_I	8	10	12	UC	12	-	19
	PSCc_II	8	10	20	RC_I	14	7	4.69
Instron	PSCc_II	8	10	20	RC_II	12	5.9	4
	PSCc_III	12	10	16				
	CC	15	15	15				

6.1.3 The numerical model of the plastometric test

One of the assumptions of the identification procedure 5.1, "Require" item b, is that the model of the experiment is given. The plastometric test is described as a rigid-plastic thermomechanical problem [46, 90] and the main equations of such a problem is provided in Chapter 3, section 3.1. The presented partial differential equations are solved with the finite element method [46, 90]. The friction on the surface sample-tool was described with the Chen-Kobayashi equation (3.9). The model is used for the simulation of axisymmetrical compression tests, as well as the plane strain compression tests. The latter, in spite of its name, involves a three-dimensional state of strains. This is due to some spread in the PSC test (see Figure 6.2). The inclusion of a 3D finite element solution to the identification procedure is possible [23, 121] but it requires very long computing times. The computations performed on a middle-class personal computer take from half a minute to one minute for one axisymmetrical compression test, while the calculations for the plane-strain compression lasted 10 times longer for one test. 3D computations for one plastometric test are even longer. One should remember that the time of the simulation depends on the mesh density, as well. In the research, which composes the identification of a substantial number of the tests, using the 3D solution was not practical. Therefore, a 2D model was used for the simulation of the PSC test but corrections proposed in [52] were applied to obtain good accuracy of the results. The idea of these corrections is explained below.

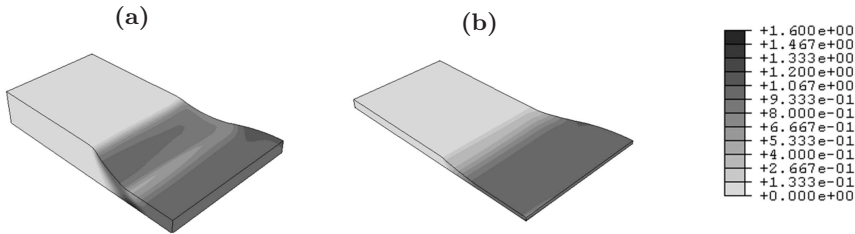


Figure 6.2: The plane strain compression sample after deformation, with some spread seen in the center. The results of the finite element method simulation of the strain distribution for the initial thickness of (a) 10 mm and (b) 2.5 mm.

The objective of the analysis in [52] was to compare the 2D and 3D simulations of the PSC tests. Three cases were considered: i) simulation of the PSC tests using the

2D code, ii) a simulation of the PSC tests using the 3D code, iii) a 3D simulation of the PSC test with an additional tool which constrained the spread. The friction coefficient on that additional vertical tool was assumed as zero. There was no heat exchange between the work-piece and this tool, either. The objective of the last set of the simulations was to evaluate the reason for the errors in the 2D simulation. These computations would explain whether the errors are due to neglecting the spread or due to the differences in the state of stress.

Since the results obtained for different tests were similar, one test only (for the nominal temperature 1000°C and the strain rate 1⁻¹) is discussed here. Figure 6.3a shows the loads measured and predicted for the friction coefficient $m_c = 0.05$. It is observed that, for the selected flow stress function, the loads predicted by the 3D solution coincide with the experimental results very well. The 2D model overestimates loads at the beginning of the compression. It is due to the influence of the rigid ends, which is stronger when the spread is constrained. The predictions of the 2D model underestimate the loads significantly in the final stage of the process. This is caused by the fact that the spread is neglected in the 2D solution and the calculated area of contact is lower than in the real process (symbol \circ in Figure 6.3a). Thus, the spread correction for the 2D model was proposed. It is based on the current width of the sample, which is calculated as [52]:

$$b = b_0 \left[1 + C - C \left(\frac{h}{h_0} \right)^{0.18} \right], \quad C = \frac{\frac{b_f}{b_0} - 1}{1 - \left(\frac{h_f}{h_0} \right)^{0.18}} \quad (6.1)$$

where b_0 is the initial width, h_0 is the initial height, b_f is the experimental final width, h_f is the experimental final height, b is the current width, h is the current height, C is the spread coefficient. When the correction accounting for the spread is introduced into the 2D data, the results, which are reasonably close to the experiment, are obtained (the symbol \triangle in Figure 6.3a). The explanation given above is confirmed by the results of the simulation using the 3D code for the PSC test with additional tools preventing the spread (the symbol \square in Figure 6.3a). It is seen that these results are close to those obtained from the 2D solution. It confirms the conclusion that the differences in the contact area are responsible for underestimating the loads by the 2D model in the final stage of compression.

The calculated distributions of strains in the vertical plane of symmetry for the three considered simulations are shown in Figure 6.3b. It is seen in this figure that, due to the spread, the length of the sample is different for the 2D and 3D simulations. The essential improvement of the agreement between the 2D results and the experimental data can be obtained when the 2D loads are multiplied by a factor connected with the spread. This solution with the 2D model will supply the values of the parameters which can be used as the starting point for further identification using the 3D model.

A similar correction was proposed in [146] for the channel test. The scheme of PSCc test is shown in Figure 6.4. 2D and 3D simulations of the plane strain compression in channel dies show that the differences in loads calculated by the two models depend

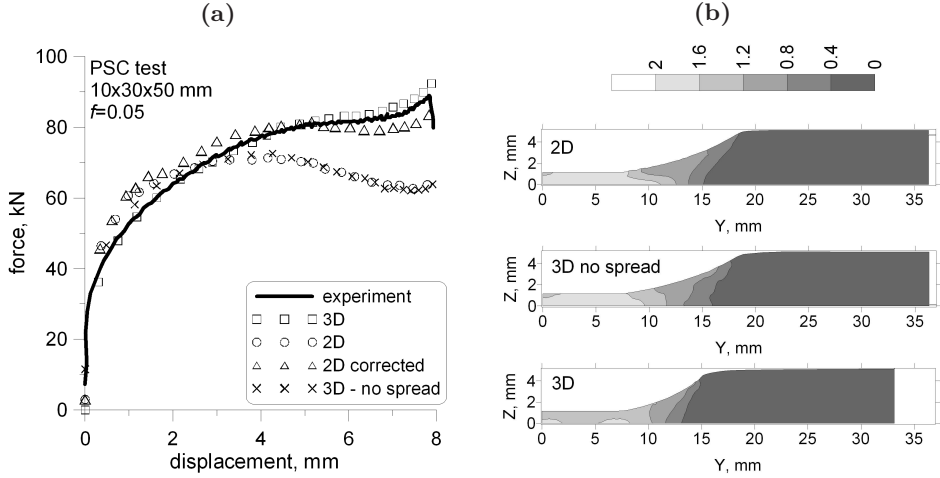


Figure 6.3: (a) Force vs. displacement curves in the PSC test obtained from various simulations compared with the experimental data, $m_c = 0.05$, (b) Distribution of strains in the vertical plane of symmetry for three simulations.

mainly on the friction coefficient and they increase with the progress of the test. An analysis of all the simulations enables the suggestion for the following correction coefficient:

$$\zeta_i = 1 + \frac{m_{c2} \Delta_2}{2 + m_{c1} \Delta_1} \quad (6.2)$$

where ζ is the coefficient which corrects the loads calculated using the 2D model, m_{c1} , m_{c2} are the friction coefficients between the sample and, respectively, the horizontal and the vertical part of the die. In Equation (6.2) Δ_1 and Δ_2 are the shape factors of the deformation zone. The coefficient Δ_1 is defined as a ratio between the length l and the height h of this zone. The coefficient Δ_2 is defined as a ratio between the length l and the width b . The influence of friction depends on the values of these factors.

To recapitulate this part of the analysis, two-dimensional finite element solutions were used for the simulations of the plane strain compression tests in the identification analysis and the corrections based on Equations (6.1) and (6.2) were used in the calculations of the loads.

Flow stress models

The flow stress σ_p is the only material parameter in the flow rule (3.6) which is a part of the thermomechanical numerical description of the plastometric test (see section 3.1). The determination of this parameter is the main objective of these investigations. The selection of the flow stress function is an important part of the identification procedure because the accuracy of the modeling of metal

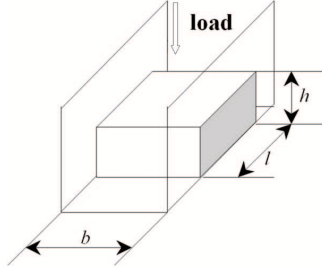


Figure 6.4: A schematic illustration of the plane strain compression in the channel die (the PSCc test).

forming processes depends on the capability of the selected function to describe the behavior of the material during deformation. The basic functions define flow stress as a function of strain, the strain rate and, for hot forming, temperature of the process.

Accounting for the influence of the history of deformation is the next difficulty faced by the flow stress models. Therefore, relatively complicated functions are often proposed [18] or more advanced models are developed, such as an internal variable model [85]. The results of the evaluation of the selected models, regarding their capabilities to describe properly the flow stress, and to determine quantitatively the errors due to the approximation of the experimental data, are presented below. The general classification of the flow stress functions is given in [32] and numerous propositions are available in [31, 50, 32, 37].

Conventional models. The first group of flow stress models are equations in which flow stress is defined as a function of the three external variables: strain, the strain rate and temperature. Neither the history of deformation nor the parameters of material microstructure are accounted for in these models, but they still give reasonably good results for certain conditions of deformation and they are widely used in simulations of metal forming processes. For cold forming, the Hollomon function of the flow stress σ_p is used:

$$\sigma_p = a\varepsilon^n \quad (6.3)$$

where ε is strain, a is a parameter, n is sensitivity to strain.

For hot forming, the general function is:

$$\sigma_p = \sigma_0 + a\varepsilon^n \dot{\varepsilon}^m \exp\left(\frac{Q}{RT}\right) \quad (6.4)$$

where a is the hardening coefficient, n is the strain exponent representing sensitivity to strain, m is the strain rate exponent representing sensitivity to the strain rate, Q represents sensitivity to temperature, ε is strain, $\dot{\varepsilon}$ is the strain rate, T is the absolute temperature, R is the universal gas constant.

As it is shown in Figure 6.5, the function (6.4) is not capable of describing material softening during deformation. Such softening can be due to dynamic recrystallization, which occurs at low values of the Zener-Hollomon parameter defined as $Z = \dot{\varepsilon} \exp(Q/RT)$. Therefore, additional terms are introduced in the function (6.4) and, in the simplest approach, the flow stress is defined as:

$$\sigma_p = a\varepsilon^n \dot{\varepsilon}^m \exp\left(\frac{Q}{RT}\right) \exp(-q\varepsilon) \quad (6.5)$$

where q is the parameter responsible for softening.

The strain softening is predicted by the function (6.5), but the shape of the curve (Figure 6.5) differs from the one observed in the experiments. The flow stress drops after the pick stress is reached. Beyond this, there is not a relation of the softening term on the Zener-Hollomon parameter and the function predicts softening even at low temperatures and high strain rates (Figure 6.5a). Therefore, more complicated functions were developed and the one proposed in [26] is:

$$\sigma_p = \sqrt{3} \left[a\varepsilon^n \exp\left(\frac{Q}{RT}\right) \exp(-q\varepsilon) + [1 - \exp(-q\varepsilon)] a_{sat} \exp\left(\frac{Q_{sat}}{RT}\right) \right] (\sqrt{3}\dot{\varepsilon})^m \quad (6.6)$$

This function has 7 coefficients and is flexible enough to reproduce the shape of the real flow stress curves. An additional hardening coefficient a_{sat} and sensitivity to temperature Q_{sat} are introduced to enable the dependence of softening on temperature and the strain rate. The problems occur when flow stress is to be described in a wide range of values of the Zener-Hollomon parameter Z . A reasonably complex relation of the pick strain on temperature and the strain rate is not reproduced properly. Therefore, a more complex function is proposed in [18] and is also analyzed in [50, 51]:

$$\sigma_p = (\sigma_{ss(e)} - \sigma_0) \left[1 - \exp\left(-\frac{\varepsilon}{\varepsilon_r}\right) \right]^{\frac{1}{2}} - R \quad (6.7)$$

where:

$$R = \begin{cases} 0 & \varepsilon \leq \varepsilon_c \\ (\sigma_{ss(e)} - \sigma) \left\{ 1 - \exp\left[-\left(\frac{\varepsilon - \varepsilon_c}{\varepsilon_{xr} - \varepsilon_c}\right)^2\right] \right\} & \varepsilon \geq \varepsilon_c \end{cases}$$

$$\sigma_i = \frac{1}{\alpha_i} \sinh^{-1} \left(\frac{Z}{A_i} \right)^{\frac{1}{n_i}} \quad i \in \{0, ss(e), ss\}$$

$$\varepsilon_r = 0.31 \left[q_1 + q_2 \sigma_{ss(e)}^2 \right] \quad \varepsilon_{xr} - \varepsilon_c = \frac{\varepsilon_{xs} - \varepsilon_c}{1.98}$$

$$\varepsilon_c = C_c \left(\frac{Z}{\sigma_{ss(e)}^2} \right)^{N_c} \quad \varepsilon_{xs} - \varepsilon_c = C_x \left(\frac{Z}{\sigma_{ss(e)}^2} \right)^{N_x}$$

Equation (6.7) has 16 coefficients, therefore, it is difficult for identification. On the other hand, it has a good predictive capability as far as complex material response

to deformation has to be described in a wide range of temperatures and strain rates.

Another proposition is the function of the form:

$$\sigma_p = a_1 \varepsilon^n U^m \left[1 + \exp \left(-a_2 \frac{\varepsilon - \varepsilon_p}{\varepsilon_b} \right) - \exp \left(-a_3 \frac{\varepsilon}{\varepsilon_b} \right) \right] \quad (6.8)$$

where:

$$\varepsilon_p = a_4 U + a_5, \quad \varepsilon_b = a_6 U^2 + a_7 U + a_8, \quad U = \ln(Z) \quad (6.9)$$

and $m, n, a_1 - a_8$ are parameters.

Equations (6.4)-(6.7) give a general explicit description of the material behavior during hot deformation. The flow stress σ_p is calculated as a function of the strain ε , the strain rate $\dot{\varepsilon}$ and the temperature T . Equation (6.4) is the model for materials which do not soften during deformation. The parameter m represents sensitivity to the strain rate and the flow stress decreases with the increasing m for $\dot{\varepsilon} < 1$ and increases with the increasing m for $\dot{\varepsilon} > 1$.

Equations (6.5)-(6.8) enable modeling of the material behavior when dynamical recrystallization occurs. In Equation (6.5) q is the softening coefficient and the process of softening depends only on strain, independently of temperature and the strain rate. Along with an increase in the strain, the flow curve described by the model (6.5) approaches zero and the parameter q decides about the rate of this approach. This is a limitation which does not allow to use this function in a wide range of Z .

Equations (6.6) and (6.7) model the softening during deformation which is dependent on the temperature and the strain rate (see parameters $\exp(-q\varepsilon)$, a_{sat} , $\exp(Q/RT)$ in Equation (6.6)). The terms $\exp(-q\varepsilon)$ and $[1 - \exp(-q\varepsilon)] a_{sat} \exp(Q_{sat}/RT)$ in Equation (6.6) control the strain, at which the softening begins, and the rate of this process. When the term $\exp(-q\varepsilon)$ in Equation (6.6) approaches zero, the stress value approaches some fixed value. It is not observed for the function (6.5). The function (6.7) allows to model the variety of materials in a wide range of Z . The main difficulty in the application of this model is a large number of parameters which have to be identified.

The internal variable model. Conventional rheological models do not account for the history of the process. After changing the conditions of deformation the response of the model moves immediately to the new equation of the state and the flow stress is a function of new values of external variables. On the other hand, it was observed experimentally [144] that some metallic materials show delay in the response to the change of the conditions. This delay is due to microstructural phenomena which require some time to proceed. Therefore, the rheological models with an internal variable (IVM) as an independent parameter, to remember the history of deformation, were developed.

The dislocation density is the main internal variable in the IVM for metallic materials. The dislocation density can be treated, in the simplest form, as an average

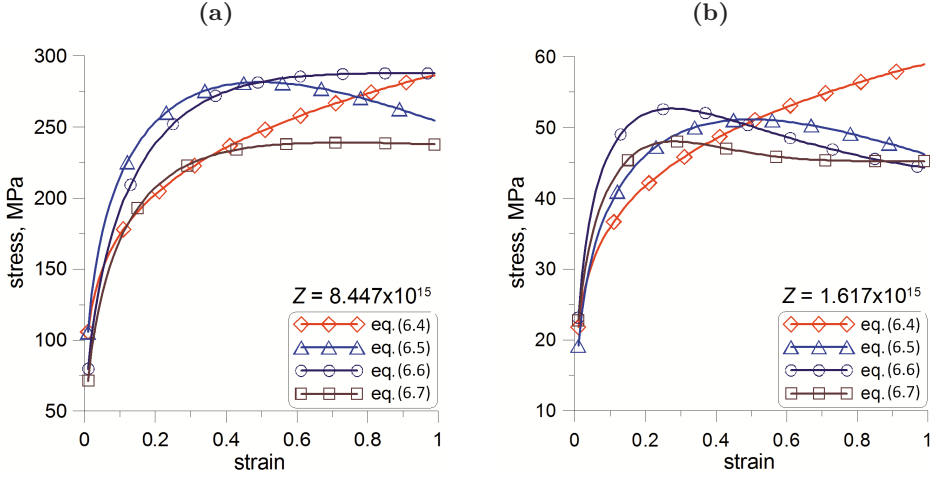


Figure 6.5: Plots of the typical flow stress functions for (a) high and (b) low values of the Zener-Hollomon parameter.

[85] or a probability function describing the distribution of dislocation density can be introduced [91]. It is obvious that the introduction of more complicated treatment of the dislocation density leads to an increase in computation costs in the finite element method used to model the deformation process. Thus, the model with the average dislocation density, which is adequate for the flow stress predictions, is discussed below. Since the stress during plastic deformation is governed by the evolution of dislocation populations, a competition of storage and annihilation of dislocations, which superimpose in an additive manner, control a hardening. The yield stress accounting for softening is proportional to the square root of the dislocation density ρ_d . The evolution of dislocation populations accounting for restoration processes is given by:

$$\frac{d\rho_d(t)}{dt} = \frac{\dot{\varepsilon}}{bl} - k_2 \dot{\varepsilon}^{-q} \rho_d(t) - \frac{k_3}{D} \rho_d(t) R[\rho_d(t) - \rho_{cr}] \quad (6.10)$$

where:

ρ_{cr} is the critical dislocation density at the onset of recrystallization, R is a function defined as:

$$R[\rho_d(t)] = \begin{cases} 0 & \text{for } \rho_d \leq \rho_{cr} \\ \rho_d(t - t_{cr}) & \text{for } \rho_d > \rho_{cr} \end{cases}$$

where t_{cr} is the time at the beginning of dynamic recrystallization, b is the Burgers vector, D is the average diameter of grain, l is the average free path for dislocations calculated as $l = A_0 Z^{-A_1}$, A_0 , A_1 are coefficients, k_2 is the self diffusion coefficient expressed as $k_2 = k_{20} \exp(Q_s/RT)$, Q_s is the activation energy for self-diffusion, k_{20} is a coefficient, k_3 is the grain boundary mobility described by $k_3 = k_{30} \exp(Q_m/RT)$, Q_m is the activation energy for the grain boundary mobility, k_{30} is a coefficient, q is a coefficient.

The flow stress σ_p is defined as:

$$\sigma_p = \sigma_0 + \alpha b \mu \sqrt{\rho_d} \quad (6.11)$$

where σ_0 is the stress accounting for elastic deformation, α is a coefficient, μ is the shear modulus.

The coefficients $A_0, A_1, k_{20}, Q_s, q, k_{30}, Q_m, \sigma_0$ and α have to be determined for a particular material.

6.1.4 The identification task

According to the algorithm 5.1, statement no. 2 in this investigations, vector \mathbf{x} of identified parameters consists of the flow stress model coefficients or the friction parameter, vector \mathbf{p} defines the process parameters such as temperature, the strain rate and strain, the sample dimensions, and vector \mathbf{y} , the model outputs, contains information of the loads recorded during the tests and the sample shape after compression. The inverse problem (statement no. 3) is defined as: to determine the flow stress and friction parameters based on the measured and calculated loads during the plastometric test and the sample shape after the test.

Referring to the functional defined by (5.1), the rheological parameters are estimated by searching for a minimum of the following functional [133, 61]:

$$\Phi(\mathbf{x}) = \frac{1}{N_t} \sum_{i=1}^{N_t} \frac{1}{N_{l_i}} \sum_{j=1}^{N_{l_i}} w_{ij}^F \left[\tilde{F}_{ij} - F_{ij}(\mathbf{x}) \right]^2 \quad (6.12)$$

where \mathbf{x} is the vector of rheological parameters, N_t is the number of tests performed for various strain rates and temperatures, N_{l_i} is the number of load measurement sampling points in the i^{th} test, and \tilde{F}, F are the measured and calculated with the finite element method loads, w^F is weighted coefficient defined as $w^F = \tilde{F}^{-2}$. The rheological parameters are estimated based on the results of the uniaxial compression (UC), the plane strain compression (PSC) or the ring compression (RC) tests.

Both the friction and the flow stress model parameters are determined from the RC test and the functional (5.1) is expressed as:

$$\Phi(\mathbf{x}) = \frac{1}{N_t} \sum_{i=1}^{N_t} \left\{ \frac{1}{N_{d_i}} \sum_{j=1}^{N_{d_i}} w_{ij}^d \left[\tilde{d}_{ij} - d_{ij}(\mathbf{x}) \right]^2 + \frac{1}{N_{l_i}} \sum_{j=1}^{N_{l_i}} w_{ij}^F \left[\tilde{F}_{ij} - F_{ij}(\mathbf{x}) \right]^2 \right\} \quad (6.13)$$

where \mathbf{x} is the vector of the rheological and friction coefficients, N_{d_i} is the number of diameter measurements along the height of the sample in the i^{th} test, \tilde{d}, d are the measured and calculated with the finite element method inner and outer diameters of the sample after the test, w^d is weighted coefficient defined as $w^d = \tilde{d}^{-2}$.

$$(6.14)$$

As it was shown in [133, 123], simultaneous determination of both the friction and the rheological parameters from the ring compression test is possible using the functional (6.13).

Another approach to determine both the friction and the rheological parameters is to use the UC test with the functional (5.1) defined as:

$$\Phi(\mathbf{x}) = \frac{1}{N_t} \sum_{i=1}^{N_t} \left\{ \frac{1}{N_{l_i}} \sum_{j=1}^{N_{l_i}} w_{ij}^F [\tilde{F}_{ij} - F_{ij}(\mathbf{x})]^2 + w_i^\beta [\tilde{\beta}_i - \beta_i(\mathbf{x})]^2 \right\} \quad (6.15)$$

where $\tilde{\beta}$, β is the measured and predicted barreling of the sample after the test, respectively, w^β is weighted coefficient. The barreling of the sample is defined as:

$$\beta = 1 - \frac{V_f}{V_0} \quad (6.16)$$

where V_0 is the initial volume of the cylinder, V_f is the volume of the cylinder with the radius equal to the radius of the contact surface and the height equal to the final height of the sample.

When the friction parameter is identified, RC is the most relevant test. This kind of a test gives information about the sample shape after compression, which is strongly sensitive to the friction. Thus, the functional (5.1) is of the following form:

$$\Phi(\mathbf{x}) = \frac{1}{N_t} \sum_{i=1}^{N_t} \frac{1}{N_{d_i}} \sum_{j=1}^{N_{d_i}} w_{ij}^d [d_{ij} - d_{ij}(\mathbf{x})]^2 \quad (6.17)$$

6.1.5 The estimation of the functional minimum

In statement 9 of the identification algorithm 5.1, the functional Φ is minimized with respect to the identified parameters \mathbf{x} . An attempt to increase the robustness of computations was made and the minimization of Φ was performed with the following procedures:

- the gradient optimization algorithm with semi-analytical sensitivity coefficients,
- a two-step optimization procedure,
- classic non-gradient optimization algorithms enriched with the results of the local sensitivity analysis,
- a multi-criterion optimization.

As the gradient optimization procedure, the Gauss-Newton algorithm was used. The method is not the fastest gradient algorithm, as the Levenberg-Marquardt procedure is, but the idea was to apply semi-analytical calculations of sensitivity coefficients instead of the numerical estimation of derivatives. Such computations are possible

if the source code of the process numerical solver is available. In those investigations, plastometric tests were simulated with the home-made software [90] and all the sources files were open to be read and modified. Calculations of semi-analytical sensitivities were performed with the procedure described in Chapter 4, section 4.1.1.

The remaining optimization methods are described below. To estimate the efficiency of the calculations, the developed algorithms were compared to each other or to classic optimization procedures.

A two-step optimization procedure

Since the identification calculations are time consuming, a two-step algorithm was applied [123], which reduces the calculation costs.

Identification calculations - Step I. The first step, which is further referred to as the preliminary identification analysis (*Step I*), performs the optimization for each available test separately. The input parameters for the optimization are the loads measured as the function of the tool displacement for a given strain rate and temperature. The simulation of each test is performed only once, therefore, the procedure does not require long computing times (see algorithm 6.1). During the simulation, the value of flow stress is determined for each time step of the computation from the following minimization task:

$$\Phi_{ij}(a) = w_{ij}^F \left[F_{ij}(a) - \tilde{F}_{ij} \right]^2 \quad (6.18)$$

$$\min_a \Phi_{ij}(a) \quad \forall i = 1 \dots N_t \quad \forall j = 1 \dots N_{l_i} \quad (6.19)$$

where \tilde{F}_{ij} , F_{ij} are the measured and calculated loads in the j^{th} time step of the i^{th} compression test, w_{ij}^F is weighted coefficient. The minimum is searched with respect to the coefficient a in the following relationship:

$$\sigma_p = a\sigma_e \quad (6.20)$$

where σ_p is the flow stress used in the finite element model of the compression test, coefficient a represents the ratio between the real flow stress which gives the minimum of the function (6.18), and the flow stress σ_e calculated directly from the experiment as:

$$\sigma_e = \frac{F}{S} \quad (6.21)$$

where S is the current value of the contact surface. The simulations are performed assuming the values of the strain rate and the temperature which are nominal for the tests. Due to inhomogeneity of deformation and due to deformation heating, the variations of the strain rate and the temperature are accounted for by the introduction of the following multiplier into the equation describing the flow stress:

$$\sigma_p = a\sigma_e \left(\frac{Z}{Z_n} \right)^m \quad (6.22)$$

where Z is the Zener-Hollomon parameter such that $Z = \dot{\varepsilon} \exp(Q/RT)$ and $Z_n = \dot{\varepsilon}_n \exp(Q/RT_n)$, $\dot{\varepsilon}_n$, T_n are the nominal values of the strain rate and temperature for the selected test, $\dot{\varepsilon}$, T are the current local values of the strain rate and temperature. The strain rate exponent m and the activation energy Q are calculated from the measurements of the loads using a simplified graphical method. The correction using Equation (6.22) accounts only for the variations of the temperatures and the strain rates from their nominal values for the considered single test. The minimization procedure with respect to the coefficient a was implemented into the finite element code [90] of the thermomechanical problem described in Chapter 3, section 3.1.

Algorithm 6.1 The preliminary step of the identification analysis (*step I*)

Require:

The measured loads in plastometric tests: $\{\tilde{F}_{ij}\}$, $i = 1 \dots N_t$, $j = 1 \dots N_{l_i}$

Accuracy of computations: δ

```

1: for all the tests  $i = 1 \dots N_t$  do
2:   for  $j = 1$  to  $N_{l_i}$  {each time step of the FE process simulation} do
3:     Set  $a$ 
4:     Calculate  $F_{ij}$ 
5:     Calculate  $\Phi_{ij}$  according to Equation (6.18)
6:     if  $\Phi > \delta$  then
7:       Determine a new value of the parameter  $a$  defined in Equation 6.22
8:       Goto Step 4
9:     else
10:      Store  $\varepsilon_{ij}, \sigma_{ij}$ 
11:    end if
12:  end for
13: end for
14: return Set of the strain-stress values:  $\{\varepsilon_{ij}, \sigma_{ij}\}$ ,  $i = 1 \dots N_t$ ,  $j = 1 \dots N_{l_i}$ 

```

Identification calculations - Step II. A set of the values of strains and stresses, which represent the real flow stress function, is obtained from the first step of the identification analysis. The further analysis includes an approximation of the stress-strain data for all the temperatures and the strain rates (N_t tests). It is performed using the function $\sigma_p = \sigma_p(\varepsilon, \dot{\varepsilon}, T, \dots)$. At this stage, an arbitrary function is used, but one has to realize that the accuracy of the approximation depends on the ability of the function to reproduce a complex stress-strain relationship. The coefficients of the flow stress function determined using the approximation technique are the starting point for the final identification analysis which is combined with the finite element simulation of all the tests (*Step II*). Since the coefficients estimated in *Step I* are close to the optimum solution, the final identification is performed in a reasonably short time.

The two-step identification procedure is applicable for the rheological parameters estimation with the functional (6.12) based on the measurements from UC or PSC tests. The algorithm and its applications are presented in [117] as well.

The modified classic non-gradient optimization algorithm

The idea of this approach is to use the results of sensitivity analysis to accelerate the optimization procedure. Although in those investigations sensitivity analysis was performed after the identification process to estimate the quality of the obtained parameter values, the identification procedure with the modified optimization algorithm was run once again to verify if the developed algorithm decreases the computation costs. The promising results were the basis to investigate such an approach in the next identification tasks.

The information obtained from sensitivity analysis is included to the optimization algorithm by customizing the optimization parameters for each identified coefficient with respect to the results of sensitivity analysis. As an example the optimization procedure of the simplex method (the Nelder-Mead algorithm [83]) is presented. At the beginning of this procedure, an initial simplex is generated. Beyond the first vertex, the simplex is not generated randomly. Next vertexes are determined in the following way: for the coefficients of the highest sensitivity, the side length is the shortest and for the coefficients of the lowest sensitivity, the side is the longest. The second modification is to adjust the procedure parameters. In the simplex method there are three parameters: reflection, expansion and contraction which are responsible for the selection of vertexes in the next iterations. The default values of these coefficients are modified based on the information of sensitivity analysis (the rule was the same as for the initial simplex generation). In Figure 6.6 the calculations results of the flow stress (6.5) parameter identification problem for various starting simplexes are presented. The identification was based on the UC test and the functional was defined by Equation (6.12). It is observed that the simplex procedure supported by the sensitivity results converges faster than the procedure with the default optimization parameters and faster than the algorithm with the values greater than default, in all the instances.

A multi-criterion optimization

Another formulation of the identification procedure introduces a multi-criterion optimization:

$$\min_{\mathbf{x}} \Phi(\mathbf{x}) = [\phi_1(\mathbf{x}), \dots, \phi_i(\mathbf{x}), \dots, \phi_m(\mathbf{x})] \quad (6.23)$$

where \mathbf{x} is the vector of the estimated parameters, $\Phi(\mathbf{x})$ is the vector of the objectives $\phi_i(\mathbf{x})$, $i = 1 \dots m$. The single objective is connected with a single set of experimentally observable traits, e.g. the shape of the sample or the loads. Therefore, one experiment could provide multiple data sources for the identification procedure. In the case of the current work, each criterion is defined by Equation (6.12) for $N_t = 1$, and thus $m = N_t$. The functional for the minimization procedure is calculated on the basis of the minimax scalarization strategy:

$$\Phi = \max \left(\frac{\phi_i(\mathbf{x})}{\phi_i^{min}} \right) \quad (6.24)$$

where ϕ_i^{min} are the minimal values of the objectives, $i = 1 \dots m$.

This approach allows to reduce the computation costs, especially for an analysis of a large group of the tests. A more conventional functional is based on the averaging of the objectives and it is defined as:

$$\Phi = \frac{1}{m} \sum_{i=1}^m \phi_i(\mathbf{x}) \quad (6.25)$$

Equation (6.25) is equivalent to the functional (6.12).

The example calculations are presented for the identification problem of the flow stress (6.8) parameters, the functional expressed by (6.12) and the UC tests. The simplex method was applied as the optimization procedure. The comparison of the minimax (6.24) and averaging the (6.25) functionals is shown in Figure 6.7 for m equal to the number of the tests N_t . For illustrative purposes, the results of the optimization which was performed with the use of Equation (6.24), were recalculated to the form of the functional (6.25). More precisely, the recalculated functional is the functional calculated from Equation (6.25) using the coefficients determined for the criterion (6.24). The axis on the right side of the plot shows corresponding values of the functional (6.24). The minimax formulation enables a more steep descent of the functional, while the final quality of the solution is similar. Therefore, the choice of a functional can be important for the total computational effort.

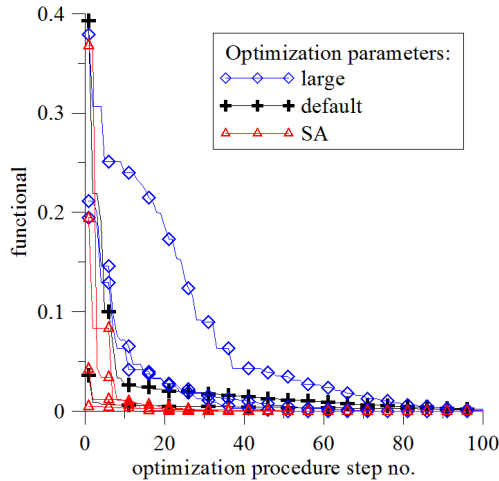


Figure 6.6: A functional in the consequent steps of the simplex optimization procedure for various optimization parameters.

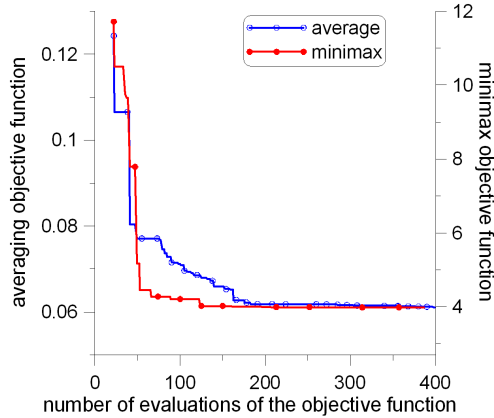


Figure 6.7: The functional values in the consequent steps of the optimization procedure with respect to the functional type.

The extended discussion of the application of various optimization techniques is also given in [116].

6.1.6 The results of the parameter identification

The identification procedure was carried out for all the tests described in section 6.1.2 with the optimization algorithms presented in section 6.1.5 applied to the functionals (6.12), (6.13), (6.15) or (6.17). The plastometric tests were simulated with a numerical model provided in section 6.1.3. The selected results are presented below.

Hot tests. Theoretically, any type of compression tests can be used to evaluate the friction model, but in order to obtain good accuracy of the solution, large sensitivity of the sample dimensions with respect to the friction is required. This sensitivity is very small for the spread in the plane strain compression, moreover, an accurate analysis of the spread requires 3D inverse calculations, which is very costly. Barreling in the uniaxial compression is more sensitive to friction and a successful attempt of using the measurements of barreling for the identification of the friction model is described in [93]. There is a common opinion [73] that the largest sensitivity of the shape of the sample to friction is observed in the ring compression and this test was used in the present work for the identification of the friction coefficient. The identification of the friction coefficient using the functional (6.17) yielded the value of $m_c = 0.11$, which was used in the identification analysis of all the tests. The selected example of comparison of the shape of the ring after compression obtained from the measurements and predicted by the finite element code with the optimized friction coefficient is shown in Figure 6.8. Due to symmetry, a quarter of the cross section is presented. A good agreement is seen in this figure. Similar results were obtained for all the RC tests.

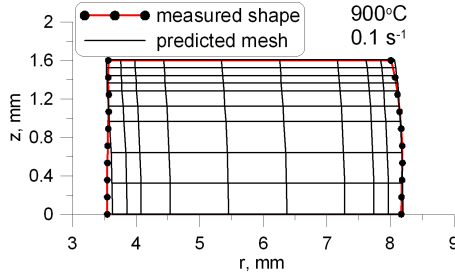


Figure 6.8: The measured shape of the ring cross section compared to the prediction for the friction coefficient of 0.11.

Parameters of the flow stress model were determined next. Figure 6.9a shows an example of the flow stress as a function of the strain calculated directly, as a load-to-contact area ratio, for the all investigated hot compression tests. It is seen in this figure that significant differences between the flow stress calculated for various tests or for various sample dimensions appear. Figure 6.9b shows the selected results obtained after *Step I* of the two-step optimization procedure for the compression tests at 1000°C. An analysis of the plots shows that a very good agreement between the tests is observed for the low strain rate of 0.1 s⁻¹. For the remaining strain rates (1 s⁻¹ and 10 s⁻¹), the largest values of the flow stress are obtained from the uniaxial compression, intermediate values are obtained from both the plane strain tests and the lowest values from the ring compression. This tendency is also observed for the remaining temperatures. However, the discrepancies are larger in lower temperatures.

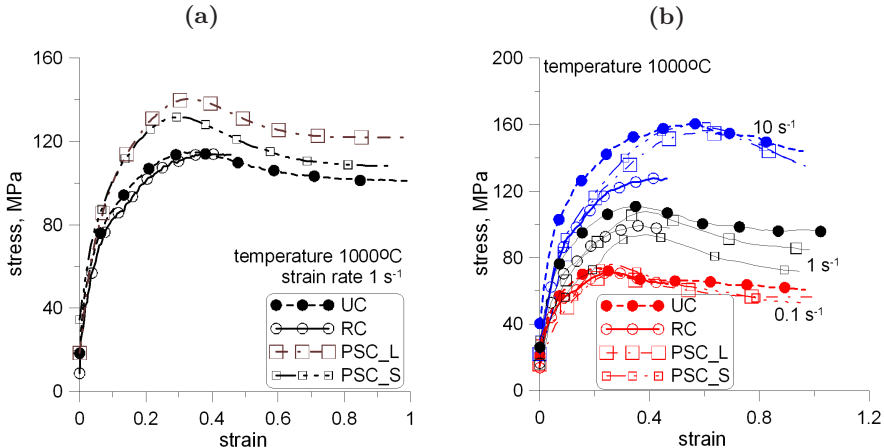


Figure 6.9: (a) An example of the flows stress calculated as a function of the strain directly from the tests as the load-to-contact area ratio, temperature 1000°C and the strain rate 1 s⁻¹, (b) The flow stress obtained from *Step I* of the identification analysis for all the hot compression tests; temperature 1000°C.

The difference between the uniaxial compression and the plane strain compression is small. The flow stress calculated from the ring compression is noticeably lower than for the remaining tests. The plane strain compression tests for different sample dimensions yield the values which are close to each other.

The identification procedure was performed for all the flow stress functions (6.4)-(6.8) and (6.11). Therefore, the two-step optimization algorithm presented in the section 6.1.5 was applied. The flow stress vs. the strain function given in a tabular form was determined first and that relationship was approximated using Equations (6.5)-(6.8) and (6.11).

The computations started from the point, which was obtained from approximation of the flow stress curves in Figure 6.9b. The values of the coefficients that were determined by the identification analysis are given in Table 6.3, while the typical result of the comparison of the values that were obtained from *Step I* and *Step II* of the identification analysis are shown in Figure 6.10b. The plots indicate good capability of Equation (6.8) to describe the flow stress relationship. The coefficients obtained from the approximation for the remaining equations, including the value of the functional (6.12), are given in Table 6.3.

Table 6.3: Coefficients of the flow stress models estimated by the inverse analysis and the value of the functional.

<i>Eq.</i>	<i>a</i>	<i>n</i>	<i>m</i>	<i>Q</i>	<i>q</i>	<i>a_{ss}</i>	<i>Q_{sat}</i>	Φ
6.4	1.933	0.216	0.16	43236	-	-	-	0.149
6.5	1.516	0.335	0.156	50723	0.672	-	-	0.095
6.6	9.742	0.331	0.155	23838	3.095	0.134	62272	0.079
6.7	<i>A</i> ₀	<i>n</i> ₀	α ₀	<i>A</i> _{ss(e)}	<i>n</i> _{ss(e)}	α _{ss(e)}	<i>A</i> _{ss}	0.044
	0.267×10^{13}	28.91	0.07	0.11×10^{13}	4.596	0.011	1.37×10^{13}	
	<i>n</i> _{ss}	α _{ss}	<i>q</i> ₁	<i>q</i> ₂	<i>C</i> _c	<i>N</i> _c	<i>C</i> _x	
	8.89	0.013	0.514	0.25×10^{-10}	0.00015	0.046	0.002	
	<i>N</i> _x	<i>Q</i>						
	0.324	32610						
6.8	<i>a</i> ₁	<i>n</i>	<i>m</i>	<i>a</i> ₂	<i>a</i> ₃	<i>a</i> ₄	<i>a</i> ₅	
	0.000134	0.348	3.838	2.139	0.957	0.0489	-1.043	
	<i>a</i> ₆	<i>a</i> ₇	<i>a</i> ₈					
	0.00214	-0.0779	0.786					

The agreement between the measurements and the numerical model calculations is reasonably good, as it is presented in Figure 6.10a for Equation (6.8). The main improvement which was achieved in *Step II* of the analysis, is connected with the estimation of the parameters ε_p and ε_b . The remaining coefficients are close to those obtained using the approximation of the results of *Step I* of the analysis. In particular, the initial estimation of the coefficient *m* was accurate. This tendency was observed for all the identification calculations performed in the work. Moreover, the identified values of the coefficient *m* were similar (less than 1% difference) for both the UC and the RC tests.

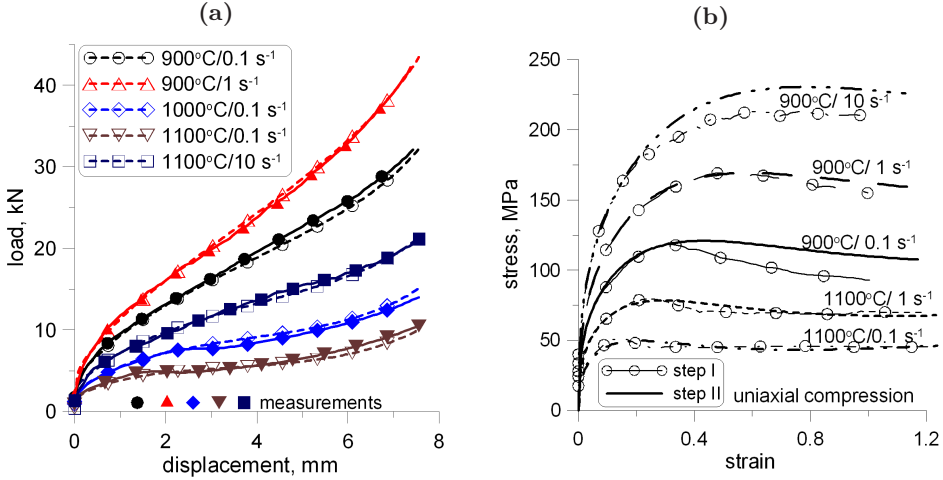


Figure 6.10: (a) Selected examples of the comparison of UC forces: measured (filled symbols) and computed by numerical model with the flow stress obtained from the identification analysis (open symbols), (b) Flow stress obtained from *Step I* and *Step II* (Equation (6.8)) of the identification analysis for the UC tests.

The coefficients of the internal variable model obtained from the identification analysis and the value of the functional are given in Table 6.4.

Table 6.4: Coefficients of the internal variable model obtained from the identification analysis and the value of the functional.

A_0	A_1	k_{20}	Q_s	q	k_{30}	Q_m	σ_0	α	Φ
0.0017	0.163	226.4	36328	0.027	0.411	223150	1.06	3.9	0.062

Figure 6.11 shows a comparison of the flow stress obtained from *Step I* of the identification procedure with the predictions based on the function (6.7) and on the internal variable model (6.11). The latter model replicates better the shape of the curve with dynamic recrystallization, but the average error is larger for this method, see Table 6.4.

The presented results of the identification analysis show that Equations (6.6) and (6.7) perform very well as constitutive models in simulations of the typical metal forming processes. Equation (6.7) gives slightly better accuracy when large range of temperatures and the strain rates is considered (Table 6.4). On the other hand, this equation has a lot of parameters and the identification involves larger costs of computations. The internal variable method is not competitive when accuracy in the reasonably stable conditions is considered. Beyond this, since it requires a solution for the differential equation in each Gauss integration point in the finite element solution, the IVM causes a noticeable increase in the computational costs. It has,

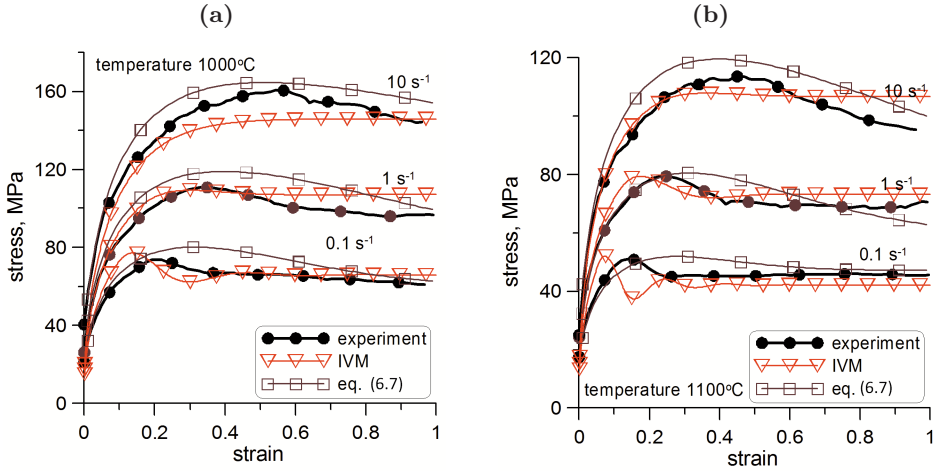


Figure 6.11: Experimental flow stress compared with approximations using the function (6.7) and the internal variable method.

however, a particular ability of accounting for the delay of the material response in the transient conditions. Thus, this method should be used only for the processes which involve varying deformation conditions and accounting for the history of deformation is important.

Cold plastometric tests. The identification procedure of the cold ring compression test yielded the friction coefficient of 0.067 and this value was used in all the further simulations. There was not a noticeable influence of the strain rate on the friction coefficient. All the results of the identification analysis for all the performed tests are presented in Figure 6.12 in the form of the constant strain rate, isothermal stress-strain relationships. An analysis of the results of inverse calculations showed that the flow stresses determined from the CC, RC and UC tests are very close to each other. The values of the flow stress determined from various PSCc tests coincide, as well, but they are lower compared to those obtained from the CC, RC and UC tests.

The results of the identification procedure lead to a suggestion that different mechanisms are responsible for cold plastic deformation in the two investigated groups of plastometric tests. In the first group, which is composed of the tests characterized by the free spread of the material (UC, CC, RC), deformation by slip is dominant. The plane strain compression (PSC) test can be added to this group. The second group of the tests, channel tests (PSCc), is characterized by the constraint of metal flow in one direction. It was observed by a number of researchers, see, for example, [2, 35, 105], that this constraint involves some softening phenomena which are due to the initiation of the micro-shear bands in the material. The results of the present numerical simulations and the identification procedure confirmed the contribution of these softening phenomena in the PSCc tests.

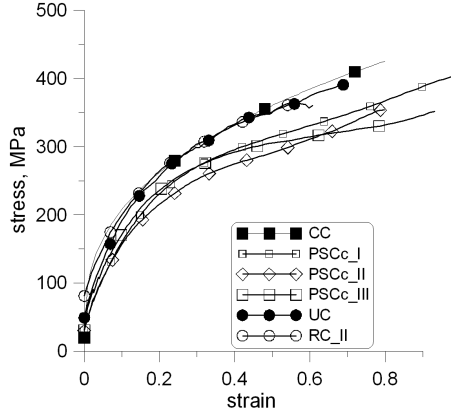


Figure 6.12: The flow stress obtained from the inverse analysis for all the cold compression tests.

6.1.7 Sensitivity analysis

The general objective of the sensitivity analysis is the determination of the influence of the investigated parameters in modeling on the output parameters which are observables in the tests. In the work, the sensitivity analysis focused on the two aspects connected with the identification procedure. The first one is the evaluation of the importance of the identified parameters in the functional calculations. These results supply information which is helpful in the selection of the type of the plastometric test, bearing in mind the fact that large sensitivity of the functional with respect to the identified parameters is required for good accuracy of the identification calculations. The second aspect was the evaluation of the sensitivity of the parameters calculated by the identification procedure with respect to the assumed process parameters. This analysis supplies information how sensitive the result of the identification procedure is with respect to the parameters which are either assumed or determined in another experiment. Sensitivity of the determined flow stress with respect to the assumed friction coefficient (if friction was not an identified parameter and the functional (6.12)) was used is an example of this analysis in the present work. These results allow the evaluation of the accuracy of the identification procedure.

Since rheological and friction parameters were determined, local sensitivity algorithm based on the finite-difference approximation scheme presented in the Chapter 4, section 4.1, was applied and the local sensitivity matrix $\hat{\mathbf{S}}$ (4.6) was calculated:

$$\hat{\mathbf{S}} = [\hat{s}_{ji}] = \left[\frac{x_i}{y_j} \frac{\partial y_j}{\partial x_i} \right] \quad (6.26)$$

where y_j is one of the model outputs representing the loads or the sample shape, and x_i is one of the rheological parameters from Equations (6.3)-(6.8) or the friction coefficient.

Sensitivity of the output parameters with respect to the process parameters and coefficients in the rheological model

For the sensitivity calculations, the model outputs \mathbf{y} were defined as the average load F during the test for all the tests, the barreling β defined by Equation (6.16) for the UC test and the outer and the inner ring diameter d after the RC test. These parameters are components of the functionals (6.12), (6.17), (6.13), (6.15). In the analysis, the sensitivity of the load and the sample dimensions with respect to the rheological parameters is considered as sensitivity of the functional to these parameters.

The average load F in the test is calculated as:

$$F = \frac{1}{\Delta h} \int_0^{\Delta h} F_x dx \quad (6.27)$$

where Δh is the reduction of the height, F_x is the current value of the load.

The sample dimensions in the sensitivity analysis were the same as in the experiments (Table 6.1). Before the sensitivity analysis was performed, the loads and barreling were calculated as functions of the rheological parameters and the selected results for the UC test are presented in Figure 6.13. The parameters m , n and q are the independent variables in these plots. The presented results supply information regarding the character of the influence of rheological parameters on the loads and on the sample dimensions.

It is seen in Figure 6.13 that the effect of the rheological parameters on the load and on the barreling is complex. Thus, the sensitivity coefficients \hat{s}_{j_i} are estimated according to Equation 6.26, where (y_j) is a component of $\mathbf{y} = (d, \beta, F)$, x_i is one of the parameters from Equations (6.3)-(6.8).

The results of the calculations of all the investigated sensitivity coefficients are demonstrated below. Since the sensitivities vary with varying values of the independent parameters, the results are presented for the following basic values of the parameters: $a = 10$ MPa, $n = 0.3$, $m = 0.15$, $Q = 36000$ J/mol and $q = 0$. Notice that in Equation (6.5) activation energy is not in the Zener-Hollomon parameter and it is not to power m . In consequence, the values of the activation energy Q in Equations (6.8) and (6.5) are different, the latter is equal to the former multiplied by m .

Figure 6.14 shows the comparison of the sensitivity coefficients determined for various plastometric tests. Sensitivity of the loads was determined for all the tests (Figure 6.14a) and the results enable the following conclusions. The UC test is the most sensitive to all the rheological parameters and it should be recommended as the experiment supplying the data for the identification calculations with the further application of the results in the simulations of bulk forming. The three remaining tests show, in general, lower sensitivity. Sensitivity with respect to the softening coefficient q is larger for the tests involving large plastic deformation, namely the

PSC of small samples and the UC tests. This sensitivity is low in the RC test (due to small deformations) and in the PSC of large samples (a reasonably uniform deformation does not cause large strains). Sensitivity of the diameters of the samples was determined for the axisymmetrical tests only (Figure 6.14b). It is seen in this figure that the shape of the sample is not dependent on the rheological parameters, except some small influence of the strain exponent m and the strain rate exponent n on the barreling in the UC test. As expected, the shape of the samples after compression depends mainly on the friction coefficient m_c . This effect is, in general, stronger in the RC test, where two diameters are measured and better accuracy is expected. This test is correctly recommended as the best test for the determination of the friction parameter.

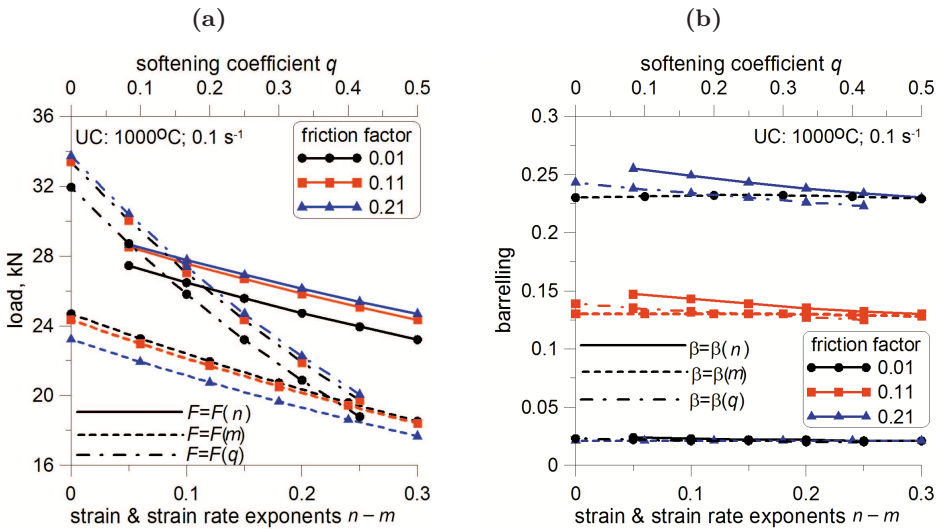


Figure 6.13: (a) Loads and (b) barreling as a function of the strain exponent n , the strain rate exponent m and the softening coefficient q in the uniaxial compression test.

Sensitivity analysis was performed for Equation (6.7) of a large number of the parameters responsible for various phenomena contributing to the overall flow stress, i.e. hardening, recovery, recrystallization. In this equation, the loads are sensitive to the activation energy Q and the parameters N_x , $\alpha_{ss(e)}$, α_{ss} , C_x , and q_1 (see Figure 6.16a). What should be emphasized is negligible sensitivity of the loads with respect to some parameters. It seems that a more detailed analysis of Equation (6.7) may lead to the simplification and a decrease in the number of parameters, which is an important advantage in the identification procedure.

The analysis of the internal variable model shows that the parameters describing the average free path of dislocations (A_0 , A_1), as well as the coefficient α , have the

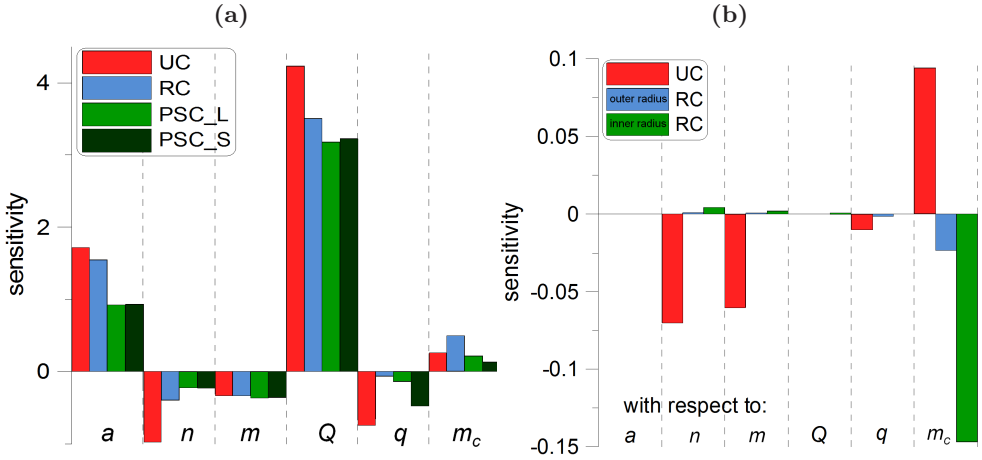


Figure 6.14: (a) Sensitivity of the loads and (b) the sample dimensions with respect to the rheological parameters and friction in various tests.

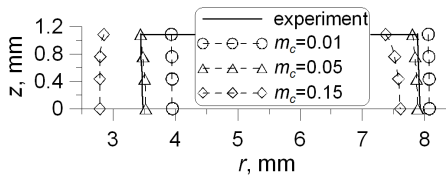


Figure 6.15: The shape of the inner and outer surfaces after the cold ring compression calculated for various friction coefficients and measured in the experiment.

strongest influence on the loads. Beyond this, the loads are also sensitive to the remaining parameters except the coefficient q which introduces the dependence of the recovery on a strain rate.

A similar analysis was performed for the cold compression tests, assuming $m = Q = q = 0$ in Equation (6.5). The calculated sensitivity of the loads and the sample dimensions with respect to the rheological parameters a and m was similar as in the hot tests. Sensitivity of the sample shape after compression with respect to the friction parameter was higher than in the hot tests [97]. Figure 6.15 presents the shape of the ring after compression calculated for various friction parameters and measured in the experiment (a quarter of the cross section is shown).

Sensitivity of the identification procedure results to the process parameters

The rheological parameters, the friction parameters and the heat transfer coefficient can be determined using the identification procedure presented in Chapter 5.

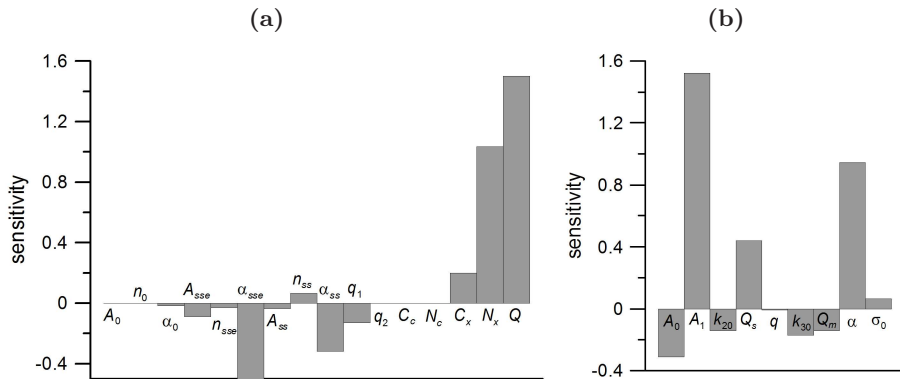


Figure 6.16: (a) Sensitivities of the loads with respect to the rheological parameters in the function (6.7), (b) sensitivities of the loads with respect to the rheological parameters in the IVM model (6.10).

The problem of the latter coefficient is well discussed in [74, 11, 13, 33] and it is not investigated in the present work. The current investigations focus on the rheological and friction models. When the rheological parameters are determined using the identification procedure, the friction coefficient has to be known. To the contrary, when the identification of the friction model is performed, the rheological parameters have to be known. This problem can be solved by using the RC tests and the functional (6.13), which enables simultaneous determination of both the friction and rheological parameters [135, 134, 123, 117]. This approach involves larger computing costs due to a greater number of the parameters which are identified, and it is common that the identification analysis is applied to estimate either the rheological or friction parameters separately, assuming that the others are known. Thus, the objective of this part of the work is to determine how far errors in the evaluation of the assumed parameters affect the solution. This analysis is divided into two parts. The effect of the friction parameter on the flow stress determined with the use of the identification procedure is investigated first. The effect of the rheological parameters on the friction parameter determined with the use of the identification procedure is evaluated next.

Figure 6.17a shows a selected example of the flow stress determined by the identification procedure for various values of the friction parameter in the RC tests. An influence of the friction is well visible. This influence is lower in the remaining tests, which can be better observed in Figure 6.17b where sensitivity of the flow stress at the strain of 0.4 with respect to the friction parameter is shown for all the tests as a function of this parameter. It can be concluded from this figure that the flow stress determined by the identification procedure is almost insensitive to friction in the PSC tests for large samples (PSC_L). This sensitivity is slightly larger for the PSC of small samples (PSC_S) and the UC test, and the largest sensitivity is observed for the RC test. The values of the flow stress for the identified friction

parameter of 0.11 are in the ellipse and they differ slightly between the tests.

Applying local sensitivity coefficient to evaluate the influence of friction on the flow stress determined from the identification procedure, the following expression was proposed:

$$\hat{\delta}_{\sigma_p, m_c} = \frac{m_c}{\sigma_p} \frac{\partial \sigma_p}{\partial m_c} \quad (6.28)$$

The values of the sensitivity coefficient $\hat{\delta}_{\sigma_p, m_c}$ calculated for various tests for the friction coefficient $m_c = 0.11$ are shown in Figure 6.18a. It is observed that the flow stresses obtained from the RC test are the most sensitive to the value of the friction parameter.

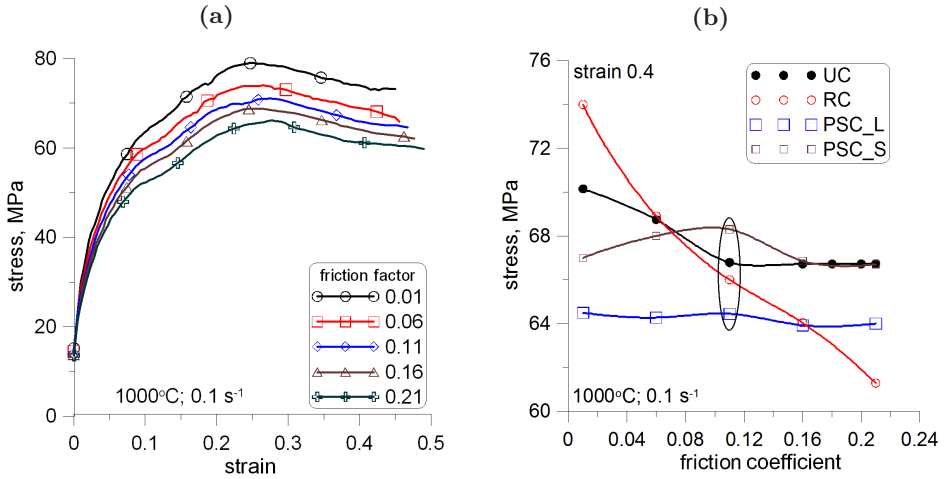


Figure 6.17: (a) The flow stress determined from the identification analysis for various values of the friction, (b) the flow stress at the strain of 0.4 determined from the identification analysis as a function of the friction coefficient.

The analysis of results shows that the sensitivity coefficient is very low for the UC and PSC tests. Some sensitivity of the result is observed with respect to the exponents n and m . The results of the identification procedure of the RC test are completely insensitive to the hardening coefficient a . The RC test is the most sensitive to the errors in the evaluation of the friction parameter. The UC test is less sensitive to the errors in the evaluation of the friction parameter and this test should be recommended as the best one for the identification of the rheological parameters.

Sensitivity of the material flow with respect to the friction coefficient for various initial dimensions of the ring $d^{out} : d^{in} : h$, where d^{out} is the outer ring diameter, d^{in} is the inner ring diameter, h is the ring height, was investigated as well. The local

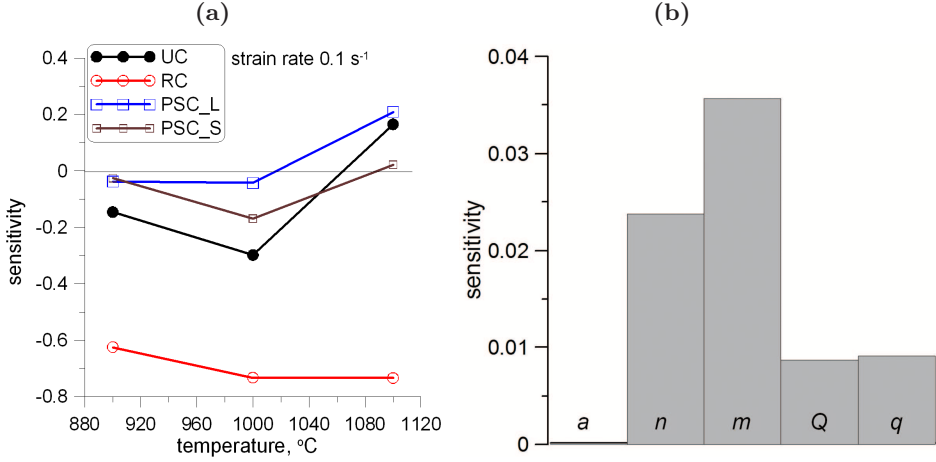


Figure 6.18: (a) Sensitivity of the friction coefficient, determined with the use of the identification analysis of the RC tests, with respect to the assumed rheological parameters of the material, (b) sensitivity of the rheological parameters of the material, determined with the use of the identification analysis of the RC tests, with respect to the assumed friction coefficient.

sensitivity coefficient was defined as:

$$\hat{s}(\mathbf{x}) = \frac{m_c}{V(\mathbf{x})} \frac{dV(\mathbf{x})}{dm_c} \quad (6.29)$$

where $\mathbf{x} = (m_c, d^{out}, d^{in}, h)$, m_c is the friction coefficient and dV is expressed by:

$$\frac{dV(\mathbf{x})}{dm_c} = \frac{V(m_c, d^{out}, d^{in}, h) - V(m_c + \Delta m_c, d^{out}, d^{in}, h)}{\Delta m_c} \quad (6.30)$$

and $V(\mathbf{x}) = V(m_c, d^{out}, d^{in}, h)$ is the volume of the inner hole after the compression test for the friction m_c :

$$V(\mathbf{x}) = \pi \int_0^{h_e} f^2(z) dz \quad (6.31)$$

where h_e is the ring height after the compression, $f(z)$ is the inner diameter in the function of the ring height after the test.

The sensitivities were calculated for various ratios of $d^{out} : d^{in} : h$ presented in Table 6.5. The computations were carried out for various densities of the mesh and for sufficiently dense meshes there was no impact of the mesh element to the calculation result. The results are shown in Figure 6.19.

An increase in the ratio of the outer to inner ring diameter reduces sensitivity of the inner hole shape to the friction parameter. The ratio $d^{out} : d^{in}$ equal 6 : 4 gives low sensitivity to friction, particularly for larger values of this parameter. The friction

Table 6.5: Initial dimensions of the rings.

d^{out} , mm	d^{in} , mm	h , mm	$d^{out} : d^{in} : h$
12	8	4	6:4:2
12	6	2	6:3:1
12	6	5	6:3:2.5
12	6	6	6:3:3
12	4	6	6:2:3
12	4	4	6:2:2
12	4	2	6:2:1

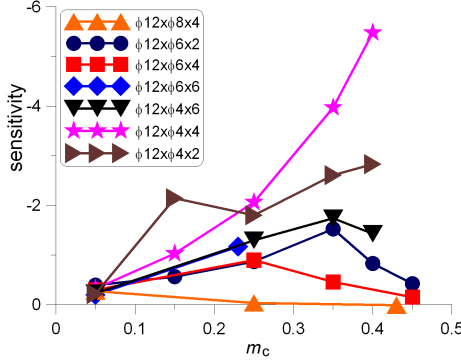


Figure 6.19: The results of sensitivity computations of the inner ring shape with respect to friction for various initial ring dimensions.

has the greatest impact on the material flow for the rings of a small inner diameter (d^{in}) and a small height (h); however at the higher friction parameters the inner diameter is close to zero (free flow of the material is not possible), thus the sensitivity decreases (see Figure 6.19 for the ring of the dimensions $d^{out} = 12$ mm, $d^{in} = 4$ mm, $h = 2$ mm). For small friction coefficients, the interpretation of the results is difficult regardless of the initial dimensions of the ring. The detailed results of this investigations are provided in [112].

6.1.8 Discussion of the results

Sensitivity analysis and the identification procedure applied to various compression tests and a wide range of the flow stress equations allow to draw the following conclusions:

- The developed method, the identification procedure presented in Chapter 5, combining the optimization task with the local sensitivity analysis application presented in section 4.1, is a powerful tool for the interpretation of the plasticometric test results independently of the type of the machine, a lubricant, a method of heating and other experiment parameters out of control. This approach guaranties that the obtained values of the material and the process parameters are very close to the real ones.

- The identification procedure gives the results, which are insensitive to the size of the sample. The lack of sensitivity to the method of testing is observed for the tests which do not constrain the flow of the material in the transverse direction.
- Functions commonly used as rheological models give, in general, good results for the processes with reasonably stable conditions. More complex functions, with a larger number of coefficients, give slightly better approximation compared to the simple equations with a smaller number of parameters. Sensitivity analysis has shown that in more complicated functions some of the parameters show a small influence on the flow stress predictions. It seems that these functions should be further explored regarding a possibility of obtaining a simpler but still accurate form.
- Loads predicted by the finite element method simulation are the most sensitive to the activation energy and then subsequently to the hardening coefficient, the strain rate exponent, the strain exponent, the softening parameter. The lowest sensitivity is observed with respect to the friction parameter.
- The flow of the material, in this analysis represented by the shape of the rings after compression, is almost not sensitive to the rheological parameters. As expected, sensitivity is observed with respect to the friction parameter. The inner diameter is much more sensitive to the changes of this parameter than the outer diameter.
- The flow stress determined from the identification procedure of the UC and PSC tests is not sensitive to the assumption of the friction parameter. The flow stress determined from the identification procedure of the RC and RSC test is slightly more sensitive to the assumed friction. It means that the exact evaluation of the friction parameter is not crucial for the accuracy of the identification procedure.
- The analysis shows that the loads are most sensitive to the rheological parameters in the UC test and the shape of the sample is most sensitive to friction in the RC test.
- The developed modified optimization algorithms applied to the identification procedure reduces the computation costs.
- The local sensitivity analysis allows to estimate the error of the identified parameters.

6.2 A quantitative fracture criterion

Fracture is a phenomenon occurring not seldom during the material deformation in metal forming processes. The formulation of the quantitative fracture criterion [87] for the materials subjected to plastic deformation is essential for the modeling of forming processes for the materials characterized by low plasticity. In order to avoid fracture during forming, it is necessary to determine precisely the material crack resistance and to use this knowledge to design the process technological parameters

which prevent fracture. The criteria based on the information on stress and the strain history, which are commonly used [87, 16], give relatively good qualitative results but the quantitative accuracy is often insufficient. It is generally due to difficulties with the determination of the material parameters in the fracture criteria. The problem of formulating a complex criterion which gives qualitatively good results is still open. In this work, the phenomena described with the fracture criteria containing the parameters characterizing the fracture of a particular material is considered. Thus, the fracture criterion is a material model which requires identification. According to the identification strategy algorithm presented in Chapter 5, the measured data is necessary to perform an identification. The Strain Induced Crack Opening (SICO) test is commonly used to supply data for identification. Therefore, the present section deals with an analysis of the SICO test in the aspect of the identification of the fracture criteria parameters.

6.2.1 Objectives of the work

The main goal of the investigations was the determination of sensitivity of the fracture criterion with respect to:

- the SICO test parameters: temperature, the die velocity,
- the material parameters: the strain rate sensitivity, the hardening coefficient, the hardening exponent and the temperature sensitivity coefficient.

The objective was to determine to what extent the value of the fracture criterion changes with the change in the SICO test parameters and the material plastic properties. Since the SICO test was performed for the reference parameters of this test [141], the local sensitivity algorithms provided in Chapter 4, section 4.1, were applied. The results contributed to design the critical value of the fracture criterion in the function of the test and the material parameters of the highest impact to the test. The critical fracture value is responsible for the initiation of the fracture process; thus, it is a very important parameter in the process modeling and avoiding the fracture. The details of the investigations are presented also in [142].

6.2.2 The experiment

The SICO test [58, 6] is commonly used to determine a tendency of materials to fracture during hot forming. The test is a hot workability technique with good reproducibility and possibility to employ large strains. The SICO test is divided into two stages: the resistance heating of the sample to get an appropriate temperature field, and upsetting until the fracture appearance. This fracture appearance, expressed as the value of the circumferential strain, is an observable data in the test. The schematic view of the sample and the real samples are shown in Figure 6.20.

In those investigations, the test conditions were as follows. The dimensions of the sample were 10×86.4 mm. The chemical composition of the carbon-manganese steel was 0.21% C, 1.32% Mn, 0.23% Si, 0.2% Cu. The sample heating rate was $5^\circ\text{C}/\text{s}$ for about 230 s, the stroke during upsetting was 16 mm, the die velocity was equal to 90

mm/s, the test temperature was 1050°C. The circumferential strain in the analyzed SICO test was equal to 0.65.

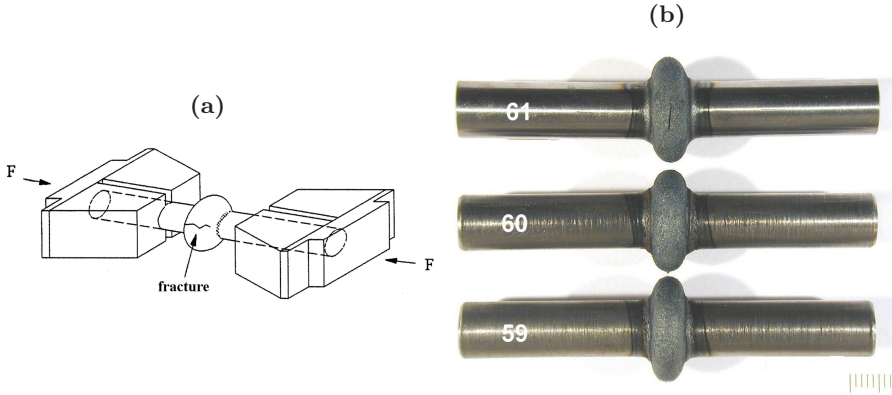


Figure 6.20: The SICO test: (a) view of the tools and the sample, (b) the samples after compression [142].

6.2.3 A numerical model of the SICO test

The identification procedure 5.1 requires to express a numerical model of a process - the SICO test. Due to inhomogeneities of the temperature, stress and strain fields in the test, the quantitative interpretation of the SICO test produces certain problems [58]. Therefore, the experiment was defined as a thermomechanical problem described with the equations provided in Chapter 3, section 3.1 and solved with the finite element method. Such an approach reflects the inhomogeneity of the strains, stresses and temperatures.

In the work, the experiment described in section 6.2.2 was reproduced. The heat transfer coefficient for the tool-workpiece interface was assumed at 20 kW/m²K for the high pressure contact and 10 kW/m²K for the sides of the sample. The temperature distribution at the cross section after the test is presented in Figure 6.21.

The material properties were described with the flow stress equation (6.4) dedicated to hot forming and for the investigated steel the parameters were equal to $a = 4.7$, $n = 0.212$, $m = 0.139$, $Q = 31020$ J/mol.

The process was simulated to the moment when the fracture occurred. The computation time of one test was approximately more than a dozen minutes.

The fracture criteria

Within the work the capability of various fracture criteria: Latham&Cockcroft, normalized Latham&Cockcroft [16] and Oyane [87], were tested. The criteria are based on the assumption that the fracture occurs when the integral of stresses with respect to strain exceeds the limiting value, called the critical value, C .

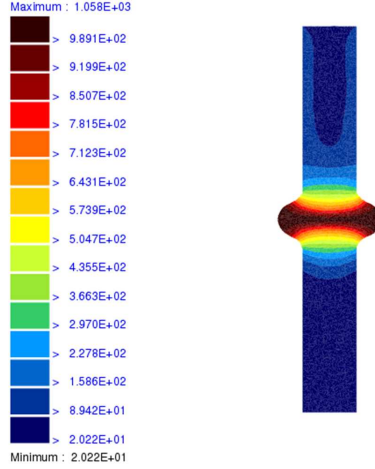


Figure 6.21: The temperature distribution at the cross section after the SICO test, Celsius degrees are presented in the scale.

- The Latham&Cockcroft criterion:

$$\chi_{LC} = \int_0^{\underline{\varepsilon}_i(t)} \sigma_1 d\underline{\varepsilon}_i(t) \geq C \quad (6.32)$$

- The normalized Latham&Cockcroft criterion:

$$\chi_{nLC} = \int_0^{\underline{\varepsilon}_i(t)} \frac{\sigma_1}{\underline{\sigma}_i} d\underline{\varepsilon}_i(t) \geq C \quad (6.33)$$

- The Oyane criterion:

$$\chi_{Oyane} = \int_0^{\varepsilon_i(t)} \left(1 + A \frac{\sigma_h}{\underline{\sigma}_i} \right) d\varepsilon_i(t) \geq C \quad (6.34)$$

where $\underline{\varepsilon}_i$ is the effective strain, σ_h is the hydrostatic stress, $\underline{\sigma}_i$ is the effective stress, σ_1 is the maximum principal stress, C is the critical value of integral, A is the constant.

The criteria (6.32)-(6.34) were implemented into the finite element code and predicting a fracture was possible.

6.2.4 Sensitivity analysis

In the identification algorithm 5.1, statement no. 1, sensitivity analysis is applied in case of introducing new models to the process model. Since the goal of the work

was to design a function describing the critical value of the fracture and the fracture criteria were involved in the thermomechanical model dedicated to the SICO test as new equations, that statement of the identification algorithm was performed with the local sensitivity methods presented in Chapter 4, section 4.1.

The objective of the sensitivity analysis was evaluation how sensitive the parameters in various fracture criteria (6.32)-(6.34) were with respect to the SICO test parameters and to the material parameters. The independent parameters of the process in the analysis were:

- the temperature at the moment of the fracture (T),
- the die velocity (v),

The parameters describing the material properties in Equation (6.4) were:

- the hardening coefficient (a),
- the hardening exponent (n),
- the strain rate sensitivity (m),
- the temperature sensitivity coefficient (Q).

In the analysis, each fracture criterion was calculated as the maximum value χ_i of that criterion in the volume of the sample:

$$\chi_i^{\max} = \max_V \chi_i \quad i \in \{Oyane, LC, nLC\} \quad (6.35)$$

Local sensitivity coefficients \hat{s}_{ij} , using the finite-difference approximation scheme (4.5), were estimated as:

$$\hat{s}_{ij} = \frac{x_j^{ave}}{\chi_i^{ave_{\max}}} \frac{\chi_i^{\max}(x_j + \Delta x_j) - \chi_i^{\max}(x_j)}{\Delta x_j} \quad (6.36)$$

where x_j is a component of the process parameter vector $\mathbf{x} = (T, v, a, n, m, Q)$ in turn, $i \in \{Oyane, LC, nLC\}$ is the value of i^{th} fracture criterion calculated for the parameter x_j , $\delta \in (0, 1)$ is a small perturbation. The superscript *ave* indicates the average value of the parameter.

Calculations were performed for various values of the temperature $T \in (950 - 1200^\circ C)$, the velocity of die $v \in (30, 220)$ mm/s, the hardening coefficient $a \in (2.5, 6.5)$, the hardening exponent $n \in (0.1, 0.3)$, the strain rate sensitivity $m \in (0.08, 0.2)$, the temperature sensitivity coefficient $Q \in (30000, 38000)$ J/mol.

Due to the idea of the sensitivity analysis, those investigations were to determine the process and material parameters of the highest impact to the fracture initiation, the sensitivity coefficient \hat{s}_{ij} was introduced and it was calculated as the average from the absolute values of the i^{th} fracture criterion:

$$\hat{s}_{ij} = \frac{1}{N_j} \sum_{j=1}^{N_j} |\hat{s}_{ij}| \quad (6.37)$$

where N_j is the number of sensitivity calculations for the parameter x_j .

The results of calculations of the sensitivity coefficients are presented in Figure 6.22.

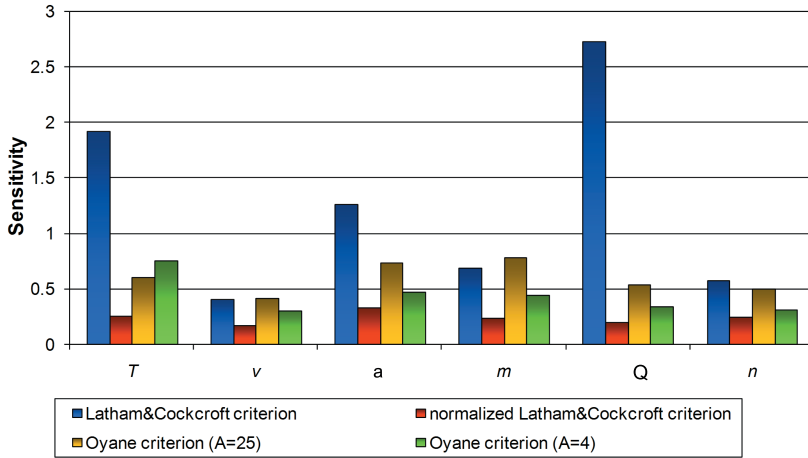


Figure 6.22: Sensitivity of fracture criteria with respect to various parameters.

6.2.5 Discussion of the results

The analysis of the sensitivity calculation results provides information regarding the importance of various parameters in the SICO tests. It is seen in Figure 6.22 that the Latham&Cockcroft criterion is more sensitive than other fracture criteria to the process conditions and the material properties. The maximal sensitivity is observed with respect to the temperature T , the hardening coefficient a and the temperature sensitivity coefficient Q . Slightly lower sensitivity is observed for the strain exponent n and the die velocity v . Finally, it can be also concluded that the fracture criteria value is much less sensitive to changes of the die velocity and to the hardening exponent.

The conclusion from the sensitivity analysis is that in the identification procedure of the SICO test, more accurate quantitative predictions of fracture initiation can be obtained when the critical value C is introduced into the numerical model of the SICO test as a function of the process and the material parameters. Thus, the suggestion is made that the critical value of the criterion should be a function of the temperature, the hardening coefficient, the temperature sensitivity coefficient and the strain rate sensitivity. The effect of the die velocity and the hardening exponent is negligible. The strain exponent can be added to the list of the independent variables, as well. The investigations of the SICO test were continued and they were the main objective of the work [140]. The function describing the critical value of fracture initiation was developed and it was implemented into the finite element code for the SICO test and the selected forging operation simulations. Values of fracture criteria were estimated for the circumferential strain determined in the analyzed SICO test based on the

algorithm 5.1. Evaluation of the sensitivity provided the information which made the identification procedure more efficient. The results of the identification are presented in details in the work [140].

6.3 The strain localization model

The accuracy of materials processing simulations depends on the quality of the description of the phenomena occurring during deformation. Rheological models usually treat material as a continuum and are unable to describe properly several important phenomena which may be either random or discontinuous or even both. Therefore, there is a continuous search for alternative models, which account for non-continuous structure of materials and for the fact, that various phenomena in materials occur on a various scale. Accounting for the stochastic character of the phenomena is an additional challenge. Multiscale models, see, e.g., [1, 17], are one of the solutions capable to overcome the mentioned difficulties. Over the last decade, multiscale modeling techniques have become very popular. The problem of identifying the parameters of such a model is discussed in this section.

6.3.1 Objectives of the work

Multiscale models based on the combination of the Finite Element (FE) and the Cellular Automata (CA) method are designed to describe the development of the strain localization during material processing [1, 64]. Numerical tests confirmed a qualitatively good predictive capability of the model. The problem of quantitative accuracy still remains open. To reach the accuracy, the values of the coefficients in the transition rules of the CAFE model have to be determined on the basis of the experimental data. It is expected that the identification procedure developed in Chapter 5 will be an efficient method to identify these parameters.

Those investigations were the first attempt to identify the CAFE model parameters. Therefore, according to the statement no. 1 of the identification algorithm 5.1, the sensitivity analysis of the model was performed. Since the calculations performed with the CAFE model are time consuming, the sensitivity analysis was based on the Morris method presented in Chapter 4, section 4.2.1. This is a screening design technique which searches the whole parameter domain in a computation cost-effective way. The objectives of the work were to perform the sensitivity analysis, to identify the key parameters of the model, to determine their influence on the model response and to formulate guidelines for the further identification of the CAFE model parameters. The details of the investigation are presented in [119, 66].

6.3.2 The experiment

The process that was considered as a case study was a simple shearing test presented in Figure 6.23. The selected material was oxygen-free high thermal conductivity copper deformed at the room temperature. The strain localization phenomena for that material and the shearing test are experimentally well investigated, which was

the reason for selecting them in the present work for validation and identification of the numerical modeling.

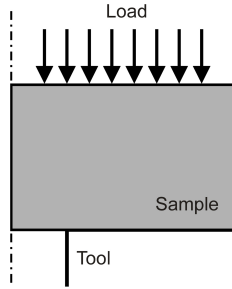


Figure 6.23: A simple shearing test with a rectangular sample.

6.3.3 The numerical model of a shearing test

A simple shearing test is defined as a multiscale problem which accounts for the phenomena that occur on a different scale in the material. In the macro-scale, the material is the continuum, and the process is described as a thermomechanical problem expressed with the equations presented in Chapter 3, section 3.1. The equations are solved with the finite element method. Micro shear bands initiate and propagate in the microscale and they are modeled in the micro-scale with the cellular automata approach. The cellular automata model is introduced and attached to the finite element model of the shearing test and multiscale (CAFE) modeling is performed. One multi-scale simulation of the shearing test takes approximately a dozen of minutes. The general ideal of the multiscale approach is presented in Figure 6.24.

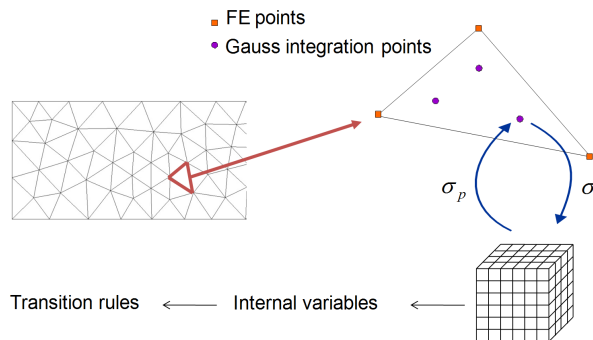


Figure 6.24: The CAFE model scheme.

In the CAFE model, the micro shear band (MSB) is defined by several state variables that describe each particular cell, as well as by a set of transition rules.

Transition rules provide information when a CA cell can change its state and become a cell with micro shear bands (*activeMSB*). Transition rules are usually logical functions, which are used to replicate mechanisms leading to the initiation of micro shear bands and next shear bands that are observed experimentally [49, 15]. When the transition rule for a particular cell is fulfilled, the cell changes its *activeMSB* state, if not the state of the cell remains unchanged. A detailed description of the developed model regarding the state of the cells and transition rules is presented in the works [64, 65, 63]. Below, the main assumptions of the model are presented.

The flow of the information between the scales is performed in both directions, from the macro-scale to the micro-scale, as well as from the micro-scale to the macro-scale. In each time increment of numerical modeling, the information about the stress tensor is sent from the finite element solver to the MSB cellular automata, where development of the micro shear bands is calculated according to transition rules. Based on the information supplied by the cellular automata, the flow stress σ_p is calculated and it is used in the finite element model during the next step of the finite element calculations.

One of the most important function of the model is the function that controls distribution of one of the internal variables for the MSB among the cells. The Gauss function was selected to model that phenomena, where the critical value for the initiation of the hard slip system, τ_{\max}^* , is a controlled variable described by:

$$\tau_{\max}^* = \frac{1}{\sigma_{dev} \sqrt{2\pi}} \exp\left(-\frac{\mu^2}{2\sigma_{dev}^2}\right) \quad (6.38)$$

where μ is the expected value, σ_{dev} is the standard deviation.

Due to that, the work was focused on the validation of the CA model, in particular, on the verification which parameters of the model were of importance in forming micro shear bands. Two parameters of the Gauss distribution function were considered as independent stochastic variables in the analysis. One was the expected value μ and the standard deviation σ_{dev} was the other one. In the CAFE model, the values of τ_{\max}^* are generated using the right hand side of Equation (6.38) and they are main parameters which control the initiation of the micro shear bands in the MSB space.

6.3.4 Sensitivity analysis

The CAFE model is time consuming; therefore, for sensitivity analysis of the CAFE model, the Morris design algorithm was selected which is provided in Chapter 4, section 4.2.1. Three parameters were selected to the analysis: two parameters of the cellular automata module - as the crucial parameters in the micro shear bands development (see Equation (6.38)) and friction coefficient m that characterizes specimen-tool contact properties implemented in the finite element model of the macro-scale. The vector \mathbf{x} containing the parameters is in the following form:

$$\mathbf{x} = (\underline{\mu}, \sigma_{dev}, m) \quad (6.39)$$

where $\underline{\mu}$ and σ_{dev} are the expected value and the standard deviation in Equation (6.38), m is the friction coefficient. The space of acceptable values for the components of vector \mathbf{x} was defined as: $\underline{\mu} \in [200, 500]$ MPa, $\sigma_{dev} \in [10, 300]$ MPa, $m \in [0, 0.80]$.

The distribution of the strain values along the profile line at the fixed time of the process is analyzed to estimate sensitivity (see Figure 6.25). The strain profile was divided into two regions in such a way that characteristic picks were observed. The output of the model was defined as the sum of the two relative strain picks:

$$y(\mathbf{x}) = \beta_1 y_1(\mathbf{x}) + \beta_2 y_2(\mathbf{x}) \quad (6.40)$$

where β_1, β_2 are weighted coefficients such that $\beta_1 + \beta_2 = 1$ and for the calculations in the work those coefficients were assumed as $\beta_1 = \beta_2 = 0.5$ which means similar significance of both strain picks, $y_i(\mathbf{x}), i = 1, 2$, is a relative strain pick, given by the formula:

$$y_i(\mathbf{x}) = \frac{\varepsilon_i^{\max}(\mathbf{x}) - \varepsilon_i^{\min}(\mathbf{x})}{\varepsilon_i^{\max}(\mathbf{x})} \quad i = 1, 2 \quad (6.41)$$

where $\varepsilon_i^{\max}, \varepsilon_i^{\min}, i = 1, 2$, the maximum and the minimum of the strain along the fixed line for the first and the second strain region, respectively.

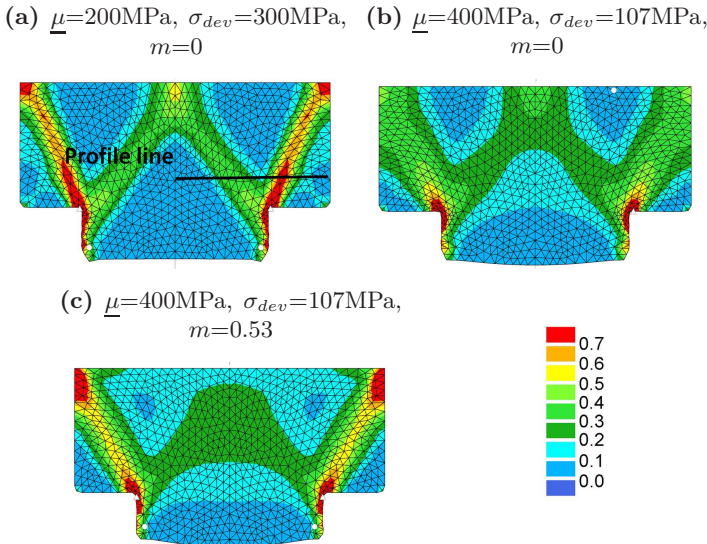


Figure 6.25: Examples of the strain distribution field obtained from the CAFE model with different input parameters.

According to Morris algorithms, each component of the \mathbf{x} vector was rescaled to the interval $[0, 1]$. The parameters of the algorithm were setup as follows: the number of the analyzed parameters $n = 3$, the number that characterizes the division of the unit interval $k = 4$, the number of independent trajectories $r = 5$. The results of the sensitivity calculations are presented in Figure 6.26. Distributions F_i for the

parameters of the vector \mathbf{x} are shown in Figures 6.26a - 6.26c, and means in function of standard deviations of elementary effects are presented in Figure 6.26b.

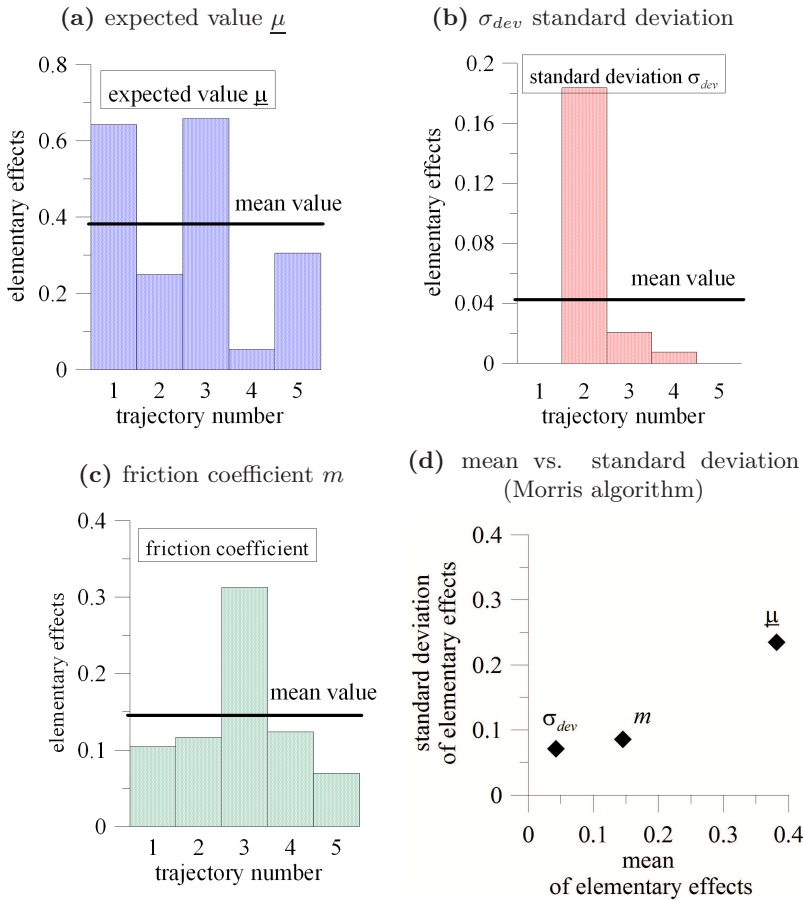


Figure 6.26: Distribution F_i of the elementary effects $\xi_i(\mathbf{x})$ and estimated mean and standard deviation of the effects for the parameters of shearing test.

The elementary effects of the expected value $\underline{\mu}$ (Figure 6.26a) vary from 0.05 to 0.66. The highest values are obtained for the conditions of the process while the fraction of the shear bands in the deformation is significantly independent of contact properties (the friction coefficient) - see trajectories 1 and 3. The elementary effects of the standard deviation σ_{dev} (Figure 6.26b) vary from 0.07 to 0.18. If the values of the standard deviation are high, the output of the model is not sensitive to this parameter (trajectories 1 and 5) or the response is weak (trajectories 3 and 4). The elementary effects of the friction coefficient m (Figure 6.26c) vary from 0.07 to 0.31. The distribution is uniform, except the trajectory 3 while the fraction of shear bands in the deformed specimen is very high. The analysis of the mean values (Figure 6.26d)

proved that the model response is the most sensitive to the expected value $\underline{\mu}$, the friction coefficient m controls the process to a minor extent, and the influence of the standard deviation σ_{dev} is weak. Standard deviations (Figure 6.26d) of the considered parameters show that the expected value $\underline{\mu}$ with the highest value interacts with other parameters (the standard deviation σ_{dev} and the friction coefficient m) or its effect is nonlinear.

6.3.5 Discussion of the results

The application of the shearing test, where the material flow is highly constrained, provides valuable data for the sensitivity analysis. The Morris algorithm of the screening design applied to the sensitivity analysis of the CAFE model highlighted the model parameters with the most important overall influence on the output. The main advantage of the Morris algorithm are the relatively low costs of calculations. This feature of the method is desirable due to excessive time of the CAFE simulation of complex deformation processes. As presented, the influence of the standard deviation is very small, that is why during further research the investigation of additional parameters that are present in the transition rules have to be considered. As expected, the value of $\underline{\mu}$ is most significant and this value has to be identified very precisely to describe the real behavior of the material properly. The obtained results are helpful in the identification procedure to estimate the model parameters and to predict the material behavior during the process with higher accuracy. Some examples of the identification parameters for selected materials are provided in the work [63].

6.4 The phase transformation model for the design of laminar cooling and continuous annealing of steels

As it was mentioned in section 6.3, the accuracy of the modeling of metal forming processes depends, to a large extent, on properly defined phenomena which occur during the deformation. While predicting the product microstructure and properties is required, phase transformation models have to be included in the modeling. Therefore, a phase transformation model was selected as the next example of the sensitivity analysis and the identification procedure in the present work.

A large number of phase transformation models are available in the literature, from the simplest ones based on the Johnson-Mehl-Avrami-Kolmogorov (JMAK) equation [4] through more advanced models based on the phase field [106] or a solution of differential equation [111] to discrete models based on the Cellular Automata method [59]. All these models are characterized by various complexity of the mathematical formulation and various predictive capabilities. Two aspects decide about the accuracy and effectiveness of the phase transformation modeling: the selection of a relevant model for a particular application and correct identification of the model parameters. In metals processing, the problem of identification of models using the inverse procedure 5.1 was widely investigated for flow stress models, see, for example, the author's papers [117, 125]. The application of the inverse procedure to identify

phase transformation models was first presented in [93, 48] and that approach was used in the present work, supported by sensitivity analysis algorithms to investigate the model parameters uncertainty, to formulate the most efficient version of the model and to decrease computational costs.

6.4.1 Objectives of the work

The selection of the relevant phase transformation model for a particular application was the primary objective of the work. The selection has to be made by searching for a balance between the model predictive capabilities and computing costs. In the investigations, a modified JMAK phase transformation model for steels was proposed. The next objective was to validate the model construction with the sensitivity analysis presented in Chapter 4, especially global sensitivity methods provided in section 4.2, to identify the model parameters of the highest impact to the model outputs, and to apply the identification procedure 5.1 to determine the model parameters for a particular material.

6.4.2 Phase transformation models

Selection of the model

Classification of phase transformation models with respect to predictive capabilities and computing costs is presented in Figure 6.27. The first group (bottom left corner in Figure 6.27) contains models commonly used for fast simulations of industrial processes and they are generally limited to the description of the kinetics of transformations and the volume fractions of the phases. The additivity rule [103] is applied in these models to account for the temperature changes during the transformations. In the second group (the centre in Figure 6.27) there are differential equations or the phase field technique models, usually applied to the technology design and the optimization of processes. These models accurately describe transformations in varying temperatures. The next group (further right in Figure 6.27) includes models based on the finite element (FE) solution of the diffusion equation with a moving boundary [88]. Beyond the parameters mentioned earlier, these models are capable of predicting the distribution of carbon concentration in austenite and the resulting hardness of bainite and martensite.

A significant extension of the predictive capabilities is obtained when the models listed above are implemented into the finite difference or finite element models which simulate industrial thermomechanical processes [92]. This coupling involves an increase in the computing costs. Finally, the most advanced models (the top right corner in Figure 6.27) connect the FE codes with discrete models, such as Cellular Automata (CA), Molecular Dynamics (MD) or Monte Carlo (MC).

The performed analysis of the phase transformation models and the published data [8] lead to the conclusion that the modified JMAK equation models are accurate and efficient enough to be applied in the modeling when the volume fractions of the phases are the optimization parameters. Since the objective of the work was fast prediction of transformation temperatures and volume fractions of the structural components in industrial processes, the modifications of the JMAK equation were considered.

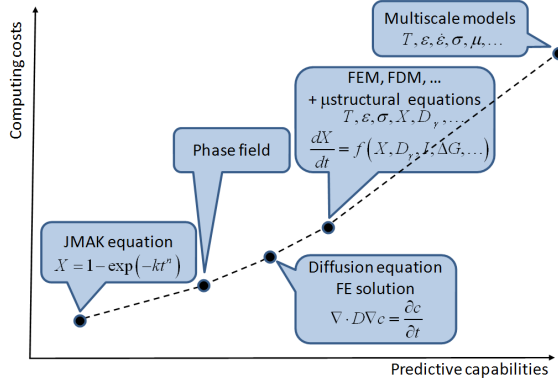


Figure 6.27: Classification of the selected phase transformation models: computing costs versus predictive capabilities.

A description of the JMAK model

The general form of the JMAK equation is:

$$X = 1 - \exp(-kt^n) \quad (6.42)$$

where X is the transformed volume fraction, t is time, k , n are the parameters.

Theoretical considerations show that, according to the transformation type (the nucleation and growth process, the site saturation process) a constant value of the parameter n in Equation (6.42) can be used. The values of n are introduced in the model as a_4 , a_{15} and a_{24} for ferritic, pearlitic and bainitic transformations, respectively. The parameter k should map the form of the Time-Temperature-Transformation (TTT) diagram. Following that observation, k is defined as a temperature function $k = f(\hat{T})$. Various forms of k were tested in the work. A too simple function may cause low accuracy of the model and a too complex function may cause problems with the identification of the model and the lack of the uniqueness of the solution. The function $k = f(\hat{T})$ has to be flexible enough to replicate complex phenomena of the nucleation and growth controlled by diffusion, interface mobility and solute-drag effect. These phenomena are reversibly dependent on the temperature. The rate of nucleation increases with the temperature drop below A_{e3} . Contrary, diffusion becomes slower at lower temperatures. That inspired the authors of [20] to propose a modified Gaussian function for the parameter k which is used for ferritic transformation in this work:

$$k = k_{\max} \exp \left[- \left(\frac{\hat{T} - T_{nose}}{a_7} \right)^{a_8} \right] \quad (6.43)$$

where \hat{T} is temperature in °C. The four parameters in this function k_{\max} , T_{nose} , a_7 , a_8 allow to describe all shapes of the TTT curves in a quite intuitive way: k_{\max} is

the maximum value of k , T_{nose} is a temperature position of the nose of the Gaussian function and represents the temperature (in °C) of the maximum rate of the transformation, a_8 is proportional to the nose width at mid height and a_7 is related to the sharpness of the curve.

Equation (6.43) is supposed to account for the influence of the austenite grain size at the beginning of the transformation. Thus, the following equations are used to calculate the parameters k_{max} and T_{nose} :

$$k_{max} = \frac{a_5}{D_\gamma} \quad (6.44)$$

$$T_{nose} = A_{e3} + \frac{400}{D_\gamma} - a_6 \quad (6.45)$$

where D_γ is the austenite grain size at the beginning of the transformation.

It was concluded from the primary model investigations that there is no need to introduce such a complex function $k(\hat{T})$ for pearlitic and bainitic transformations. Therefore, a slightly simpler function was selected for the pearlitic transformation:

$$k = \frac{a_{14}}{D_\gamma^{a_{16}}} \exp\left(a_{13} - \frac{a_{12}\hat{T}}{100}\right) \quad (6.46)$$

In the bainitic transformation the dependence on the grain size D_γ is neglected:

$$k = a_{23} \exp\left(a_{22} - \frac{a_{21}\hat{T}}{100}\right) \quad (6.47)$$

In the model phases incubation times should be accounted for. Equation (6.42) combined with the function (6.43) does not require the incubation time. It is assumed that ferritic transformation begins when the volume fraction of ferrite achieves 5%. Incubation times of the remaining transformations (τ_p, τ_b) are calculated as:

- for pearlite

$$\tau_P = \frac{a_9}{(A_{e1} - \hat{T})^{a_{11}}} \exp\left(\frac{a_{10} \times 10^3}{RT}\right) \quad (6.48)$$

- for bainite

$$\tau_b = \frac{a_{17}}{(a_{20} - \hat{T})^{a_{19}}} \exp\left(\frac{a_{18} \times 10^3}{RT}\right) \quad (6.49)$$

Additional relationships in the model and equilibrium carbon concentrations are:

$$c_\gamma = \frac{(c_0 - X_f c_\alpha)}{1 - X_f} \quad X_{f0} = \frac{c_{\gamma\alpha} - c_0}{c_{\gamma\alpha} - c_\alpha} \quad (6.50)$$

$$c_{\gamma\alpha} = c_{\gamma\alpha 0} + c_{\gamma\alpha 1} \hat{T} \quad c_{\gamma\beta} = c_{\gamma\beta 0} + c_{\gamma\beta 1} \hat{T} \quad c_\alpha = f(\hat{T}) \quad (6.51)$$

where c_γ is the average carbon content in the austenite, c_α is carbon content in the ferrite, c_0 is carbon content in the steel, $c_{\gamma\alpha}$ is carbon concentration in the austenite at the γ - α boundary, $c_{\gamma\beta}$ is carbon concentration in the austenite at the γ -cementite boundary, X_{f0} is equilibrium (maximum) ferrite volume fraction in the steel in the considered temperature. The equilibrium concentrations $c_{\gamma\alpha}$ and $c_{\gamma\beta}$, as well as carbon content in the ferrite c_α , are introduced as the temperature functions. These functions are polynomials and they are determined using ThermoCalc software based on the information on the steel chemical composition.

Modeling of phase transformations starts with Equation (6.42) when the temperature drops below A_{e3} . The additivity rule [103] is applied to the model to account for the temperature variations during transformation. The transformed ferrite volume fraction $X_f(\hat{T}^{(i)})$ is calculated with respect to the maximum volume fraction of ferrite $X_{f0}(\hat{T}^{(i)})$ for the temperature $\hat{T}^{(i)}$. Thus, the volume fraction of ferrite with respect to the whole volume of the material is $F_f = X_{f0}X_f$ for the fixed temperature $\hat{T}^{(i)}$. The value of X_f calculated from Equation (6.42) for the varying temperature has to be corrected due to a change in the equilibrium (maximum) ferrite volume fraction X_{f0} , which is the temperature function (see Table 6.7):

$$X_f(\hat{T}^{(i+1)}) = X_f(\hat{T}^{(i)}) \frac{X_{f0}(\hat{T}^{(i)})}{X_{f0}(\hat{T}^{(i+1)})} \quad (6.52)$$

where i is the iteration number, $\hat{T}^{(i)}$ is temperature in the i^{th} iteration. The simulation continues until the transformed volume fraction achieves 1. However, when carbon content in the austenite exceeds the limiting value $c_{\gamma\beta}$ (see Equations (6.50) and (6.51)), the austenite-pearlite transformation begins in the remaining volume of the austenite.

The bainite initial temperature T_{bs} and the martensite initial temperature T_{ms} are functions of the chemical composition of the austenite:

$$T_{bs} = a_{20} - 425[\text{C}] - 42.5[\text{Mn}] - 31.5[\text{Ni}] \quad (6.53)$$

$$T_{ms} = a_{26} - a_{27}c_\gamma \quad (6.54)$$

Fraction of the austenite which transforms into the martensite, is calculated according to the model of Koistinen and Marburger [47], described also in [143, 93]:

$$X_m = 1 - \exp\left[-0.011\left(T_{ms} - \hat{T}\right)\right] \quad (6.55)$$

Equation (6.55) represents the volume fraction of martensite with respect to the volume of austenite which was remaining at the temperature T_{ms} . The volume fraction of martensite with respect to the whole volume of the material is:

$$F_m = (1 - F_f - F_p - F_b) X_m \quad (6.56)$$

where F_f , F_p , F_b are the volume fractions of ferrite, pearlite and bainite with respect to the whole volume of the sample.

Since continuous annealing was selected as a case study in this work (see section 6.6), the transformation of the ferritic-pearlitic microstructure into the austenite also has to be considered. Kinetics of the austenitic transformation during heating is described by Equation (6.42) with the coefficient $n = a_{30}$ and the coefficient k defined as:

$$k = a_{28} \exp\left(\frac{-a_{29} \times 10^{-3}}{RT}\right) \quad (6.57)$$

Incubation time for the ferrite-austenite transformation is calculated from the equation:

$$\tau_a = \frac{a_1}{(\hat{T} - A_{e_1})^{a_3}} \exp\left(\frac{a_2 \times 10^3}{RT}\right) \quad (6.58)$$

The phase transformation model described by Equations (6.42)-(6.58) was applied to predict the phases distribution in the material for the selected industrial process: continuous annealing after cold rolling presented in section 6.6. To perform the numerical modeling of a process the model was validated with sensitivity analysis first and next identified using the identification procedure.

6.4.3 Sensitivity analysis

Sensitivity of the modified JMAK phase transformation model with respect to the model coefficients was estimated using three global sensitivity methods from Chapter 4: the Morris design provided in section 4.2.1, correlation ratios presented in section 4.2.2, and Sobol' indices from section 4.2.2. The model inputs were: $\mathbf{x} = (cr, \mathbf{a})$, where cr is the cooling rate, $\mathbf{a} = (a_4, \dots, a_{27}, D_\gamma)$ are coefficients of the JMAK model. Ten model outputs $\mathbf{y} = (T_{ij}, F_i)$ were analyzed, where T_{ij} is temperature, F_i is the phase volume fraction, $i \in \{f, p, b, m\}$ indicates the ferrite, pearlite, bainite or martensite phase, $j \in \{s, e\}$ indicates the beginning/end of the phase transformation, respectively. The modified JMAK model includes information on the steel chemical composition, as well as information on the phase equilibrium conditions. Hence, the calculations were performed for the selected dual phase steels. One of them was used in modeling of the industrial process presented in section 6.6. The chemical composition of the steels are listed in Table 6.6 while the parameters describing the carbon concentration equilibrium, determined with the ThermoCalc software, are provided in Table 6.7.

Table 6.6: Chemical composition of the investigated steels, weight%.

C	Mn	Si	P	S	Cr	Mo	Cu	Al	V	Nb	Ti	N
DP1203:												
0.071	1.45	0.25	0.01	0.006	0.55	0.03	0.02	0.022	0.005	0.005	0.002	0.0039
DP1205:												
0.11	1.45	0.19	0.014	0.006	0.27	0.03	0.01	0.034	0.005	0.004	0.013	0.0038

The sensitivity results for all the parameters $\mathbf{a} = (a_4, \dots, a_{27}, D_\gamma)$ obtained for the investigated steels by the Morris algorithm are presented in Figure 6.28. It is

Table 6.7: Parameters in Equations (6.50)-(6.51) describing the carbon concentration equilibrium.

	$c_{\gamma\alpha 0}$	$c_{\gamma\alpha 1}$	$c_{\gamma\beta 0}$	$c_{\gamma\beta 1}$
DP1203:	4.85	-0.005776	-1.47	0.00289
DP1205:	4.57	-0.005412	-0.94	0.00228
	$c_{\alpha} = \begin{cases} -0.069 + 0.000435\hat{T} - 9.1658 \times 10^{-7}\hat{T}^2 + 6.487 \times 10^{-10}\hat{T}^3 & \text{for } \hat{T} < 637^{\circ}C \\ -0.0487268 + 0.00017839\hat{T} - 1.50788 \times 10^{-7}\hat{T}^2 & \text{for } \hat{T} \geq 637^{\circ}C \end{cases}$			

observed that some of the model parameters do not impact any model outputs, some of them influence the model outputs in a negligible way. These parameters cannot be identified based on the analyzed model outputs or they should be eliminated from the model.

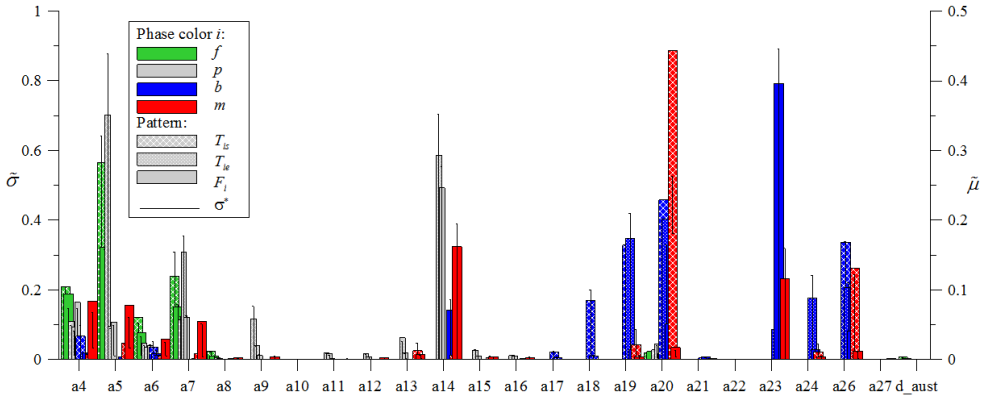


Figure 6.28: Sensitivity analysis results obtained by Morris design for the modified JMAK model of the cooling process.

The conclusions are formulated as the summary results from the application of three sensitivity methods: Morris design, correlation ratios and Sobol' indices:

- *Ferrite*. The results for ferrite transformation obtained from all the sensitivity methods are presented in Figure 6.29. Initial temperature of ferrite transformation is most sensitive to a_7 (a parameter in the k equation (6.43)) - a high impact of this parameter on T_{fs} and F_f is observed. The following remarks are made for the next parameters: a_4 (an exponent in Equation (6.42)) - slight sensitivity to the temperature start T_{fs} , higher sensitivity to the volume fraction F_f , a_5 (a parameter in the k_{max} equation (6.44)) and a_6 (a parameter in the T_{nose} equation (6.45)) - both outputs: T_{fs} and F_f are sensitive to these parameters, a_8 (a parameter k in Equation (6.43)) - a low impact of this parameter on T_{fs} and F_f , a_{20} (a parameter in the T_{bs} equation (6.53) and the bainite incubation time τ_b in Equation (6.49)) - it determines T_{bs} and it indirectly influences F_f - thus higher sensitivity to F_f , low sensitivity to T_{fs} . D_{γ} (a parameter in the k_{max} equation (6.44)) - the same sensitivity conclusions as

for a_{20} . Suggestion: the parameter a_8 can be eliminated in modeling the ferrite phase transformation. The lack of the model sensitivity on the D_γ parameter is questionable. This problem should be investigated by performing dilatometric tests for various grain sizes.

- *Pearlite*. For the considered chemical composition of steels, the contribution of pearlite transformation is negligible and observed for low cooling rates, below 1°C/s. The conclusions on the model sensitivity are formulated based on the Morris Design calculations - Figure 6.28. The initial phase transformation temperature T_{ps} is sensitive to the parameter a_5 in the k_{max} equation (6.44) for ferrite transformation which indirectly influences the beginning of the pearlite transformation. The end phase transformation temperature T_{pe} and the phase volume fraction F_p are sensitive first of all to the parameter a_{14} in the k equation (6.46) for pearlite. Some sensitivity is observed for the parameters a_4 and a_7 which are related to the ferrite phase. For the dual phase steels that were chosen for the analysis, those parameters determine whether the pearlite transformation begins, hence their impact on the pearlite model outputs. Regarding that fact, the model of the pearlite transformation for DP steels can be simplified.
- *Bainite*. The results for bainite transformation obtained from all the sensitivity methods are presented in Figure 6.30. Three bainite phase model outputs: the phase transformation temperature start/end T_{bs}/T_{be} and the phase volume fraction F_b are sensitive to the a_{20} parameter from the T_{ms} equation (6.53) and the bainite k equation (6.49) and next to the a_{26} parameter from Equation (6.54) defining the phase initial temperature of martensite. Next T_{bs} is sensitive to the a_{19} and a_{18} - parameters from the bainite incubation time τ_b (Equation (6.49)). Lower sensitivity to these parameters is observed for T_{be} . The model output T_{be} is sensitive to a_{24} which is the exponent n in Equation (6.42)). The remaining parameters defining bainite transformation: a_{17} , a_{21} , a_{22} , a_{23} do not impact the bainite model outputs or their impact is very low. Suggestion: the bainitic transformation model can be simplified.
- *Martensite*. The results for martensite transformation obtained from all the sensitivity methods are presented in Figure 6.31. The phase temperature start T_{ms} is sensitive to the a_{20} parameter from the T_{bs} equation (6.53) and next to the a_{26} parameter from the T_{ms} equation (6.54). The results for the phase volume fraction F_m are not consistent but the impact of the parameters a_{20} and a_{26} listed above is observed. Moreover, a slight influence of a_4 - a_7 , a_{14} and a_{23} is noticed.

To sum up, the sensitivity analysis indicated the set of parameters of the highest impact on the model outputs and in the parameters identification process they should be determined. The parameters of the low impact should be fixed or, if it is possible, eliminated from the model of the investigated steels.

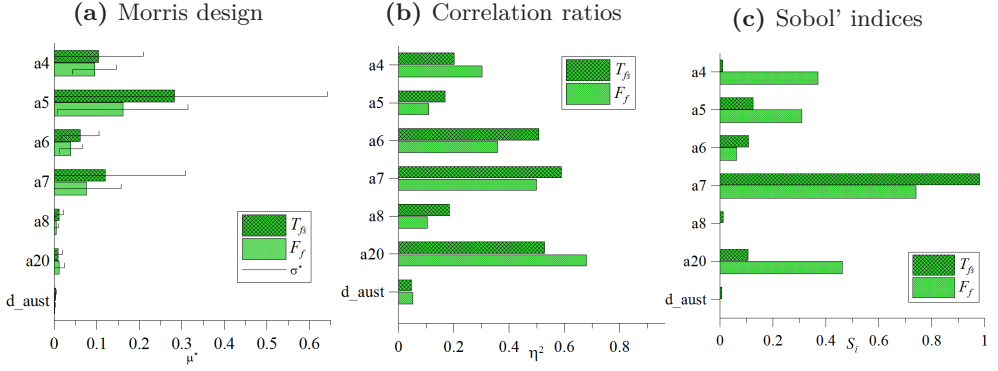


Figure 6.29: Ferrite phase sensitivity indices calculated with respect to the parameters of the modified JMAK model estimated by the three SA methods.

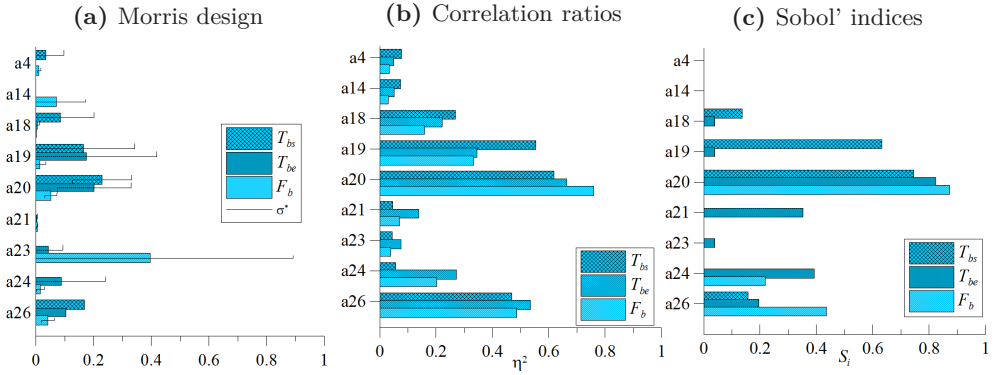


Figure 6.30: Bainite phase sensitivity indices calculated with respect to the parameters of the modified JMAK model estimated by the three SA methods.

6.4.4 Identification of the model parameters

According to the functional (5.1) defined in the identification strategy algorithm 5.1, the functional to solve the identification problem of the JMAK model is expressed as:

$$\Phi(\mathbf{a}) = \frac{1}{n_T} \sum_{i=1}^{n_T} \beta_i^T [T_i^m - T_i(\mathbf{a})]^2 + \frac{1}{n_F} \sum_{i=1}^{n_F} \beta_i^F [F_i^m - F_i(\mathbf{a})]^2 \quad (6.59)$$

where $\mathbf{a} = (a_1, \dots, a_{30})$ is the vector of the identified coefficients of the JMAK model, T_i^m, T_i are measured and calculated initial and final temperatures of the phase transformations, β_i^T are weighted coefficients defined as $1/(T_i^m)^2$, n_T is the number of temperature measurements, F_i^m, F_i are the measured and calculated phases volume fractions at the room temperature, β_i^F are weighted coefficients defined as $1/(F_i^m)^2$,

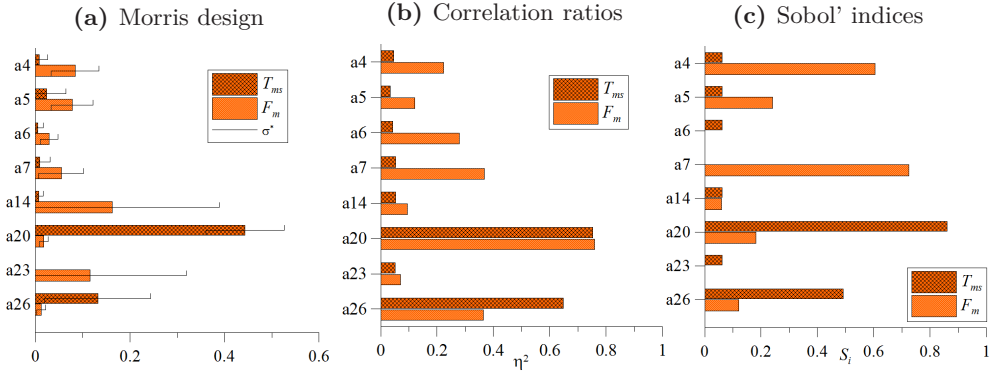


Figure 6.31: Martensite phase sensitivity indices calculated with respect to the parameters of the modified JMAK model estimated by the three SA methods.

n_F is the number of measurements of the phase volume fractions, i indicates the phase transformation.

The functional (6.59) was minimized using the modified particle swarm algorithm provided in Chapter 4, section 4.1.2, to increase the calculation efficiency. The values of the \mathbf{a} parameters obtained from the identification procedure are given in the Table 6.8. The whole JMAK model for all the transformations contains 30 parameters. However, after the simplification based on the sensitivity analysis only 26 of them were active in the transformation model for the considered dual phase steels and they were used in the present work.

The model described by the parameters presented in Table 6.8 was validated. It was used to simulate all the performed dilatometer tests. Figure 6.32a shows the comparison of the measured (filled symbols) and predicted (open symbols) initial and final temperatures of the phase transformations for DP1203 steel. The shape of the symbol refers to the temperature in the legend. An analysis of the results confirms that the model predicts initial and final temperatures for the transformations quite well, although the accuracy is slightly worse for the pearlite initial and bainite final temperatures. Figure 6.32b shows the calculated volume fractions of the phases for the same steel. Similarly good results were obtained for DP1205 steel.

6.4.5 Discussion of the results

An analysis and identification of the phase transformation models for steels was performed. The following observations were made:

- The model based on the modified JMAK equation is efficient and satisfactorily accurate and it can be used for the optimization of the manufacturing of steels when volume fraction of the phases are the objectives of the optimization.

Table 6.8: Coefficients in the phase transformation model calculated using the identification analysis for the investigated DP steels.

	a_1	a_2	a_3	a_4	a_5	a_6	a_7	a_8	a_9
DP1203:	1039	4.861	2.866	1.333	0.673	157.9	39.83	1.983	64.76
DP1205:	1039	4.861	2.866	1.690	0.858	187.9	39.06	1.779	64.84
	a_{10}	a_{11}	a_{12}	a_{15}	a_{17}	a_{18}	a_{19}	a_{20}	a_{21}
DP1203:	1.106	0.618	0.153	1.285	1842	66.59	3.489	692.7	0.181
DP1205:	1.106	0.618	0.153	1.285	1600	64.64	3.495	669.2	0.118
	a_{22}	a_{23}	a_{24}	a_{25}	a_{26}	a_{27}	a_{28}	a_{29}	a_{30}
DP1203:	0.074	0.406	1.049	0	435.8	1.732	9636	79.4	0.229
DP1205:	0.074	0.344	1.037	0	421.7	1.830	9636	79.4	0.229

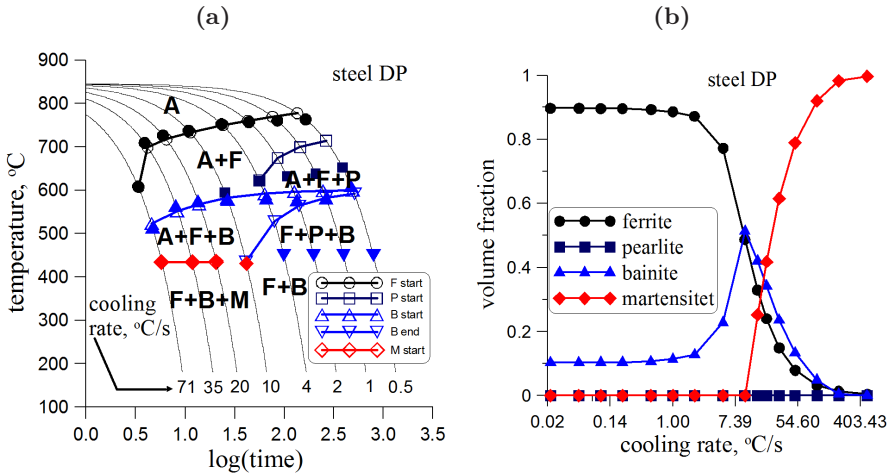


Figure 6.32: Comparison of the predictions of the optimized phase transformation model (the coefficients in Table 6.8 for DP1203 steel) with measurements for (a) the transformations initial and final temperatures and for (b) volume fractions of the phases.

- Sensitivity analysis allowed to simplify the modified JMAK equation model by removing the relation of the temperature dependent coefficients describing kinetics of the pearlite transformation.
- The identification procedure is efficient to determine a large number of the phase transformation model parameters and the application of sensitivity analysis reduced the dimension of the parameter domain.

6.5 Design of the hot rolling technology of dual phase steel strips

Optimization of product properties in the metal forming industry is a complex task. This is particularly challenging for innovative materials, e.g. dual phase steels, which

require precise thermomechanical treatment. Numerical modeling of the production of dual phase steels includes thermomechanical model for the rolling and phase transformation model for microstructure properties. Both of the models are characterized by the material parameters and the model predictions are related to the accuracy of the determination of these parameters. The phase transformation model was the subject of the investigations presented in section 6.4. This section deals with the problem of the parameter identification of another part of the production cycle - the hot rolling process.

6.5.1 Objectives of the work

Difficulties in the optimization of material properties after hot rolling are usually related to a large number of control variables which should be considered in the technology design. Thus, the objective of the work was to apply the sensitivity analysis to evaluate the importance of all variables as far as their influence on the finishing rolling temperature and the grain size. An arbitrary hot rolling process characterized only by a number of passes and cooling conditions between the passes was selected for the analysis. Such process parameters as the initial temperature, interpass times, heat exchange coefficients and rolling velocities were selected as independent variables. The next objective was to define the task of the production cycle design based on the information from performed the sensitivity analysis the of rolling process and sensitivity analysis of the phase transformation model presented in section 6.4, and to make the identification procedure 5.1 robust for the formulated problem.

6.5.2 The experiment

The pilot hot rolling mill installed in the Institute for Ferrous Metallurgy in Gliwice, Poland, was used in the analysis. This mill enables an arbitrary configuration of the process composed of passes, controlled cooling/heating between the passes followed by the controlled cooling after rolling. Hot rolling in the reverse pilot mill of the 4 mm strip from 100×240 mm slab in 6 passes was investigated. The technical parameters of the rolling mill have an influence on the results but they are not controllable parameters and they were not the variables in the sensitivity analysis. These parameters are: the work roll diameter 250 mm, the length of the roll 700 mm, the maximum cross section of the stock slab 500×100 mm, the maximum rolling velocity 1.1 m/s, the pressure in the descaler 25 MPa, the maximum rolling force 2.5 MN. The detailed information on the semi-industrial line is presented in [25].

The investigated material was DP1205 steel of chemical composition presented in Table 6.6 in section 6.4. The plastometric and stress relaxation tests were performed to supply data for the identification and validation of the flow stress and the microstructure evolution models. All the tests were performed at the Institute for Ferrous Metallurgy in Gliwice. Axisymmetrical compression tests for the temperatures 800-1200°C and the strain rates $0.1-100\text{s}^{-1}$ were performed for the identification of the flow stress model. Stress relaxation tests were performed for the identification of the microstructure evolution model. The microstructure of the sample after cooling

characteristic for the DP steels (fast cooling to 680°C, maintaining at this temperature for 10 s and again fast cooling to the room temperature) is shown in Figure 6.33b. The microstructure is composed of 72% of ferrite, 8% of bainite and 20% of martensite. Mechanical properties of the DP steel sample were above the standard: $R_e = 462$ MPa, $R_m = 723$ MPa, $A_2 = 35.7\%$, $Z = 61\%$.

Multi-stage plane strain compression (PSC) tests, which simulated the rolling process, were performed for the validation of the flow stress and the microstructure evolution models. The strains (the strain rates, s^{-1}) in those tests were as follows: 0.4(5) → 0.3(5) → 0.2(10) → 0.2(10) → 0.2(30) → 0.2(50) → 0.2(50). The interpass times were, respectively: 30 s, 10 s, 10 s, 3 s, 3 s and 1 s. The recorded stresses and temperatures during the test are shown in Figure 6.33a. An analysis of the results shows that partial recrystallization of the austenite is observed in the last 4 passes in the range of temperatures 900-850°C. Flow stress value increases and in the last pass is about 3 times higher than in the first one.

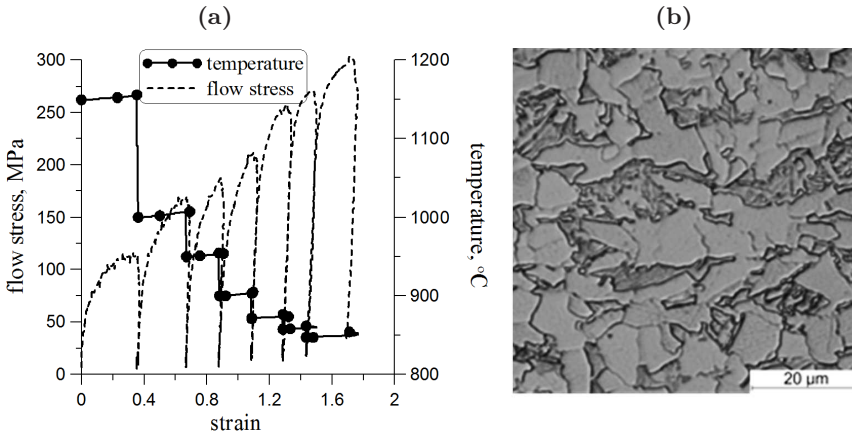


Figure 6.33: (a) Stress-strain relationship and changes of temperature in the multi-stage PSC test, (b) microstructure after the physical simulation of rolling and cooling characteristic for the DP steels.

6.5.3 The numerical model of the process

The numerical model of the hot rolling process described in the previous section is considered. The problem of each pass is formulated as an one-dimensional mechanical problem with time, combined with the heat equation solved using the finite element method [61], described by the equations provided in Chapter 3, section 3.1. The microstructure evolution model introduced to the finite element code is based on the fundamental works of Sellars [104].

The flow stress model parameters were estimated with the identification procedure 5.1 presented in section 6.1, based on the data from the experiments from the previous

section.

The flow stress model for the considered dual phase steel was:

$$\sigma_p = 3255.3\varepsilon^{0.19} \exp(-0.283\varepsilon) \dot{\varepsilon}^{0.119} \exp\left(-0.003007\hat{T}\right) \quad (6.60)$$

where \hat{T} is temperature in °C, ε is strain, $\dot{\varepsilon}$ is the strain rate.

The microstructure evolution model, as it was mentioned above, was based on Sellars research work [104]. Due to lower temperatures and higher strain rates in the finishing rolling dynamic recrystallization was neglected. The following equations were used:

- the kinetics of static recrystallization

$$X_{st} = 1 - \exp\left[\ln(0.5) \left(\frac{t}{t_{0.5}}\right)^{1.7}\right] \quad (6.61)$$

- time for 50% recrystallization

$$t_{0.5} = 8.5 \times 10^{13} \varepsilon^{-1.834} \dot{\varepsilon}^{-0.536} D_0^{1.8} \exp\left(\frac{218630}{RT}\right) \quad (6.62)$$

- the grain size after static recrystallization

$$D_{SRX} = 96.43 \varepsilon^{-0.408} D_0^{0.2} \dot{\varepsilon}^{0.14} \exp\left(-\frac{25371}{RT}\right) \quad (6.63)$$

- the grain growth

$$D^2 = D_{SRX}^2 + 10^A t \quad A = 9.5 + \frac{10920}{\hat{T}} \quad (6.64)$$

where X_{st} is the recrystallized volume fraction, D_0 is the grain size prior to deformation.

The flow stress and the microstructure models were implemented to the finite element solver of the rolling process.

6.5.4 Sensitivity analysis

Manufacturing of dual phase steel strips consists of hot rolling, laminar cooling, cold rolling and annealing processes. The design of the whole production cycle requires deep knowledge of each step of the process. Laminar cooling and annealing processes were investigated in the author's papers [113, 82]. In this work, the hot rolling process is considered. The formulation of the design task of hot rolling process with the numerical approach was the objective of the investigations and while the identification algorithm 5.1 was applied, the problem was formulated as the optimization task. The optimization for the production cycles has already been theoretically formulated for forging, see, for example, [57, 132] and for the identification problem in rolling [130]. Due to a large number of the optimization variables, a practical solution for rolling

is difficult. The hot rolling design problem is nonlinear and, when the finite element method is used to model this problem, computation costs are relatively high (the computation time of a few-stage rolling process is about two minutes). Moreover, there is no precise information on the design parameter domain - it is defined on the basis of experts' and technologists' knowledge. Thus, according to the identification algorithm 5.1, statement no. 1, the preliminary step to validate the hot rolling model should be preformed. This is crucial for the proper and effective process design. The validation was carried out with global sensitivity analysis methods provided in Chapter 4, section 4.2 because the whole parameter domain was going to be investigated and verified. Sensitivity analysis of the finishing rolling temperature and the final austenite grain size with respect to controllable process parameters was performed. It was expected that the number of process parameters would decrease and the ranges of their variability would be contracted.

Formulation of the hot rolling problem design

The model input parameters characterize the process, boundary conditions and the material. The model outputs are the final temperature of rolling and the average grain size after the last pass. The design of a hot rolling process is an identification problem that was transformed to the optimization task according to the algorithm 5.1. The functional of this identification problem includes the information on the final rolling temperature and the material microstructure, especially the desired value of the grain size:

$$\Phi(\mathbf{x}) = \|\mathbf{y}(\mathbf{x}) - \mathbf{y}^m\|^2 \quad (6.65)$$

where $\mathbf{x} = (a_{ij_k})$ is the vector of the selected process parameters: $i \in \{0, \dots, 6\}$ is the pass number; $j \in \{0, A, B, P\}$: 0 is the furnace, A, B is the transportation time, P is the pass; $k \in \{\widehat{T}, t, v, h\}$: \widehat{T} is temperature, t is the interpass time in s, v is the roll rotational speed in rpm., h is the heat transfer coefficient at the strip-roll interface in $\text{W}/(\text{m}^2\text{K})$; $\mathbf{y} = (T_{6P}, D_{\gamma 6P})$ are the model outputs: temperature and the grain size, respectively, m indicates the measured data.

The functional (6.65) is minimized with respect to \mathbf{x} (the parameters of the rolling process). To control the efficiency and robustness of the optimization procedure, the sensitivity analysis was carried out.

The sensitivity computations

The sensitivity indices: $\tilde{\mu}_i - \tilde{\sigma}_i$, $\tilde{\eta}^2$ and S_i were estimated for the rolling mill process. The indices were calculated with respect to the selected model parameters $\mathbf{x} = (a_{ij_k})$. The model outputs were the components of the functional (6.65): T_{6P} , $D_{\gamma 6P}$. The parameter domain was defined according to the technological constraints (see Table 6.9). The results are presented in Figures 6.34 and 6.35.

Table 6.9: Constraints of the process parameters $\mathbf{x} = (a_{ij_k})$.

a_{00_T}	a_{00_t}	a_{1A_t}	a_{1B_t}	a_{iP_h}	a_{iP_v}	$a_{iP_t, i \neq 6}$	a_{6P_t}
1100-1200	5-25	0.5-2	1-5	5×10^3 - 5×10^4	10-50	4-20	3-6

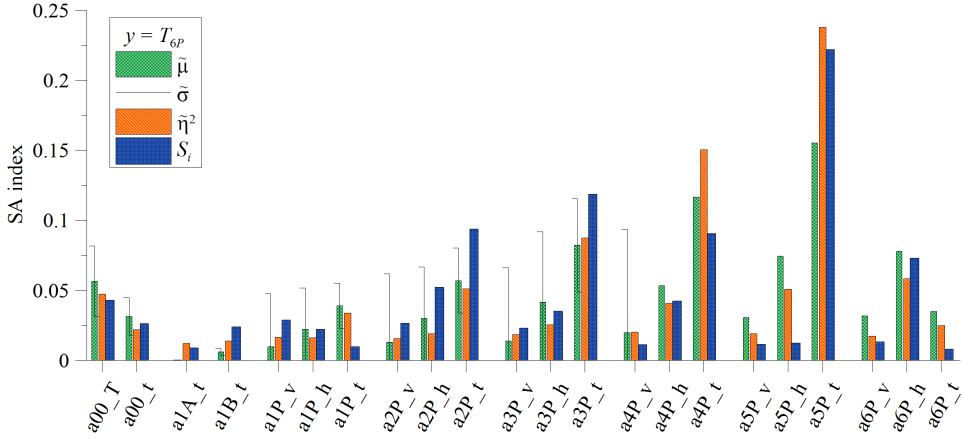


Figure 6.34: Sensitivity indices for the temperature T_{6P} after the last pass of the hot rolling process.

6.5.5 Discussion of the results

The performed analysis provided the information on the sensitivity of the model outputs with respect to the selected model inputs. The most important parameters are: the interpass times a_{iP_t} , the exit temperature from the furnace a_{00_T} , (see Figures 6.34 and 6.35). These parameters should be optimized in the hot strip rolling process design. The effect of the interpass time increases with the subsequent passes and the largest effect is for the interval after the 5th pass. Much lower sensitivity is observed for the roll rotational speed a_{iP_v} . The sensitivity to the heat transfer coefficients a_{iP_h} is reasonable, thus errors in the evaluation of these parameters will probably not influence the optimization.

The sensitivity analysis for hot strip rolling indicated the process variables of the highest importance to the temperature and the grain size after the last pass of rolling. These process variables compose interpass times and the exit temperature from the furnace and they will become the components of the optimization vector of the whole manufacturing process design.

The applied sensitivity analysis methods provided the information which was helpful in the identification of the model parameters of the highest impact to the model outputs. While the selected parameters are going to be decision variables in the process design formulated as the optimization task, the computation costs will be reduced, which was the main objective of those investigations.

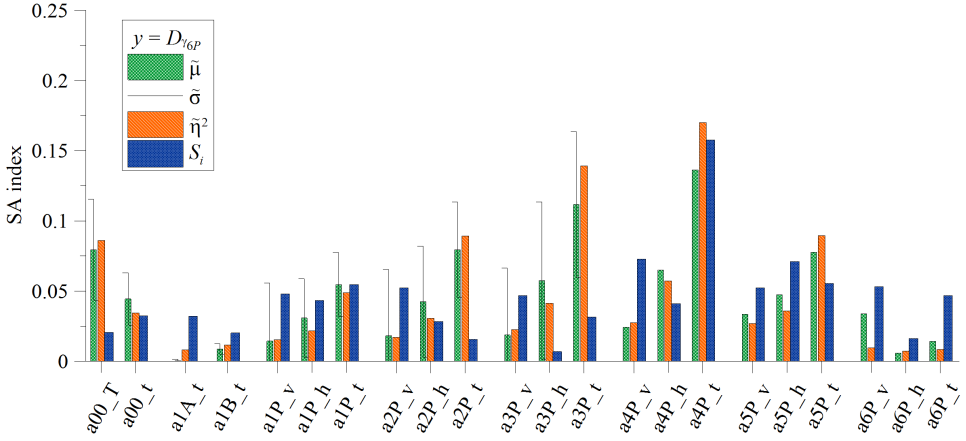


Figure 6.35: Sensitivity indices for the grain size $D_{\gamma_{6P}}$ after the last pass of the hot rolling process.

6.6 Design of the continuous annealing process

Continuous annealing after cold rolling was selected as a testing process for the identified phase transformation model described in section 6.4. The investigations were performed for DP1205 steel of chemical composition presented in Table 6.6 in section 6.4. Sensitivity analysis of the annealing process with respect to the controllable parameters of the cycle was carried out first, the results were presented in [113]. Physical simulations of that process were performed to validate the model, as well [94]. The main conclusions from [113] are:

- with respect to the phase volume fractions the most important parameter is the intercritical temperature T_{h1} which decides of ferrite volume not transformed into austenite during heating stage,
- next the annealing phase transformation model is sensitive to the parameters of the first, rapid step of the cooling stage: the cooling rate C_{r1} and the final temperature T_{r1} ; this step is crucial for producing ferrite microstructure from austenite and influences the beginning of the bainite and martensite transformations,
- the remaining parameters of the annealing process are not so much important.

Simulations of the continuous annealing after cold rolling were performed to test the predictive capabilities of the model. Four thermal profiles characteristic for the continuous annealing were considered. A schematic illustration of the typical continuous annealing thermal cycle is shown in Figure 6.36a and the investigated cycles are shown in Figure 6.36b. Heating/cooling rates, as well as the final temperature for each part of the cycle were the controllable parameters of the cycle. The values

of these parameters are given in Table 6.10. In the last part of each cycle C_{r5} was 20°C/s and the final temperature was equal to the room temperature.

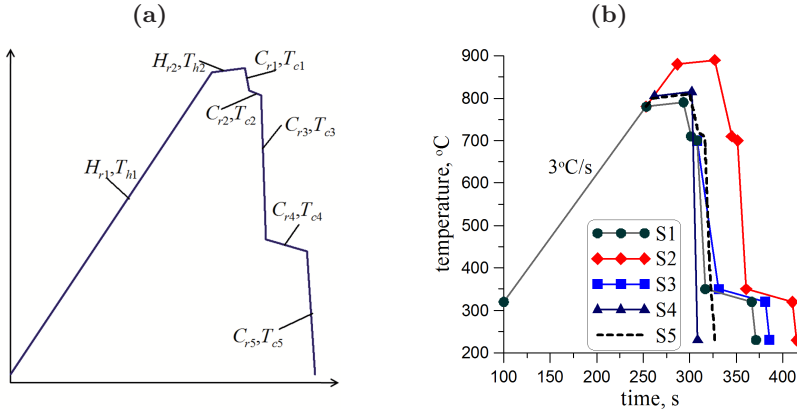


Figure 6.36: (a) A typical continuous annealing thermal profile, (b) thermal profiles for annealing processes investigated in the work.

The results of simulations of the annealing thermal cycles S1-S4 in Table 6.10 are presented in Figures 6.37 and 6.38.

Table 6.10: Heating/cooling rates, $^\circ\text{C/s}$, and final temperatures, $^\circ\text{C}$, for each part of the thermal cycles for the investigated annealing processes.

cycle	H_{r1}	T_{h1}	H_{r2}	T_{h2}	C_{r1}	T_{c1}	C_{r2}	T_{c2}	C_{r3}	T_{c3}	C_{r4}	T_{c4}
S1	3	780	0.25	790	8	710	6.67	700	8.75	350	0.6	320
S2	3	880	0.25	890	18	710	6.67	700	8.75	350	0.6	320
S3	3	780	0.25	790	8	710	6.67	700	23.3	350	0.6	320
S4	3	805	0.25	815	9.94	710	6.67	700	20	350	0.6	320
S5	3	790	0.25	800	10	700	7.4	689	5.65	350	0.6	320

Changes of volume fractions of the phases are presented in Figures 6.37a and 6.38a. The thermal cycles S1 and S2 differed with the maximum temperature of the cycle. This temperature was 890°C for the case S2 and full austenitization after heating was obtained. The maximum temperature in the case S1 was 765°C , which was in the lower part of the inter critical region. In consequence, over 70% of ferrite remained in the microstructure after heating. The cases S3 and S4 represent annealing in the inter critical region of the temperature but with the maximum temperature of 790°C , which is higher than in the case S2. The differences between S3 and S4 were in the temperatures of heating and in the cooling rates during fast cooling (see Table 6.10). Changes in the average carbon concentration in austenite are presented in Figures 6.37b and 6.38b. It is seen in this figure that the largest carbon concentration was obtained for the case S1, in which the final volume fraction of ferrite was the largest. Volume fractions of the phases after various annealing cycles are shown in

Figure 6.39a. It is observed that the required volume fraction of ferrite at the level of 0.7 was obtained for the case S3, but the disadvantageous excess of bainite over martensite was observed. The volume fraction of ferrite was slightly too low in the case S4, but only a negligible amount of bainite was obtained in that case.

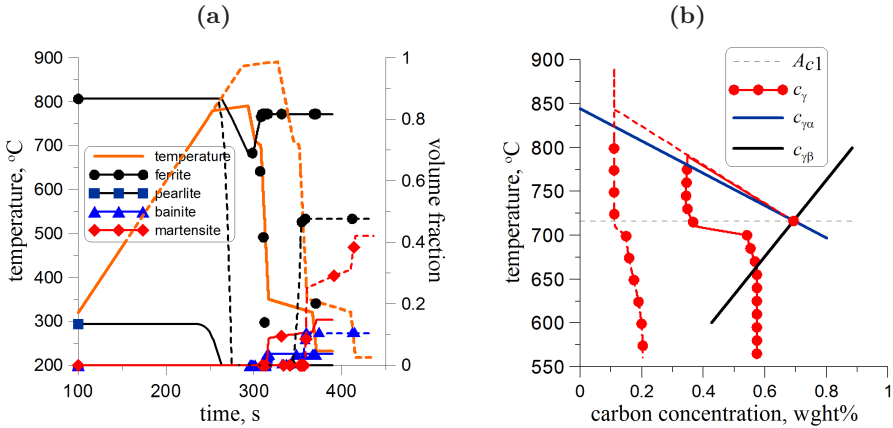


Figure 6.37: (a) The temperature and kinetics of the transformations during the annealing cycles S1 (solid lines) and S2 (dotted lines), (b) changes in the average carbon concentration in austenite during the annealing cycles S1 (solid line) and S2 (dotted line).

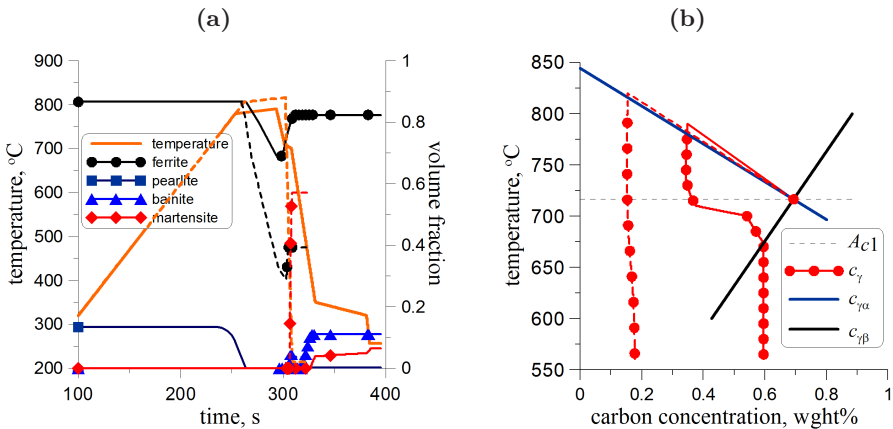


Figure 6.38: (a) The temperature and kinetics of the transformations during the annealing cycles S3 (solid lines) and S4 (dotted lines), (b) changes in the average carbon concentration in austenite during the annealing cycles S3 (solid line) and S4 (dotted line).

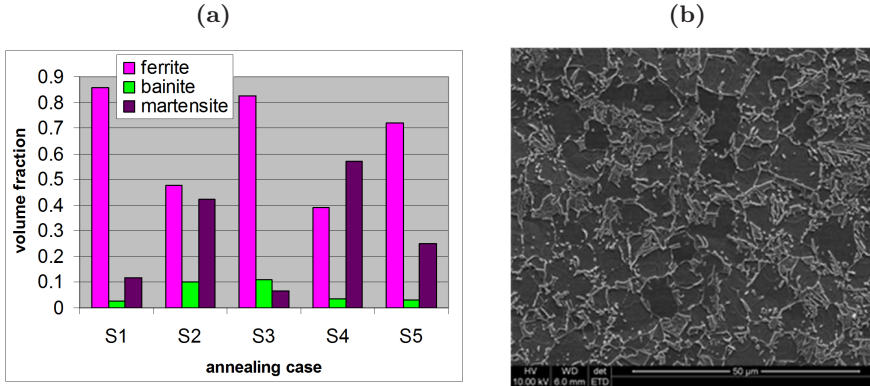


Figure 6.39: (a) Volume fractions of the phases after various annealing cycles, (b) microstructure after the thermal cycle A5, composed of 32% of hard constituents, approximately 25% of martensite and 7% of bainite (courtesy of Professor Roman Kuziak from the Institute for Ferrous Metallurgy in Gliwice).

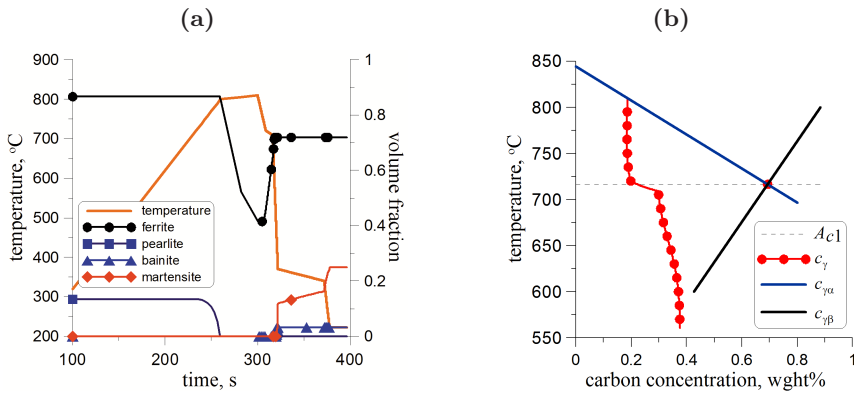


Figure 6.40: (a) The temperature and kinetics of the transformations during the annealing cycle S5, (b) changes in the average carbon concentration in austenite during the annealing cycle S5.

On the basis of these simulations and the sensitivity analysis performed in [113], it was possible to formulate an optimization task to obtain the required volume fraction of martensite of around 0.25 with a negligible amount of bainite. The parameters of this case are given as S5 in Table 5 and in Figure 6.36b. It is observed in case S5 that a slight decrease of the temperature T_{c2} allowed to predict the desired material microstructure presented in Figure 6.39b. Volume fractions of the phases after this annealing cycle are shown in Figure 6.40a and changes in the average carbon concentration in austenite are presented in Figure 6.40b.

The presented example for the physical model of continuous annealing confirmed good predictive capabilities of the model. It was also proved that the application of inverse analysis combined with sensitivity analysis allowed for efficient optimization of the annealing process. Physical simulation for the optimal parameters of the annealing cycle confirmed good accuracy of the method.

7 Conclusions

7.1 Summary

The main output of the work is the development and implementation of the identification strategy algorithm for the problems of the model parameter estimation in metal forming. The procedure is described in Chapter 5. The sensitivity analysis application, presented in Chapter 4, as a module combined with the primarily developed software for the inverse calculations for a rigid-plastic thermomechanical model, forms a robust tool for the parameter identification. The sensitivity analysis package provides:

- local methods with numerical and semi-analytical estimation of sensitivities,
- global methods, including algorithms for points generation (design for the experiment),

and it is applied for both the numerical model of the problem and the identification problem.

In the work, various problems were solved with the developed identification procedure 5.1 and the calculations are presented in Chapter 6. Each case study includes the description of the applied sensitivity analysis method with regard to the identification algorithm and the advantages of the sensitivity analysis results are listed. The calculated sensitivity indices:

- allow to validate the model,
- provide information whether it is possible to determine model parameters based on the assumed functional of the identification problem,
- enclose or extend the parameter domain,
- estimate an error and/or an accuracy of determined parameters,
- allow to adjust parameters of the optimization procedure.

The above items lead to a decrease in the calculations costs and the parameter estimation uncertainty.

The following problems were studied in Chapter 6:

- the identification of rheological and friction parameters using the results from the uniaxial compression test, the ring compression test, the 2D and 3D plane strain compression test for various flow stress models

- sensitivity analysis of the quantitative fracture criterion based on the results of the SICO test,
- sensitivity analysis of the cellular automata finite element model for the strain localization,
- identification of the phase transformation model parameters for steels,
- a design of the hot rolling technology of dual phase steel strips.

Within the work, the mathematical background of the identification problem in metal forming, formulated as an inverse problem, was investigated. Ill-posedness of the models based on thermomechanical differential equations is presented in Chapter 3, particular in terms of stability. In addition, due to the phenomenological character of many models, the assumption of a unique model solution is discussed. Therefore, alternative methods, such as sensitivity analysis algorithms, are required to support the estimation of the identified parameters.

The performed investigations and the developed algorithm of the identification parameters strategy showed that *it is possible to obtain the optimal or close to the optimal solution for the ill-posed inverse problems of identification with the application of sensitivity analysis methods combined with the optimization procedures. Sensitivity analysis decreases the computational costs of the identification and increases the reliability of the solution.*

The significance of the obtained results. It was shown in the literature review (Chapter 1) that up to date, neither theoretical investigation of the identification problems for metal forming numerical models nor the application of the global sensitivity algorithms have been discussed. The identification problems were the subject of a great number of scientific papers on metal forming but the uniqueness of the solution, uncertainty of the estimated quantities have not been studied in detail. This work is also an attempt to link the theoretical background of the inverse problems with practical applications in the metal forming numerical modeling and identification problems. The following conclusions can be drawn on the basis of performed analysis using the developed identification strategy:

- The identification problems in metal forming are ill-posed problems as presented in Chapter 3. Solving such kind of problems requires regularization which transforms the tasks to the well-posed problems. Construction of an inverse operator for the identification tasks of metal forming is hard, thus, the optimization problem is formulated. Searching for the solution of the optimization task with the classical algorithms is not satisfactory and using the bio-inspired techniques is computationally too expensive in many cases. Application of the developed sensitivity analysis methods as a preliminary step of the identification increases the robustness of the inverse analysis and reduces the computational costs. Application of the local sensitivity algorithms to the results of inverse analysis allows to estimate the accuracy of the obtained solution. It was shown in the case studies provided in Chapter 6.

- The identification procedure presented in Chapter 5 combining the optimization task and the local sensitivity procedure, is a powerful tool for the interpretation of the plastometric test results and yields the material properties independent of the type of the machine, the size of the sample, a lubricant, a method of heating and other test parameters. The approach guaranties that the obtained values of the material and process parameters are very close to the real ones.
- In identification of the friction coefficient, the flow of the material represented by the shape of the sample (usually ring) after compression is almost not sensitive to the rheological parameters. It means that the identification of friction coefficient can be performed separately, independently of the tested material.
- The flow stress determined from the identification procedure for the PSC test is only slightly sensitive to the assumption of the friction. More sensitivity but also not essential was observed for the UC. The flow stress determined from the identification procedure for the RC and RSC tests is more sensitive to the assumed friction. It means that the exact evaluation of the friction parameter is not crucial for the accuracy of the identification procedure. However, to assure the accurate solution of the identification problem both friction and rheological parameters should be the design variables and the functional of the optimization task should be composed of both loads and shape of the sample after compression.
- All the actions undertaken to improve robustness and accuracy of the inverse analysis for the tests performed to determine the material properties, were successfully applied to the designed identification problems. Application of the identification strategy algorithm allowed to estimate the optimal parameters of such processes as hot rolling, laminar cooling and continuous annealing.

7.2 Future prospects

Within the work, identification problem in metal forming is studied and the identification strategy procedure is developed to obtain *the optimal (good enough)* solution for that task. It is obvious, that not all the issues have been resolved and there are still some challenges. Some open problems, which are being solved and which are going to be solved with regard to the metal forming identification problems, are listed below:

- the construction of a regularizator for inverse thermomechanical rigid-plastic problem in terms of the theorem 3.4.1,
- sensitivity analysis for multiscale models and stochastic models,
- sensitivity analysis for the multi-cycle of production,
- sensitivity analysis combined with the *hp*-adaptation finite element code,
- parallel computation for sensitivity to increase the effectiveness of computation,

- the application of sensitivity analysis for various evolutionary optimization methods, algorithms based on artificial immune systems or other bio-inspired optimization procedures.

It can be assumed that, as for identification problems considered in the work, the developed identification strategy procedure would apply to the problems mentioned above, it would reduce the costs of computations and uncertainty of the identified parameters.

A Appendix

Functional analysis - fundamentals

For this appendix, it is assumed that K is a linear operator: $K : X \rightarrow Y$ and X, Y are normed spaces over the field $\mathbb{K} = \mathbb{R}$ or \mathbb{C} .

Definition A.0.1 (Boundedness of the operator). *The linear operator K is bounded if there exists $c > 0$ such that $\|Kx\| \leq c \|x\|$ for all $x \in X$.*

Theorem A.0.1. *The following assertions are equivalent:*

1. *The operator K is bounded.*
2. *The operator K is continuous for every $x \in X$.*

The proof of this theorem can be found in [43].

Definition A.0.2 (Compact operator). *The operator $K : X \rightarrow Y$ is compact if it maps every bounded set A into a relatively compact set $K(S)$.*

Definition A.0.3. *A set $B \subset Y$ is relatively compact if every bounded sequence $(y_i) \subset B$ has an accumulation point in \bar{B} (i.e. the closure \bar{B} is compact).*

Below there are definitions which explain the used terms. It is convenient to introduce the term *ball* for the formal definitions of these terms:

Definition A.0.4 (Ball). *The ball B of the radius r and the center $x \in X$ is the set such that*

$$B(x, r) := \{y \in X : \|y - x\| < r\}$$

Definition A.0.5 (Bounded, open, closed and other sets). *A subset $A \subset X$ is*

1. *bounded if there exists $r > 0$ and $A \subset B(x, r)$.*
2. *open if for every $x \in A$ there exists $\epsilon > 0$ such that $B(x, \epsilon) \subset A$.*
3. *closed if the complement $X \setminus A$ is open.*

Let $(x_i)_i \subset A$ be a sequence.

1. *A sequence $(x_i)_i$ is bounded if there exists $c > 0$ such that $\|x_i\| < c$ for all i .*
2. *A sequence $(x_i)_i$ is convergent if there exists $x \in X$ such that $\|x - x_i\|$ convergence to zero in \mathbb{R} .*
3. *$x \in X$ is an accumulating point if there exists a subsequence $(a_{i_n})_n$ that convergence to x .*

A set $A \in X$ is compact if every sequence in A has an accumulating point in A .

A set $\bar{A} := \left\{ x \in X : \exists (x_i)_i \subset A \wedge x = \lim_{i \rightarrow \infty} x_i \right\}$ is called closure of A .

In finite-dimensional spaces, every compact set is bounded and closed. In finite-dimensional spaces, the inverse properties are also true (*Bolzano-Weierstrass theorem*): in finite-dimensional normed spaces, every closed and bounded set is compact. The theorem is not true for infinite-dimensional spaces.

Definition A.0.6 (Orthogonal complement). X is a Hilbert space.

- Elements $x, y \in X$ are called orthogonal if $(x, y) = 0$.
- Let $A \subset X$. The set $A^\perp := \{x \in X : (x, y) = 0 \quad \forall y \in A\}$ is called the orthogonal complement of A .

Definition A.0.7 (Orthonormal Systems). A countable set of elements $A = \{x_i : i = 1, 2, 3, \dots\}$ is called the orthonormal system if $(x_i, x_j) = 0 \quad \forall i \neq j$ and $\|x_i\| = 1 \quad \forall i \in (N)$

Theorem A.0.2 (Adjoint operator). $K : X \rightarrow Y$ is a linear, bounded operator, X and Y are Hilbert spaces. There exists one and only one linear, bounded operator $K^* : Y \rightarrow X$ such that $(Kx, y) = (x, K^*y)$ for all $x \in X, y \in Y$. The operator K^* is called the adjoint operator to K . If $X = Y$ and $K^* = K$ the operator K is called self-adjoint.

Definition A.0.8 (Spectrum. Eigenvalues. Eigenvectors). Let $K : X \rightarrow Y$ is a linear operator between the normed spaces X and Y . The spectrum $\sigma(K)$ is the set of the (complex) number λ such that the operator $K - \lambda I$, where I is the identity on X , does not have a bounded inverse on X . $\lambda \in \sigma(K)$ is called an eigenvalue of K if $K - \lambda I$ is not one-to-one. If λ is an eigenvalue. Then the nontrivial elements x of the kernel $\mathcal{N}(K - \lambda I) = \{x \in X : Kx - \lambda x = 0\}$ are called eigenvectors of K .

Theorem A.0.3 (Spectral radius). $K : X \rightarrow Y$ is a linear operator.

- $x_j \in X, j = 1, \dots, n$ is a finite eigenvectors set corresponding to the pairwise different eigenvalues $\lambda_j \in \mathbb{C}$. Then $\{x_1, \dots, x_n\}$ are linear independent. If X is a Hilbert space and operator K is self-adjoint (i.e. $K = K^*$), then the eigenvalues λ_j are of real-values and the corresponding vectors x_1, \dots, x_n are pairwise orthogonal.
- If $K : X \rightarrow X$ is a self-adjoint and X is Hilbert space, then $\|K\| = \sup_{\|x\|=1} (Kx, x) = r(K)$, where $r(K) = \sup \{|\lambda| : \lambda \in \sigma(K)\}$ is called the spectral radius of K .

Definition A.0.9 (Singular values). Let $K : X \rightarrow Y$ be a compact operator between the Hilbert spaces X and Y with adjoint operator $K^* : Y \rightarrow X$. The square roots $\mu_j = \sqrt{\lambda_j}, j \in J$, of the eigenvalues λ_j of the self-adjoint operator $K^*K : X \rightarrow X$ are called singular values of K . Notice that $J \subset \mathbb{N}$ or $J = \mathbb{N}$.

Comment: every eigenvalue λ of K^*K is nonnegative: $K^*K = \lambda x \Rightarrow \lambda(x, x) = (K^*Kx, x) = (Kx, Kx) \geq 0$. It means that $\lambda \geq 0$.

Theorem A.0.4 (Singular Value Decomposition). *Let $K : X \rightarrow Y$ be a linear compact operator, $K^* : X \rightarrow Y$ - adjoint operator to K and $\mu_1 \geq \mu_2 \geq \dots > 0$ the sequence of the positive singular values of K , ordered and counted to its multiplicity. Then there exist the orthonormal systems $(x_j) \subset X$ and $(y_j) \subset Y$ of the properties $Kx_j = \mu_j y_j$ and $K^*y_j = \mu_j x_j$ for all $j \in J$. The system (μ_j, x_j, y_j) is called a singular system for K .*

Every $x \in X$ has the emphsingular value decomposition of the form $x = x_0 + \sum_{j \in J} (x, x_j) x_j$ for some $x_0 \in \mathcal{N}(K)$ and $Kx = \sum_{j \in J} \mu_j (x, x_j) y_j$.

Theorem A.0.5 (Picard). *Let $K : X \rightarrow Y$ be a linear compact operator with singular system (μ_j, x_j, y_j) . The equation $Kx = y$ is solvable if and only if $y \in \mathcal{N}(K^*)^\perp$ and $\sum_{j \in J} \frac{1}{\mu_j^2} |(y, y_j)|^2 < \infty$. Then $x = \sum_{j \in J} \frac{1}{\mu_j} (y, y_j) x_j$ is a solution of equation $Kx = y$.*

Bibliography

- [1] O. Allix. Multiscale strategy for solving industrial problems. *CMAS*, volume 6, pages 107–126, 2006.
- [2] L. Annad and S.R. Kalidindi. The process of shear band formation in plane strain compression of fcc materials: effects of crystallographic texture. *Mech Mater*, volume 17, pages 223–243, 1994.
- [3] B. Aviztur. *Metal forming: processes and analysis*. Mc Graw Hill, 1968.
- [4] M. Avrami. Kinetics of phase change. *J Chem Phys*, volume 7, pages 1103–1112, 1939.
- [5] B. Barabasz, S. Migórski, R. Schaefer and M. Paszyński. Multi-deme, twin adaptive strategy *hp*-HGS. *Inverse Probl Sci En*, volume 19, pages 3–16, 2011.
- [6] P. Bariani, T. Dal Negro and S. Bruschi. Testing and modelling of material response to deformation in bulk metal forming. *CIRP Ann-Manuf Techn*, volume 52, pages 573–594, 2004.
- [7] W. Beluch, T. Burczyński and W. Kuś. *Parallel problem solving from nature*, volume 6239 of *Lecture Notes in Computer Science*, chapter Parallel artificial immune system in optimization and identification of composite structures, pages 171–180. Springer, 2010.
- [8] H.K.D.H. Bhadeshia. *Bainite in steels*. University Press, Cambridge, 2001.
- [9] R. Białecky, T. Burczyński, A. Długosz, W. Kuś and Z. Ostrowski. Evolutionary shape optimization of thermoelastic bodies exchanging heat by convection and radiation. *Comput Method Appl M*, volume 194, pages 1839–1859, 2005.
- [10] G. Blom. *Probability and statistics: theory and applications*. Springer, New York, 1989.
- [11] A Buczek and T. Telejko. Determination of heat transfer coefficient and thermal conductivity using the solution of inverse heat conduction problem. In P.F. Bariani, editor, *Proceedings of 8th International Conference on Technology of Plasticity ICTP*, Verona, October 2005. CD-ROM.
- [12] T. Burczyński, J. Działkiewicz, W. Kuś and E. Majchrzak. Identification of microscale heat transfer parameters using bioinspired algorithms. In H.A. Mang, J. Eberhardsteiner, H.J. Böhm and F.G. Rammerstorner, editors, *Proceedings of 6th European Congress on Computational Methods in Applied Sciences and Engineering ECCOMAS*, Vienna, September 2012. CD-ROM.
- [13] A. Cebo-Rudnicka, Z. Malinowski, T. Telejko and J. Gielżecki. Inverse determination of the heat transfer coefficient distribution on a steel plate cooled by a water spray nozzle. *WIT Trans Eng Sci*, volume 75, pages 345–355, 2012.
- [14] C.C. Chen and S. Kobayashi. Rigid-plastic-finite-element analysis of ring compression. In H. Armen and R. F. Jr. Jones, editors, *Proceedings of the Winter Annual Meeting of ASME, AMD: Application of numerical methods to forming processes*, volume 28, pages 163–174, 1978.

- [15] P. Cizek. Characteristics of shear bands in an austenitic stainless steel during hot deformation. *Mater Sci Eng*, volume A324, pages 214–218, 2002.
- [16] M.G. Cockcroft and D.J. Latham. Ductility and the workability of metals. *J I Met*, volume 96, pages 33–39, 1968.
- [17] S. Das, E.J. Palmiere and I.C. Howard. CAFE: a tool for modeling thermomechanical processes. In E.J. Palmiere, M. Mahfouf and C. Pinna, editors, *Proceedings of International Conference on Thermomechanical Processing: Mechanics, Microstructure & Control*, pages 296–301, Sheffield, June 2002.
- [18] N.J. Davenport, S.B. ans Silk, C.N. Sparks and C.M. Sellars. Development of constitutive equation for the modeling of hot rolling. *Mater Sci Tech*, volume 16, pages 1–8, 1999.
- [19] D. Deb. *Multi-objective optimization using evolutionary algorithms*. Wiley, 2001.
- [20] B. Donnay, J.C. Herman, V. Leroy, U. Lotter, R. Grossterlinden and H. Pircher. Microstructure evolution of C-Mn steels in the hot deformation process: the STRIPCAM model. In J.H. Beynon, P. Ingham, H. Teichert and K. Waterson, editors, *Proceedings of 2nd International Conference on Modelling of Metal Rolling Processes*, pages 23–35, London, December 1996.
- [21] H.W. Engl, M. Hanke and A. Neubauer. *Regularization of inverse problems*. Mathematics and its applications. Kluwer Academic Publishers, 1996.
- [22] G.S. Fishman. *Monte Carlo: concepts, algorithms and applications*. Springer-Verlag, New York, 1996.
- [23] R. Forestier, E. Massoni and Y. Chastel. Estimation of constitutive parameters using an inverse method coupled to a 3D finite element software. *J Mater Process Tech*, volume 125, pages 594–601, 2002.
- [24] D. Frederick and T.S. Chang. *Continuum Mechanics*. Allyn and Bacon, Inc., Boston, 1965.
- [25] B. Garbarz, W. Burian and D. Woźniak. Semi-industrial simulation of in-line thermomechanical processing and heat treatment of nano-duplex bainite-austenite steel. In J. Kusiak, J. Majta and D. Szeliga, editors, *Proceedings of the 14th International Conference on Metal Forming, Steel Res Int*, pages 1251–1254, Kraków, September 2012.
- [26] A. Gavras, E. Massoni and J. L. Chenot. An inverse analysis using a finite element model for a rheological parameter identification. *J Mater Process Tech*, volume 60, pages 447–454, 1996.
- [27] A. Gavras, E. Massoni and J. L. Chenot. The rheological parameter identification formulated as an inverse problem. *Inverse Probl Sci En*, volume 7, pages 1–41, 1999.
- [28] A. Gavras, E. Massoni and J. L. Chenot. Thermoviscoplastic parameter identification formulated ad an inverse finite element analysis of the hot torsion test. *Steel Res Int*, volume 70, pages 259–268, 1999.
- [29] J. Gawąd, R. Kuziak, L. Madej, D. Szeliga and M. Pietrzyk. Identification of rheological parameters on the basis of various types of compression and tension tests. *Steel Res Int*, volume 76, pages 131–137, 2005.

- [30] J. Gawąd, D. Szeliga, A. Bator, V. Pidvysotsky and M. Pietrzyk. Interpretation of the results of tensile tests based on two-criterion optimization. In M. Pietrzyk, editor, *Proceedings of 11th Conference on Computer Methods in Materials Technology KomPlasTech*, page 27–34, Zakopane, January 2004. Wydawnictwo Naukowe Akapit. (in Polish).
- [31] J.C. Gelin and O. Ghouati. An inverse method for determining viscoplastic properties of aluminium alloys. *J Mater Process Tech*, volume 45, pages 435–440, 1994.
- [32] F. Grosman. Application of the flow stress function in programmes for computer simulation of plastic working processes. *J Mater Process Tech*, volume 64, pages 169–180, 1997.
- [33] B. Hadała, Z. Malinowski, T. Telejko, A. Cebo-Rudnicka and A. Szajding. Influence of the finite element model on the inverse determination of the heat transfer coefficient distribution over the hot plate cooled by the laminar water jets. *Arch Metall Mater*, volume 58, pages 105–112, 2013.
- [34] J. Hadamard. *Lectures on Cauchy’s problem in linear partial differential equations*. New Haven, 1923.
- [35] S.V. Harren, H.E. Deve and R.J. Asaro. Shear band formation in plane strain compression. *Acta Metall Mater*, volume 36, pages 2435–2480, 1988.
- [36] P. Hartley, I. Pillinger and C. Sturgess. *Numerical modelling of material deformation processes. Research, development and applications*. Springer-Verlag, 1992.
- [37] P.D. Hodgson and D.C. Collinson. The calculation of hot strength in plate and strip rolling of niobium microalloyed steels. In S. Yue, editor, *Proceedings of International Symposium on Mathematical Modelling of Hot Rolling of Steel*, pages 239–250, August 1990.
- [38] S.C Hora and R.L. Iman. A comparison of maximum/bounding and bayesian/monte carlo for fault tree uncertainty analysis. Technical Report SAND85-2839, Sandia National Laboratories, 1986.
- [39] R.L. Iman and S. C. Hora. A robust measure of uncertainty importance for use in fault tree system analysis. *Risk Anal*, volume 10, pages 401–406, 1990.
- [40] P. Jojczyk and R. Schaefer. Global impact balancing in the hierarchic genetic search. *Comput Inform*, volume 28, pages 181–193, 2009.
- [41] J. Kennedy and R.C. Eberhart. Particle swarm optimization. In *Proceedings of the IEEE International Conference on Neural Networks*, volume 4, pages 1942 – 1948, Perth, WA, November/December 1995.
- [42] I.Y. Kim and O.L. de Weck. Adaptive weighted-sum method for bi-objective optimization: Pareto front generation. *Struct Multidiscip O*, volume 29, pages 149–158, 2005.
- [43] A. Kirsch. *An introduction to the mathematical theory of inverse problems*. Springer, 1996.
- [44] M. Kleiber, H. Antunez, T.D. Hien and P. Kowalczyk. *Parameter sensitivity in non-linear mechanics*. Wiley, 1997.

- [45] J. P. Kleinermann, J. P. Ponthot and M. Hogge. Parameter identification for inverse problems in metal forming simulations. *Solid Mech Appl*, volume 109, pages 81–99, 2003.
- [46] S. Kobayashi, S. Oh and T. Altan. *Metal forming and the finite-element method*. Oxford University Press, 1989.
- [47] D.P. Koistinen and R.E. Marburger. A general equation prescribing the extent of the austenite-martensite transformation in pure iron-carbon alloys and plain carbon steels. *Acta Metall Mater*, volume 7, pages 59–60, 1959.
- [48] T. Kondek, D. Szeliga and M. Pietrzyk. Computer code for identification of parameters in constitutive equations using results of axisymmetrical compression tests. In F. Grosman and et al., editors, *Proceedings of 10th Conference on Computer Methods in Materials Technology KomPlasTech*, page 207–214, Wisła–Jawornik, January 2003. (in Polish).
- [49] A. Korbel. Structural and mechanical aspects of homogeneous and non-homogeneous deformation in solids. *Cism Cour L*, volume 386, pages 21–98, 1998.
- [50] B. Kowalski, C.M. Sellars and M. Pietrzyk. Development of a computer code for the interpretation of results of hot plane strain compression tests. *ISIJ Int*, volume 40, pages 1230–1236, 2000.
- [51] B. Kowalski, C.M. Sellars and M. Pietrzyk. Identification of rheological parameters on the basis of plane strain compression tests on specimens of various initial dimensions. *Comp Mater Sci*, volume 35, pages 92–97, 2006.
- [52] B. Kowalski, W. Wajda, M. Pietrzyk and C.M. Sellars. Influence of strain and strain rate inhomogeneity on constitutive equations determined from plane strain compression tests. In A.M. Habraken, editor, *Proceedings of the 4th International ESAFORM Conference on Material Forming*, pages 561–564, Liege, April 2001.
- [53] W. Kuś and R. Górski. Parallel identification of voids in a microstructure using the boundary element method and the bioinspired algorithm. *Computer Methods in Materials Science*, volume 13, pages 251–257, 2013.
- [54] J. Kusiak. Approximation-based technique in application to the optimization of metal forming processes. In B. Buchmayr, editor, *Proceedings of 24. Verformungskundliches Kolloquium*, page 167–174, Planneralm, February 2005.
- [55] J. Kusiak, A. Danielewska-Tulecka and P. Oprocha. *Optymalizacja. Wybrane metody z przykładami zastosowań*. Państwowe Wydawnictwa Naukowe, Warszawa, 2009.
- [56] J. Kusiak, D. Szeliga and Ł. Sztangret. *Microstructure evolution in metal forming processes*, chapter Modelling techniques for optimizing metal forming processes, page 35–66. Oxford: Woodhead Publishing Limited, 2012.
- [57] R. Kuziak, V. Pidvysotsky and M. Pietrzyk. Selection of the best thermomechanical processing parameters during manufacturing of forgings made of the CuCr alloys. *Computer Methods in Materials Science*, volume 10, pages 181–189, 2010.
- [58] R. Kuziak and M. Pietrzyk. Interpretation of SICO test for rod steels. In *Proceedings of 43rd Conference on Mechanical Working and Steel Processing*, volume 39, page 65–73, Charlotte, North Carolina, October 2001.

- [59] Y.J. Lan, D.Z. Li and Y.Y. Li. Modeling austenite decomposition into ferrite at different cooling rate in low-carbon steel with cellular automaton method. *Acta Mater*, volume 52, pages 1721–1729, 2004.
- [60] F. Leja. *Rachunek różniczkowy i całkowy*. PWN, Warszawa, 1976.
- [61] J.G. Lenard, M. Pietrzyk and L. Cser. *Mathematical and physical simulation of the properties of hot rolled products*. Elsevier, Amsterdam, 1999.
- [62] J. H. Lienhard (IV) and J. H. Lienhard (V). *A heat transfer textbook*. Phlogiston Press, Cambridge, Massachusetts, USA, 2003.
- [63] L. Madej. *Development of the modeling strategy for the strain localization simulation based on the digital material representation*. Wydawnictwa AGH, 2010.
- [64] L. Madej, P.D. Hodgson and M. Pietrzyk. Multi scale rheological model for discontinuous phenomena in materials under deformation conditions. *Comp Mater Sci*, volume 38, pages 685–691, 2007.
- [65] L. Madej, P.D. Hodgson and M. Pietrzyk. The validation of a multi scale rheological model of discontinuous phenomena during metal rolling. *Comp Mater Sci*, volume 41, pages 236–241, 2007.
- [66] L. Madej, D. Szeliga, L. Sztangret and M. Pietrzyk. Validation of parameters of cellular automata finite element model dedicated to strain localization phenomena. *Steel Res Int*, volume 81, pages 1426–1429, 2010.
- [67] E. Majchrzak, J. Dziaekiewicz and G. Kałuża. Application of sensitivity analysis in microscale heat transfer. In A.J. Nowak and R.A. Bialecki, editors, *Proceedings of International Conference on Numerical Heat Transfer NHT*, Wrocław, September 2012. CD-ROM.
- [68] E. Majchrzak, K. Freus and S. Freus. Shape sensitivity analysis. implicit approach using boundary element method. *Scientific Research of the Institute of Mathematics and Computer Science*, volume 1, pages 151–161, 2011.
- [69] E. Majchrzak, J. Mendakiewicz and M. Paruch. *Evolutionary and deterministic methods for design, optimization and control with applications to industrial and societal problems (A Series of Handbooks on Theory and Engineering Applications of Computational Methods)*, chapter Application of evolutionary algorithms for inverse solidification problems solution, pages 281–286. CIMNE, Barcelona, 2011.
- [70] E. Majchrzak, J. Mendakiewicz and A. Piasecka-Belkhatay. Algorithm of mould thermal parameters identification in the system casting-mould-environment. In L. A. Dobrzański, editor, *Proceedings of 13th International Scientific Conference on Achievements in Mechanical and Materials Engineering*, pages 411–414, Gliwice-Wisła, May 2005.
- [71] E. Majchrzak and B. Mochnacki. Sensitivity analysis of transient temperature field in microdomains with respect to the dual phase lag model parameters. In H.A. Mang, J. Eberhardsteiner, H.J. Bohm and F.G. Rammerstorner, editors, *Proceedings of 6th European Congress on Computational Methods in Applied Sciences and Engineering ECCOMAS*, Vienna, September 2012. CD-ROM.
- [72] E. Majchrzak, B. Mochnacki and J.S. Suchy. Identification of substitute thermal capacity of solidifying alloy. *J Theor Appl Mech*, volume 46, pages 257–268, 2008.

- [73] A.T. Male and M.G. Cockcroft. A method for the determination of the coefficient of friction of metals under conditions of bulk plastic deformation. *J I Met*, volume 93, pages 38–46, 1964-65.
- [74] Z. Malinowski, J.G. Lenard and M.E. Davies. A study of heat transfer coefficient as a function of temperature and pressure. *J Mater Process Tech*, volume 41, pages 125–142, 1994.
- [75] MathWorks. <http://www.mathworks.com/>, May 2013.
- [76] M.D. McKay. Evaluating prediction uncertainty. Technical Report NUREG/CR-6311 (LA-12915-MS), Los Alamos National Laboratory, 1995.
- [77] M.D. McKay. Nonparametric variance-based methods of assessing uncertainty importance. *Reliab Eng Syst Safe*, volume 57, pages 267–279, 1997.
- [78] M.D. McKay, W.J. Conover and R.J. Beckman. A comparison of three methods for selecting values of input variables in the analysis of output from a computer code. *Technometrics*, volume 21, pages 239–245, 1979.
- [79] P.T Moe, W. Wajda, L. Madej, D. Szeliga, S. Storen and M. Pietrzyk. An approach for evaluating constitutive models for hot aluminium extrusion – rod extrusion of AA6060 as a case study. *Steel Grips*, volume 2, pages 723–729, 2004.
- [80] M. Morawiecki, L. Sadok and E. Wosiek. *Przeróbka plastyczna. Podstawy teoretyczne*. Śląsk, Katowice, 1986.
- [81] M.D. Morris. Factorial sampling plans for preliminary computational experiments. *Technometrics*, volume 33, pages 161–174, 1991.
- [82] K. Myczkowska, D. Szeliga and J. Kusiak. Sensitivity analysis of the cooling cycle for the dp steels. *Rudy i Metale Nieżelazne*, volume 56, pages 692–696, 2011. (in Polish).
- [83] J. A. Nelder and R. Mead. A simplex method for function minimization. *Comput J*, volume 7, pages 308–313, 1965.
- [84] J. Nocedal and S. J. Wright. *Numerical optimization*. Springer, 1996.
- [85] J. Ordon, R. Kuziak and M. Pietrzyk. History dependant constitutive law for austenitic steels. In M. Pietrzyk, J. Kusiak, J. Majta, P. Hartley and I. Pillinger, editors, *Proceedings of 8th International Conference on Metal Forming*, pages 747–753, Kraków, September 2000.
- [86] A.B. Owen. A central limit theorem for latin hypercube sampling. *J Roy Stat Soc B Met*, volume 54, pages 541–551, 1992.
- [87] M. Oyane, T. Sato, K. Okimoto and S. Shima. Criteria for ductile fracture and their application. *J Mech Work Technol*, volume 4, pages 66–81, 1980.
- [88] M. Pernach and M. Pietrzyk. Numerical solution of the diffusion equation with moving boundary applied to modeling of the austenite-ferrite phase transformation. *Comp Mater Sci*, volume 44, pages 783–791, 2008.
- [89] V. Pidvysotsky, W. Wajda, M. Pačko, R. Kuziak and M. Pietrzyk. Identification of the flow stress for copper in the room temperature. *Naukovi Visti, Suchasni Problemi Metalurgii*, volume 5, pages 255–258, 2002.

- [90] M. Pietrzyk. Comp_axi – komputerowy program do symulacji plastometrycznej próby speczania próbek osiowosymetrycznych. *Hutnik-Wiadomosci Hutnicze*, volume 60, pages 190–197, 1993. (in Polish).
- [91] M. Pietrzyk. Numerical aspects of the simulation of hot metal forming using internal variable method. *Metallurgy and Foundry Engineering*, volume 20, pages 429–439, 1994.
- [92] M. Pietrzyk and R. Kuziak. Coupling the thermal-mechanical finite-element approach with phase transformation model for low carbon steels. In J. A. Covas, editor, *Proceedings of the 2nd International ESAFORM Conference on Material Forming*, pages 525–528, Guimaraes, April 1999.
- [93] M. Pietrzyk, R. Kuziak and T. Kondek. Physical and numerical modelling of plastic deformation of steels in two-phase region. In *Proceedings of 45th Conference on Mechanical Working and Steel Processing*, volume 41, pages 209–220, Chicago, November 2003.
- [94] M. Pietrzyk, R. Kuziak, K. Radwański and D. Szeliga. Physical and numerical simulation of the continuous annealing of DP steel strips. *Steel Res Int*, volume 84, 2013. (accepted for publication).
- [95] M. Pietrzyk and J. G. Lenard. *Thermal-mechanical modelling of the flat rolling Process*. Springer-Verlag, 1991.
- [96] M. Pietrzyk, J. Majta, D. Szeliga and R. Kuziak. Inverse analysis of axisymmetrical compression of hsla steel. *Steel Res Int*, volume 78, pages 546–553, 2007.
- [97] M. Pietrzyk, V. Pidvysotsky and M. Pačko. Flow stress model accounting for the strain localization during plastic deformation of metals. *CIRP Ann-Manuf Techn*, volume 53, pages 235–238, 2004.
- [98] A. Poteralski, M. Szczepanik, G. Dziaekiewicz, R. Górski, W. Kuś and T. Burczyński. *Evolutionary and deterministic methods for design, optimization and control with applications to industrial and societal problems (A Series of Handbooks on Theory and Engineering Applications of Computational Methods)*, chapter Artificial biological systems in optimization of structures analysed by the boundary element method, pages 140–148. CIMNE, Barcelona, 2011.
- [99] D. G. Rees. *Essential statistics*. Boca Raton : Chapman & Hall, 2001.
- [100] H.H. Rosenbrock. An automatic method for finding the greatest or least value of a function. *The Computer Journal*, volume 3, pages 175–184, 1960.
- [101] A. Saltelli, Chan K. and E.M. Scot. *Sensitivity analysis*. Wiley, New York, 2000.
- [102] R. Schaefer and B. Barabasz. Asymptotic behavior of *hp*-hgs (*hp*-adaptive finite element method coupled with the hierarchic genetic strategy) by solving inverse problems. *Lect Notes Comput Sc*, volume 5103, pages 682–691, 2008.
- [103] E. Scheil. Anlaufzeit der austenitumwandlung. *Archiv für Eisenhüttenwesen*, volume 12, pages 565–567, 1935.
- [104] C.M. Sellars. *Hot working and forming processes*, chapter Physical metallurgy of hot working, pages 3–15. The Metals Soc., London, 1979.
- [105] A.L. Semiatin and G.D. Lahoti. The occurrence of shear bands in isothermal hot forging. *Metall Mater Trans A*, volume 13A, pages 275–288, 1982.

- [106] J.P. Simmons, C. Shen and Y. Wang. Phase field modeling of simultaneous nucleation and growth by explicitly incorporating nucleation events. *Scripta Mater*, volume 43, pages 935–942, 2000.
- [107] I.M. Sobol: Sensitivity analysis for non linear mathematical models. *Mathematical Modeling and Computational Experiment*, volume 1, pages 407–414, 1993.
- [108] W. Sosnowski. *Numeryczna symulacja, analiza wrażliwości i optymalizacja nieliniowych procesów deformacji konstrukcji*. Wydawnictwo Uniwersytetu Kazimierza Wielkiego, 2003. (in Polish).
- [109] W. Sosnowski, I. Marczevska and A. Marczewski. Sensitivity based optimization of sheet metal forming tools. *J Mater Process Tech*, volume 124, pages 319–328, 2002.
- [110] Statistica. <http://www.statsoft.com/>, May 2013.
- [111] M. Suehiro, T. Senuma, H. Yada and K. Sato. Application of mathematical model for predicting microstructural evolution to high carbon steels. *ISIJ Int*, volume 32, pages 433–439, 1992.
- [112] D. Szeliga. Sensitivity analysis – methods and applications. *Computer Methods in Materials Science*, volume 5, pages 170–178, 2005. (in Polish).
- [113] D. Szeliga. Design of the continuous annealing process for multiphase steel strips. In *Proceedings of 21st International Conference on Metallurgy and Materials METAL*, Brno, May 2012. CD-ROM.
- [114] D. Szeliga, J. Gawąd, T. Kondek and M. Pietrzyk. Identification of parameters of material models based on inverse analysis. In R. Tadeusiewicz, A. Ligęza and M. Szymkat, editors, *Proceedings of 4th National Conference on Metody i systemy komputerowe w badaniach naukowych i projektowaniu inżynierskim*, page 761–766, Kraków, November 2003. (in Polish).
- [115] D. Szeliga, J. Gawąd and M. Pietrzyk. Genetic algorithms for inverse calculations to the interpretation of the ring compression test results. *Rudy i Metale Nieżelazne*, volume 46, pages 516–517, 2001. (in Polish).
- [116] D. Szeliga, J. Gawąd and M. Pietrzyk. Parameters identification of material models based on the inverse analysis. *Int J Appl Math Comp*, volume 14, pages 549–556, 2004.
- [117] D. Szeliga, J. Gawąd and M. Pietrzyk. Inverse analysis for identification of rheological and friction models in metal forming. *Comput Method Appl M*, volume 195, pages 6797–6798, 2006.
- [118] D. Szeliga, J. Gawąd, M. Pietrzyk and R. Kuziak. Inverse analysis of tensile tests. *Steel Res Int*, volume 76, pages 807–814, 2005.
- [119] D. Szeliga and L. Madej. Sensitivity analysis of the cellular automata finite element model for the strain localization. *Computer Methods in Materials Science*, volume 9, pages 264–270, 2009.
- [120] D. Szeliga, P. Matuszyk, R. Kuziak and M. Pietrzyk. Identification of rheological parameters on the basis of various types of plastometric tests. *J Mater Process Tech*, volume 125–126, pages 150–154, 2002.

- [121] D. Szeliga, P. Matuszyk, V. Pidvysotskyk and M. Pietrzyk. 3D model of cube compression for inverse analysis. In M. Pietrzyk, Z. Mitura and J. Kaczmar, editors, *Proceedings of the 5th International ESAFORM Conference on Material Forming*, pages 171–174, Kraków, April 2002.
- [122] D. Szeliga and M. Pietrzyk. Problem of the starting point generation for the inverse analysis of compression tests. *Metallurgy and Foundry Engineering*, volume 27, pages 167–181, 2001.
- [123] D. Szeliga and M. Pietrzyk. *Metal forming science and practice: a state-of-the-art volume in honour of Professor J. A. Schey's 80th birthday – pioneer in the field of metal forming*, chapter Identification of rheological and tribological parameters, page 227–258. Elsevier, Amsterdam, 2002.
- [124] D. Szeliga and M. Pietrzyk. Testing of the inverse software for identification of rheological models of materials subjected to plastic deformation. *Arch Civ Mech Eng*, volume 7, pages 35–52, 2007.
- [125] D. Szeliga and M. Pietrzyk. Identification of rheological models and boundary conditions in metal forming. *Int J Mater Prod Tec*, volume 39, pages 388–405, 2010.
- [126] D. Szeliga, M. Pietrzyk, R. Kuziak and V. Pidvysotskyk. Rheological model of Cu based alloys accounting for the preheating prior to deformation. *Arch Civ Mech Eng*, volume 11, pages 451–467, 2011.
- [127] Ł. Sztangret and J. Kuziak. Modified approximation based optimization strategy. *Lect Notes Comput Sc*, volume 7268, pages 600–607, 2012.
- [128] Ł. Sztangret, D. Szeliga and J. Kuziak. Sensitivity analysis as a supporting procedure in optimization of metallurgical processes. *Hutnik-Wiadomości Hutnicze*, volume 76, pages 721 – 725, 2010.
- [129] Ł. Sztangret, D. Szeliga, J. Kuziak and M. Pietrzyk. Constitutive material model identification basing on the inverted metamodel solution. *Mechanik*, volume 84, pages 32–34, 2011.
- [130] Ł. Sztangret, D. Szeliga, J. Kuziak and M. Pietrzyk. Identification of material properties of the dp steel based on plastometric tests and on industrial hot strip rolling. *Computer Methods in Materials Science*, volume 11, pages 542–550, 2011.
- [131] Ł. Sztangret, D. Szeliga, J. Kuziak and M. Pietrzyk. Application of inverse analysis with metamodeling for identification of metal flow stress. *Can Metall Quart*, volume 51, pages 440–446, 2012.
- [132] Ł. Sztangret, A. Milenin, W. Walczyk, M. Pietrzyk and J. Kuziak. Computer aided design of the best forging technology for crank shafts. *Computer Methods in Materials Science*, volume 11, pages 237–242, 2011.
- [133] D. Szyndler. *Inverse problem applied to identification of metal forming processes parameters*. PhD thesis, Akademia Górniczo-Hutnicza, Kraków, Poland, 2001. (in Polish).
- [134] D. Szyndler, M. Pietrzyk and P.D. Hodgson. Identification of parameters in the internal variable constitutive model and friction model for hot forming of steels. In K. Mori, editor, *Proceedings of the 7th International Conference on Numerical Methods in Industrial Forming Processes NUMIFORM*, pages 297–302, Toyohashi, June 2001.

- [135] D. Szyndler, M. Pietrzyk and R. Kuziak. Estimation of rheological and friction parameters in hot forming processes as an inverse problem. In A.M. Habraken, editor, *Proceedings of the 4th International ESAFORM Conference on Material Forming*, pages 191–194, Liege, April 2001.
- [136] J. Talar, D. Szeliga and M. Pietrzyk. Application of genetic algorithms for identification of rheological and friction parameters in copper deformation processes. *Arch Metall*, volume 47, pages 27–41, 2002.
- [137] T. Telejko and Z. Malinowski. Sensitivity investigations of the inverse method involved in the thermal conductivity determination of steels. In M. Pietrzyk, Z. Mitura and J. Kaczmar, editors, *Proceedings of the 5th International ESAFORM Conference on Material Forming*, page 175–178, Kraków, April 2002.
- [138] T. Telejko and Z. Malinowski. Application of an inverse solution to the thermal conductivity identification using the finite element method. *J Mater Process Tech*, volume 146, pages 145–155, 2004.
- [139] A. Torn and A. Zilinskas. *Global optimization*, volume 350 of *Lecture Notes in Computer Science*. Springer, Berlin, 1989.
- [140] L. Trębacz. *Identification of plastic fracture criteria based on the experimental results*. PhD thesis, Akademia Górniczo-Hutnicza, 2012. (in Polish).
- [141] L. Trębacz, W. Mitkowski and M. Pietrzyk. Parameter sensitivity of the SICO test. In D.R.J. Owen, E. Onate and B. Suarez, editors, *Proceedings of 8th International Conference on Computational Plasticity Fundamentals and Applications COMPLAS*, pages 995–998, Barcelona, September 2005.
- [142] L. Trębacz, D. Szeliga and M. Pietrzyk. Sensitivity analysis of quantitative fracture criterion based on the results of the sico test. *J Mater Process Tech*, volume 177, pages 296–299, 2006.
- [143] M. Umemoto, A. Hiramatsu, A. Moriya, T. Watanabe, S. Nanba, N. Nakajima, G. Anan and Y. Higo. Computer modelling of phase transformation from work-hardened austenite. *ISIJ Int*, volume 32, pages 306–315, 1992.
- [144] J.J. Urcola and C.M. Sellars. Effect of changing strain rate on stress-strain behaviour during high temperature deformation. *Acta Metall Mater*, volume 35, pages 2637–2647, 1987.
- [145] R. H. Wagoner and J. L. Chenot. *Metal forming analysis*. Cambridge University Press, 2001.
- [146] W. Wajda, J. Kusiak and M. Pietrzyk. Ocena błędu wynikającego z zastosowania rozwiązania 2D do symulacji próby kanalikowej. In F. Grosman, A. Piela, J. Kusiak and M. Pietrzyk, editors, *Proceedings of 8th Conference on Computer Methods in Materials Technology KomPlasTech*, pages 93–100, Korbielów, 2001. (in Polish).
- [147] O.C. Zienkiewicz, R.L. Taylor and J.Z. Zhu. *The finite element method: its basis and fundamentals*. Elsevier, 2005.
- [148] A. Zmudzki, J. Kusiak and A. Danielewska-Tulecka. Optimization of materials processing using a hybrid technique based on artificial neural networks. *Arch Metall Mater*, volume 50, pages 609–620, 2005.

- [149] A. Zmudzki, R. Kuziak, M Papaj and M. Pietrzyk. Identification of friction model in extrusion. In J. Lisowski, E. Szymańska and T. Zielniewicz, editors, *Proceedings of the 16th International Scientific and Technological Conference on Design and Technology of Drawpieces and Die Stampings*, page 213–222, Poznań–Wąsowo, June 2004.
- [150] A. Zmudzki, M Papaj, R. Kuziak, J. Kusiak and M. Pietrzyk. Optimum die shape design for evaluation of material properties. In V. Brucato, editor, *Proceedings of the 6th International ESAFORM Conference on Material Forming*, page 139–142, Salerno, April 2003.
- [151] A. Zmudzki, M. Papaj, R. Kuziak, J. Kusiak and M. Pietrzyk. Validation of the forward-backward extrusion test, designed for evaluation of friction coefficient and flow properties of metal alloys deformed in semi-solid state. *Steel Grips*, volume 2, pages 541–545, 2003.
- [152] A. Zmudzki, M. Pietrzyk, R. Kuziak and M Papaj. Identification of material model for aluminium alloy using forward-backward extrusion test. In D. Buche and N. Hofmann, editors, *Proceedings of the 1st Invited Conference on Automatic Process Optimization in Materials Technology COST 526*, page 183–192, Morschach, May 2005.

ISSN 0867-6631
ISBN 978-83-7464-625-3